

**Technical University of Crete  
Department of Electronic Engineers & Engineers of  
Computers**



**Master thesis**

**‘Modelling of epithelial transport phenomena related  
with the acetowhitening optical characteristics:  
Potential for the *in-vivo* diagnosis of Cervical  
Neoplasia’**

Papoutsoglou Georgios

Committee: Assoc. Prof. Costas Balas (Supervisor)  
Prof. Michalis Zervakis  
Prof. Giorgos Stavrakakis

Chania 2007

## AKNOWLEDGEMENTS

---

Mathematical modelling of biological procedures involves a bundle of sciences participating in the most creative manner. Under mathematics physics, chemistry and medicine, that provide the knowledge, are united. However, the lack of scientific information over certain issues is, of course, a major drawback for such a quest that can potentially lead to unrealistic results. Perhaps, the most efficient way to overcome such problems is to keep it stupid, simple.

First of all, I would like to acknowledge my supervising Professor Costas Balas for the assignment of this, doubtless, interesting thesis, for his continuous support and guidance, the outmost patience during the endless arguing over the model and for his ideas that in essence have been implemented in this project. Also, I would like to thank both professors Michalis Zervakis and Giorgos Stavrakakis for their participation in the three-party committee of this thesis. Special thanks should be directed to some people whose contribution to the overall work was significant: Antonis Potirakis whose thesis guided me through all my research, John Skiadias and Manolis Papagiannakis for sharing with me their knowledge on biological and chemical aspects, helping me to gain insight about the overall problem. Many thanks should be also directed to the Electronics Laboratory fellow students, Thanasis Tsapras, Manolis Terzakis and Antonopoulos Aggelos, that encouraged me during the development of my thesis. I should not forget to thank the Electronics Laboratory teaching and technical staff member John Chatzakis for his continuous interest in the progress of my work.

Of course, I should thank all my friends for their psychological support especially in times of utter desperation. Above all, I want to thank my family to whom I owe my principles and values, whose love and caring supported me during my academic years.

Master thesis

**‘Modelling of epithelial transport phenomena related with the acetowhitening optical characteristics: Potential for the *in-vivo* diagnosis of Cervical Neoplasia’**

Papoutsoglou Georgios

Supervisor: Assoc. Professor Costas Balas

**Abstract**

Cervical Intraepithelial Neoplasia (CIN) grade I, II and III is the precursor of invasive cervical carcinoma. Diagnosis is based on the visual examination of the tissue. Topical application of acetic acid (AA) solution highlights abnormal areas. The agent-tissue interaction generates an optical signal perceived as transient tissue whitening, known as acetowhitening and is associated with the lesion’s grade. Screening techniques with promising results are emerging. However, no systematic approach exists thus far towards the understanding and the identification of the biological factors affecting the dynamic optical characteristics of the acetowhitening phenomenon. It is very essential to identify the biological factors that are affected by neoplasia development and are affecting the acetowhitening dynamic optical characteristics. By establishing such a correlation, the *in vivo* quantitative assessment of the latter would provide quantitative indices expressing disease-specific microstructural and functional alterations. Here, we attempt to interpret the biophysical processes involved during acetowhitening and determine the *in vivo* measured dynamic scattering characteristics.

Based on the assumption that acetic acid dynamics designate the acetowhitening phenomenon, a compartmental model of the epithelium has been developed. We used a set of biophysical differential equations to predict the epithelial transport phenomena that are expected to be correlated with the dynamic characteristics of the backscattered light. For model validation, an imaging device capable of measuring the acetowhitening kinetics has been developed. Model predictions have been compared with experimental data obtained from patients with cervical neoplasia of different grade and correlated with the model predictions.

Both the model and the experimental results showed that the acetowhitening is reversible in nature. Provided that the effect lasts approximately 4 minutes, the conformational changes provoked in cellular components (proteins in particular), which can in turn cause a local variation in the refractive index and consequently an alteration in the light scattering characteristics, is attributed to the intracellular proton concentration.

Using different AA concentrations (3% and 5%), results strongly suggest that the model provides valid predictions for the epithelial transport phenomena. Both intracellular proton concentrations and diffuse reflectance peak values are increasing with the concentration of administered AA. In addition, the slopes before the maximum of both model predicted and experimental curves become steeper as the concentration increases. These, in correlation with the functional status of the tissue, further confirm that the acetowhitening effect follows the dynamics of the intracellular proton concentration.

Comparisons in different CIN grades using histology as reference revealed that the higher the grade the greater the number of abnormal epithelial volume and consequently the greater the total intracellular proton volume in the epithelium at a given time point. By increasing the total intracellular volume of the protons in the total abnormal epithelium, the volume of cellular components subjected to conformational changes is expected to increase accordingly. This

implies that the alteration of the refractive index will occur in a greater number of cells, which in turn will increase back scattering cross section of the epithelial tissue.

Furthermore, the developed model was also tested in providing information across the third (vertical) direction of the epithelium. Results evidenced that the proton intracellular concentration falls remarkably across the epithelium which indicates that, in high grade cases, acetic acid is consumed in the epithelium totally.

Comparisons, confirmed the validity of the interpretation of the phenomenon and particularly the fact that dynamic scattering characteristics are largely determined by the intracellular proton concentration kinetics. In addition, the correlation of the latter with both structural and functional alterations, associated with cervical neoplasia development, has been predicted theoretically and confirmed experimentally. This highlights the potential of the developed imaging method and technology for the non-invasive diagnosis, guided therapeutics and screening of cervical neoplasia.

# TABLE OF CONTENTS

<b>CHAPTER I.....</b>	<b>1</b>
<b>MOTIVATION AND OBJECTIVES .....</b>	<b>1</b>
1.1 INTRODUCTION .....	1
1.1 CHAPTERS SUMMARY .....	4
<b>CHAPTER II .....</b>	<b>6</b>
<b>INTEGRATION OF CELLS INTO EPITHELIAL TISSUES .....</b>	<b>6</b>
2.1 PRELIMINARIES.....	6
2.2 FROM INDIVIDUAL CELLS TO ORGANIZED TISSUES .....	8
2.3 EPITHELIAL TISSUES .....	10
2.3 DIFFUSION PATHWAYS IN EPITHELIAL TISSUES.....	12
2.3.1 <i>Transcellular pathway</i> .....	13
2.3.1.1 Cell membrane .....	13
2.3.1.2 Simple passive diffusion .....	15
2.3.1.3 Protein mediated transport.....	16
2.3.1.3.1 Passive transport .....	18
2.3.1.3.2 Active transport.....	19
2.3.2 <i>Paracellular pathway</i> .....	20
2.3.3 <i>Intercellular pathway</i> .....	22
2.4 pH REGULATION .....	25
2.4.1 <i>Short-term mechanisms</i> .....	25
2.4.2 <i>Long-term mechanisms</i> .....	27
<b>CHAPTER 3 .....</b>	<b>29</b>
<b>BACKGROUND INFORMATION FOR MODEL DEVELOPMENT.....</b>	<b>29</b>
3.1 CERVICAL INTRAEPITHELIAL NEOPLASIA.....	29
3.2 STRUCTURE OF NORMAL AND ABNORMAL CERVICAL EPITHELIA.....	30
3.3 TRANSPORT PHENOMENA IN NORMAL AND ABNORMAL CERVICAL EPITHELIA.....	31
3.3.1 <i>Gap Junctions</i> .....	32
3.3.2 <i>Tight Junctions</i> .....	33
3.3.3 <i>Tumor pH</i> .....	34
3.4 INTERPRETATION OF THE TEMPORAL CHARACTERISTICS OF THE AW PHENOMENON - MODEL ASSUMPTIONS .....	35
3.5 TRANSPORT PATHWAYS OF ACETIC ACID IN NORMAL AND ABNORMAL EPITHELIA .....	37
3.7 CORRELATION BETWEEN EPITHELIAL TRANSPORT KINETICS OF ACETIC ACID AND DYNAMIC SCATTERING CHARACTERISTICS OF THE AW PHENOMENON .....	42
<b>CHAPTER 4 .....</b>	<b>45</b>
<b>COMPARTMENTAL MODELLING OF THE CERVICAL EPITHELIUM.....</b>	<b>45</b>
4.1 INTRODUCTION .....	45
4.2 MODEL FORMULATION .....	47
4.2.1 <i>Estimation of epithelial dysplastic layers and of the number of the corresponding compartments (n)</i> .....	47
4.2.2 <i>Acetic acid ionization (<math>J_{ion}</math>)</i> .....	48
4.2.3 <i>Concentration change rates by acetic acid passive diffusion through the cell membrane and tight junction (<math>J_{AA}^m, J_{AA}^{tj}</math>)</i> .....	49
4.2.4 <i>CONCENTRATION CHANGE RATES OF IONIC DIFFUSIONS (<math>J_{H^+}^{tj}, J_{Ac^-}^{tj}, J_{Ac^-}^{tj}</math>)</i> .....	51
4.2.5 <i>Active Proton and Vasculature Flux (<math>J_{H^+}^p, J_{AA}^v, J_{Ac^-}^v, J_{H^+}^v</math>)</i> .....	53
4.3 THE MODEL DIFFERENTIAL EQUATION SYSTEM .....	53
4.4 <i>Model approximation</i> .....	54
4.5 MODEL PARAMETERS.....	56

<b>CHAPTER 5 .....</b>	<b>59</b>
<b>SIMULATION RESULTS.....</b>	<b>59</b>
5.1 MULTISTAGE CIN.....	59
5.2 THE DIFFUSION ROUTES .....	61
5.3 THE BUFFERING EFFECT .....	66
5.4 INITIAL CONCENTRATION.....	67
<b>CHAPTER 6 .....</b>	<b>69</b>
<b>MODEL VALIDATION AND DISCUSSION .....</b>	<b>69</b>
6.1 EXPERIMENTAL SET-UP.....	69
6.2 CLINICAL DATA .....	71
6.3 MODEL VALIDATION .....	72
<b>CONCLUSION – FUTURE WORK.....</b>	<b>78</b>
<b>REFERENCES .....</b>	<b>80</b>
<b>APPENDIX .....</b>	<b>86</b>

## LIST OF FIGURES

---

FIGURE 1 THE CELL AS A FACTORY .....	7
FIGURE 2 PROTEIN FOLDING STAGES: FROM AN 'OPEN' AMINO ACID TO A 3-D STRUCTURE.....	8
FIGURE 3 CELL ADHESION MOLECULES: A) TIGHT JUNCTIONS B) DESMOSOMES .....	9
FIGURE 4 CLASSIFICATION OF EPITHELIA .....	10
FIGURE 5 SECRETION AND ABSORPTION CAN BE EITHER THROUGH MICROVILLIS (A), GLANDS (B) OR DIRECTLY THROUGH THE MEMBRANE (C) .....	11
FIGURE 6 THE EPITHELIAL CELL PRIME JUNCTIONS .....	12
FIGURE 7 TRANSPORT PATHWAYS IN EPITHELIAL TISSUES .....	13
FIGURE 8 DIFFUSION SCHEMES THROUGH THE MEMBRANE'S LIPID MATRIX.....	14
FIGURE 9 COMPOSITION OF THE CELL'S MEMBRANE .....	15
FIGURE 10 THE DISSOLVE-DIFFUSE MECHANISM OF PASSIVE MEMBRANE DIFFUSION .....	15
FIGURE 11 TRANSPORT PROTEINS .....	17
FIGURE 12 PASSIVE TRANSPORT.....	18
FIGURE 13 PRIMARY (A) AND SECONDARY (B) ACTIVE TRANSPORT.....	20
FIGURE 14 EPITHELIAL TIGHT JUNCTIONS .....	21
FIGURE 15 THE GAP JUNCTION PLAQUES CONSISTING OF SEVERAL GAP JUNCTION CHANNELS .....	22
FIGURE 16 THE BALL AND CHAIN GATING PROCEDURE .....	24
FIGURE 17 pH REGULATION PROCEDURES IN RESPONSE TO ACUTE ACID LOADS.....	25
FIGURE 18 THE CERVIX .....	29
FIGURE 19 CERVICAL EPITHELIAL LAYERS.....	30
FIGURE 20 THE STRUCTURE OF THE CERVICAL EPITHELIUM IN NORMAL AND PROGRESSIVE CIN AND INVASION .....	31
FIGURE 21 DIFFUSION PATHWAYS IN NORMAL AND ABNORMAL CERVICAL EPITHELIA.....	31
FIGURE 22 INTENSITY OF THE BACKSCATTERED LIGHT AS MEASURED IN NORMAL AND CIN TISSUES ....	36
FIGURE 23 TIME SEQUENCE OF IMAGES FROM A CERVIX WITH BIOPSY CONFIRMED CLN III. THE IMAGES WERE TAKEN (A) IMMEDIATELY AFTER APPLICATION OF ACETIC ACID, (B) 20 S AFTER, (C) 60 S AFTER, (D) 80 S AFTER, (E) 90 SEC AFTER. ....	37
FIGURE 24 THE LESS THE pH THE LESS THE IONIZATION OF ACETIC ACID .....	39
FIGURE 25 A) AA ENTERS THE ICS AND ECS VIA THE TRANSCELLULAR AND PARACELLULAR PATHWAY RESPECTIVELY AND IONIZES. B) AA AND PROTONS ARE EXTRUDED THROUGH THE MEMBRANE TO THE ECS. BOTH AA AND IONS PERMEATE THE INTERCELLULAR PATHWAY AND THROUGH THE GAP JUNCTIONS TO ADJACENT CYTOPLASMS (METABOLIC COOPERATION). C) THE INTRACELLULAR pH DROP CLOSES GAP JUNCTIONS AND CAUSES CYTOSKELETAL CONTRACTS THAT OPEN THE PARACELLULAR PATHWAY. D) REACHING THE ECS OF A NEOPLASTIC CELL, pH IS DROPPED, IONS RECOMBINE AND AA ENTERS THE ICS.....	41
FIGURE 26 STRUCTURAL CHANGES DURING CIN DEVELOPMENT AS A STACK OF DYSPLASTIC CELL LAYERS.....	45
FIGURE 27 (A) EPITHELIAL COMPARTMENTS AND TRANSPORT FLUXES (B) THE TWO-COMPARTMENT CELL MODEL AND TRANSPORT FLUXES.....	47
FIGURE 28 TWO-COMPARTMENT STEADY STATE PASSIVE DIFFUSION THROUGH A POROUS MEMBRANE ..	50
FIGURE 29 INTRACELLULAR CONCENTRATION PROFILES OF (A) H <sup>+</sup> AND (B) AA IN THE TOTAL EPITHELIAL DYSPLASTIC LAYERS.....	60
FIGURE 30 CONCENTRATION PROFILES OF (A) PROTONS AND (B) IN THE ENTIRE EPITHELIUM (BOLD LINE) AND IN EACH LAYER INDEPENDENTLY (SOFT LINES) .....	62
FIGURE 31 DROPPING THE PARACELLULAR DIFFUSION RATE AND THE EFFECT ON (A) ICS PROTON CONCENTRATION AND (B) ICS AA CONCENTRATION .....	63
FIGURE 32 pH PROFILES IN (A) CIN I (B) CIN II AND (B) CIN III.....	65
FIGURE 33 THE ICS BUFFERING EFFECT ON (A) PROTONS AND (B) AA INTRACELLULAR CONCENTRATIONS .....	67
FIGURE 34 THE ECS BUFFERING EFFECT ON (A) PROTONS AND (B) AA INTRACELLULAR CONCENTRATIONS .....	67

FIGURE 35 THE EFFECT OF THE INITIAL AA CONCENTRATION ON (A) PROTONS AND (B) AA INTRACELLULAR CONCENTRATIONS .....	68
FIGURE 36 EXPERIMENTAL SETUP .....	70
FIGURE 37 (A) POLARIZED IMAGE OF A CERVIX WITH HIGH GRADE CERVICAL NEOPLASIA.....	72
FIGURE 38(A) THE ACETOWHITENING MAP PSEUDOCOLOR IMAGE OVERLAID ONTO THE COLOR IMAGE OF THE CERVIX THE DR VS. TIME CURVES OF .....	73
FIGURE 39 (A)THE INTRACELLULAR CONCENTRATION (M) VS. TIME CURVES FOR 5% AND 3% ACETIC ACID AS PREDICTED BY THE MODEL .....	74
FIGURE 40 (A) INTRACELLULAR CONCENTRATION VS. TIME CURVES CORRESPONDING TO CIN I, CIN II AND CIN III AS PREDICTED BY THE MODEL. THE PEAK CONCENTRATION VALUES ARE PROPORTIONAL WITH THE CIN GRADE. ....	74
FIGURE 41 MODEL PREDICTED ICS PROTON CONCENTRATION VS. TIME CURVES CORRESPONDS TO BOTH CIN III LESIONS AND TO ITS CONSTITUTING EPITHELIAL LAYERS. INTRACELLULAR CONCENTRATION DROPS FAST WITHIN THE UPPER 10 LAYERS. ....	76

# CHAPTER I

## Motivation and objectives

### *1.1 Introduction*

Cervical cancer is a major health care issue. Recent estimates indicate that 493,000 new cases occur every year, while 274,000 women die of cervical cancer annually [1]. The problem of cervical cancer is more pronounced in the developing world where about 83% of all the new cases appear and 85% of all the lethal cervical cancers are recorded. The main cause of cervical cancer is the persistent infection with human papillomavirus (HPV), the most common sexually transmitted infection worldwide, which affects an estimated 50 to 80 percent of sexually active women at least once in their lifetime [2]. Cervical Cancer arises as the rather rare end-point of a series of stages, which begin with a sexually transmitted high risk HPV virus sub-type infection of the cervical epithelium. The infection may progress slowly to the immediate precursor of invasive squamous carcinoma, which is known as Cervical Intraepithelial Neoplasia (CIN) grade I, II, III, Microinvasive and Invasive. Grade II or more severe lesions are characterized as High Grade Squamous Intraepithelial Lesion (HSIL), while grade I or less severe lesions are characterized as Low Grade (LSIL). The discrimination between HSIL and LSIL lesions is very essential for the lesion's management decision-making (immediate treatment or follow-up respectively).

Currently, the standard method for preventing cervical cancer comprises three stages: cytology screening, colposcopic examination and subsequent biopsy sampling for women with abnormal screening results and finally treatment for the precancerous abnormalities [3]. The Cervical smear is the primary screening method for cervical neoplasia and its implementation, mainly in developed countries, has reduced the mortality remarkably. However, the accuracy of this method is limited by both sampling and reading errors, leading to low sensitivity (~0.59) [4-6]. An abnormal cervical smear is followed by referral to colposcopy, which determines the location of the most severe

dysplastic region for biopsy sampling [7, 8]. Colposcopy plays a critical role in the diagnostic chain, since its accuracy in locating and sampling the true positive for disease region determines the reliability of the definitive diagnosis, provided by histology. Colposcopic examination is based on the visual examination of the tissue with the aid of a low magnification microscope (colposcope). In order to highlight abnormal areas, topical application of acetic acid solution 3-5% is routinely used as a contrast agent for more than 70 years. The agent-tissue interaction generates an optical signal, which is perceived as transient tissue whitening. Clinical evidence supports that the degree and duration of the latter is associated with the lesion's grade and the phenomenon is known as acetowhitening (AW) effect. Visual assessment of macroscopic features of diagnostic importance, including the AW pattern, is subjective, qualitative and depends heavily on the visual acuity and training of the examiner. This fact is considered to be the source of significant limitations associated with the traditional colposcopic practice. Colposcopy suffers from low sensitivity (56%), high biopsy sampling error rate and high inter- and intra-observer disagreement in identifying cervical lesions [5, 7, 8].

Research works have provided a novel approach to the problem of non-invasive diagnosis, based on the in vivo quantitative assessment of the dynamic scattering characteristics of the AW effect [9]. In [10] a more elaborate analysis of these characteristics with the aid of dynamic spectral imaging is presented. In [11] and [12] the application of this new method and technology in larynx epithelium and in skin has been demonstrated and the obtained encouraging results highlighted the platform potential of this approach. In a very recent development, this approach has been tested in a multisite clinical trial, conducted in Europe, enrolling 308 women with abnormal pap-test. The presented results [13] showed a significant improvement in sensitivity over both colposcopy (26%) and cytology (20%), at similar specificity levels, highlighting the clinical potential of this new approach.

Nowadays, the scientific interest on AW-based diagnostic tests has been increased remarkably and its potential as an alternative screening tool is under intensive investigation. The interest has been attracted due to the fact

that acetic acid is a biomarker of very low cost, it is routinely used with no side effects and physicians have been trained to interpret AW patterns. Developing countries are seeking for alternative cost-effective solutions for diagnosis and screening, because they cannot afford to implement and maintain cytology-based primary screening methods. Very recently, the results from a large clinical study investigating the performance of the Visual Inspection with Acetic acid (VIA), have been published [14]. According to this publication, approximately 50,000 women have been enrolled in the study and a reduction in cervical cancer incidence by 30% has been observed in the group examined with VIA, compared with the control group attending the established diagnostic chain (cytology, colposcopy, histology). Despite this remarkable success, the problems of subjectivity and lack of reproducibility, associated with VIA, remain the major restricting factor for its clinical adoption [14].

Although there is an age long accumulated experience in the clinical use of the AW test and there are strong evidences that it could improve the performance of in-vivo diagnosis through quantitative assessment of its optical characteristics, surprisingly limited knowledge exists regarding the actual biophysical mechanism involved in the generation of the AW effect. This may be attributed to the fact that the latter is a result of a series of complex biological processes, involving both the structural and functional characteristics of the total epithelium. Furthermore, it is well understood that especially the functional characteristics of the epithelium cannot be fully reproduced and assessed with in vitro experiments. Experiments referring to cell cultures have improved our knowledge in the field and particularly in rooting out the cell nucleus as the location where AW effect occurs [15, 16]. Nevertheless, no systematic approach exists thus far towards the understanding and the identification of the biological factors affecting the dynamic optical characteristics of AW phenomenon. It is very essential to identify the biological factors that are affected by neoplasia development and are affecting the AW dynamic optical characteristics. By establishing such a correlation, the in vivo quantitative assessment of the latter would provide quantitative indices expressing disease-specific microstructural and functional alterations.

In this thesis, we attempt to explain the biophysical basis of the AW effect, emphasizing to the epithelial transport phenomena associated with the effect. On the basis of these explanations we have developed a biophysical model for predicting the AW dynamic characteristics in normal and pathologic conditions. Finally, we compare model predictions with experimental data and discuss our findings.

### ***1.1 Chapters summary***

The purpose of the current model is the early and reliable diagnosis of precancerous/dysplastic lesions using an *in-vivo* biophysical mathematical model. Here, we present the steps from which we were guided through in order to achieve such an enterprise.

In chapter 2 we provide the elementary knowledge the reader should acquire concerning the biophysics of an epithelial tissue. We begin by giving the aspects of evolution from a single cell to an organized tissue. Then we introduce the term of diffusion and analyze the different pathways of a solute penetrating an epithelial tissue. Ending, we present the biochemical theory of pH regulation and buffering, which may be the outmost crucial cellular mechanisms.

The main concern in chapter 3 is to pass through a more elaborate analysis over the cervical epithelial tissue. Transferring the knowledge acquired in chapter 2 we give the structural and functional characteristics of the cervical epithelium. We relate these characteristics with literature reports on cervical intraepithelial neoplasia and provide a short analysis of the changes exhibited. We then develop a theory over the kinetics of acetic acid in the dysplastic epithelium and adjoin its ionization with the corresponding pH drop and the acetowhitening phenomenon.

The core information of the mathematical model is given in chapter 4. There, we break down the acetic acid diffusion into unidirectional fluxes and introduce the basis of our compartmental modelling. Afterwards, we begin by supplying the reader with the appropriate differential equations of every

epithelial flux mentioned earlier. Then we combine these fluxes according the mass action laws producing a differential system that serves our method. Finally we accommodate the qualitative and quantitative analysis of the model's parameters which were used for the systems solution.

In chapter 5 we give the simulation results of the proposed model. We begin with picturing the model's main output which is the concentration profiles of both acetic acid and  $H^+$ . Then we try to interpret the effect of the model's parameters on these profiles and their physiological meaning.

In chapter 6 we put the model's validation. We begin by showing the instrumentation and clinical data taken from a series of gynecological examinations. After, we counterpoise the model's output and the experimental results. The remarkable results are then discussed trying to provide the reader with the potentials of the current screening method.

Finally, in chapter 7 we conclude our approach and outline the important adjustments of the current technique. We describe the problems that motivate our next steps towards the system's accuracy in terms of specificity and sensitivity according to our present analysis.

# CHAPTER II

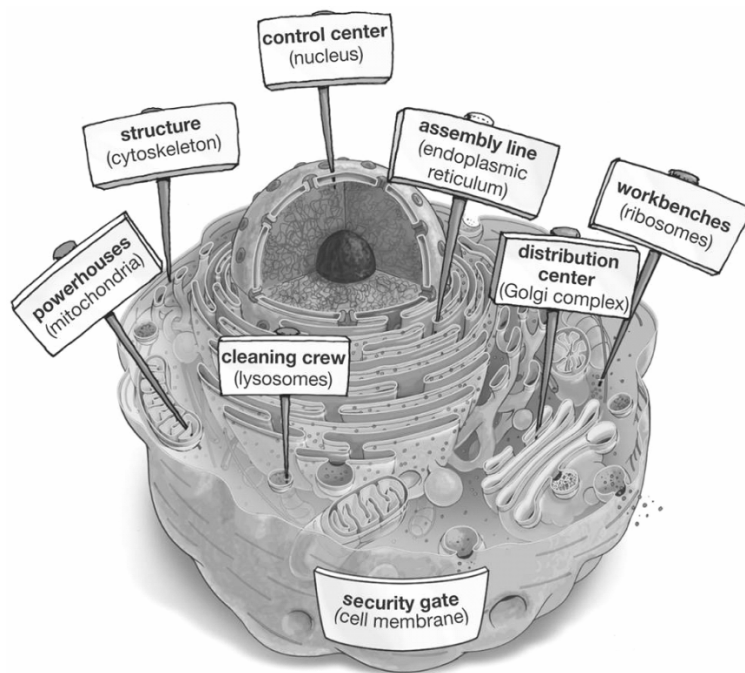
## Integration of cells into epithelial tissues

### *2.1 Preliminaries*

The cell is the structural and functional unit of all known living organisms. It is the simplest unit of an organism that is classified as living, and is sometimes called the building block of life. Development begins with the fertilized egg cell dividing into two, four, then eight cells, forming the very early embryo. Continued cell proliferation and then differentiation into distinct cell types gives rise to every tissue in the body. Cells differ in contents, shape, size, color, mobility, and surface composition. To create the human body cells must be properly arranged and organized into tissues, organs, and appendages. In addition, many cells exhibit distinct functional and/or structural asymmetries, a property often called polarity. From such polarized cells arise asymmetric, polarized tissues such as the lining of the intestines and structures like hands and hearts.

Cells can be divided into two basic components: the nucleus and the cytoplasm. The former contains most of the cell's genetic material, organized as multiple long linear DNA molecules in complex with a large variety of proteins, to form chromosomes. The latter comprises of all cell contents, but not the nucleus. The cytoplasm contains membrane bound intracellular organelles and is delimited by the plasma membrane.

In sort, mitochondria produce the chemical energy the cell needs. The Golgi complex is a stack of levelled membrane substances that accepts and differentiates, chemically, molecules that arise in the endoplasmic network which are to be extruded from cell's membrane. Lysosomes are responsible for the intracellular digestion and ribosomes are responsible for synthesizing the proteins used by the cell. Figure 1 depicts these cell functions provided by the cellular structures.



Copyright © 2005 Pearson Prentice Hall, Inc.

**Figure 1 The cell as a factory**

Generally, all cellular functions emanate from proteins. Proteins work as enzymes catalyzing reactions, as structures and regulators, as molecular machines for power and movement and organize the cell's defence and signalling. In sort, proteins are amino acid polymers connected through a long chain which is folded in a 3-dimensional structure after a sequence of conformational stages, unique for each protein (figure 2). The peptide bond is responsible for protein folding as it has the potentiality of "bending" itself. In the wide sense, the term "protein folding" includes structural, thermodynamic and kinetic aspects of transition of initially unfolded protein chain into its final native 3D structure, as well as structural transitions and dynamics of this structure in a working protein [17]. Such phenomenon is produced by chemical reactions (e.g. due to the hydrophilic and hydrophobic attribute of chemical combinations), violation of the systems' entropy (e.g. temperature) or other physical conditions (e.g. electrical, changes in pH) surrounding the protein. As a result protein properties change through denaturation.

In conclusion, the cell is the cornerstone of every living organism. Structures called organelles house cell functions producing nutrients, preserving the homeostasis and removing hazardous elements. Foremost important

organelle is the nucleus, controlling and designating cell's activities. Proteins serve as the intermediate of every cell function and their unique conformation is essential for their identification and differentiation. All these are enclosed by a plasma membrane protecting the inner environment from unwanted external stimuli.

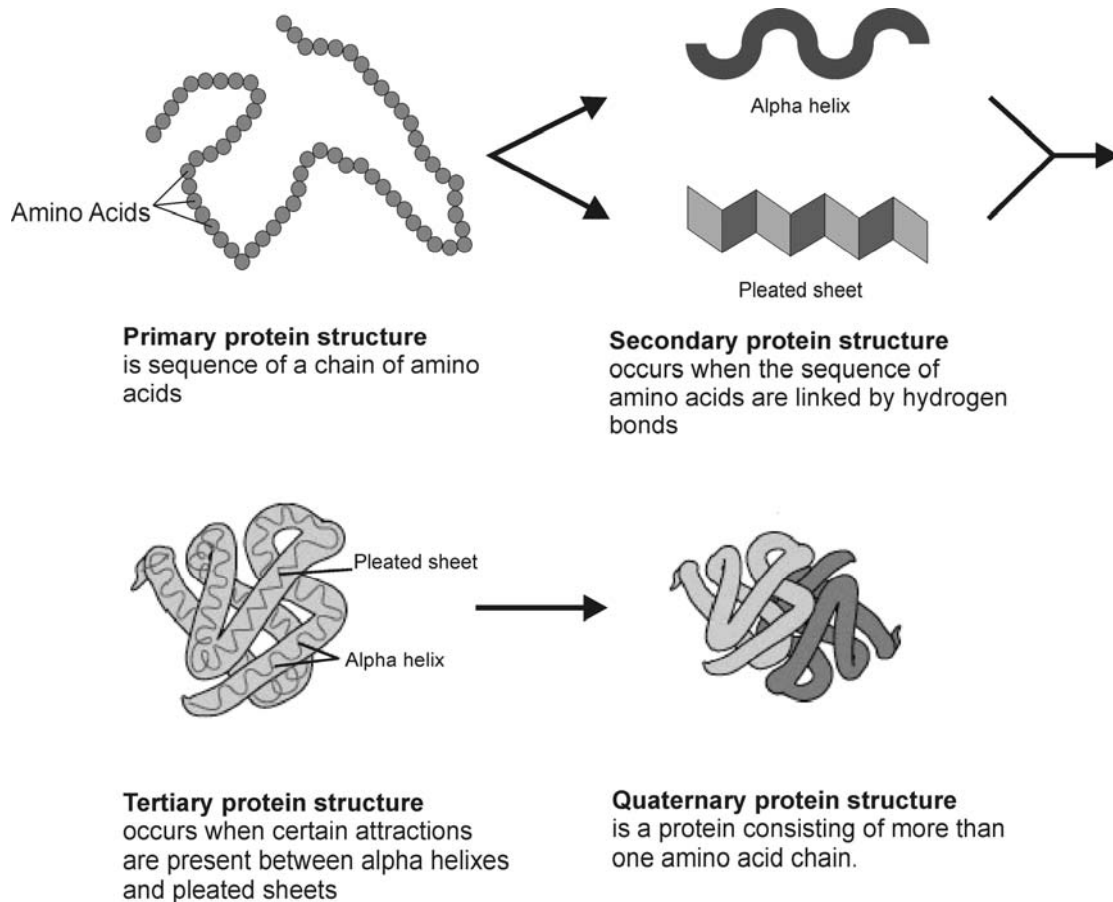


**Figure 2 Protein folding stages: from an 'open' amino acid to a 3-D structure**

## ***2.2 From individual cells to organized tissues***

In the development of complex multicellular organisms such as animals, progenitor cells differentiate into distinct “types” that have characteristic compositions, structures, and functions. Cells of a given type often aggregate into a tissue to cooperatively perform a common function, i.e. muscle contracts. Equally, they organize into an organ. For instance, the muscle valves and blood vessels of a heart cooperate to pump blood through the body. The coordinated functioning of many types of cells within tissues, as

well as of multiple specialized tissues, permits the organism as a whole to move, metabolize, reproduce, and carry out other essential activities.

Despite their diverse forms and functions, all animal cells can be classified as being components of just five main classes of tissue: epithelial tissue, connective tissue, muscular tissue, nervous tissue, and blood. Various cell types are arranged in precise patterns of staggering complexity to generate the different tissues and organs. This assembly of distinct tissues and their organization into organs are determined by molecular interactions at the cellular level and would not be possible without the temporally and spatially regulated expression of a wide array of adhesive molecules as depicted in (figure 3).

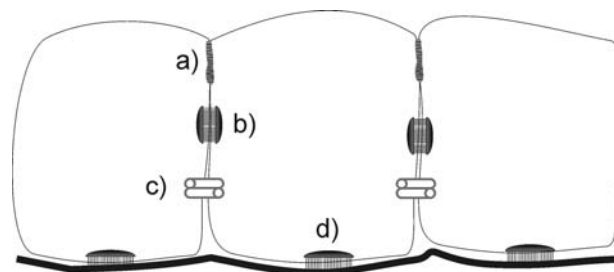


**Figure 3 Cell adhesion molecules: a) Tight junctions b) Desmosomes  
c) Gap junctions d) Hemidesmosomes**

As it will be described shortly, cells in tissues can adhere directly to one another through specialized integral membrane proteins called cell-adhesion molecules that often cluster into specialized cell junctions. In addition, cells in animal tissues also adhere indirectly through the binding of adhesion receptors in the plasma membrane to components of the surrounding extracellular matrix. These two basic types of interactions not only allow cells to aggregate into distinct tissues but also provide a means for the bidirectional transfer of information between the exterior and the interior of cells.

In this thesis we are interested in exploring the structure and function of epithelia, which will be extensively described, while their cell-cell interactions will provide us with the background to mathematically model their biophysical transport processes.

## 2.3 Epithelial tissues

Epithelia are tissues lining cavities and tubes, covering exposed surfaces of the body. They comprise of firmly coherent cells with minimal interval. One surface of the epithelium is exposed to the lumen and the other usually rests on a basement membrane (basal lamina) as depicted in figure 4a. Thus, they function as interfaces between different biological compartments. As such, they mediate a wide range of activities such as selective diffusion, absorption and/or secretion, physical protection and containment. They are classified according to their cellular shape, number of cell layers, cilia coating and keratin containment. The basal lamina, a thin fibrous network of collagen and other extracellular matrix components, supports all epithelia and connects them to the underlying connective tissue. Adding, epithelial tissues are usually polarized keeping basal and apical cellular surfaces structurally and functionally different exhibiting distinctive characteristics.

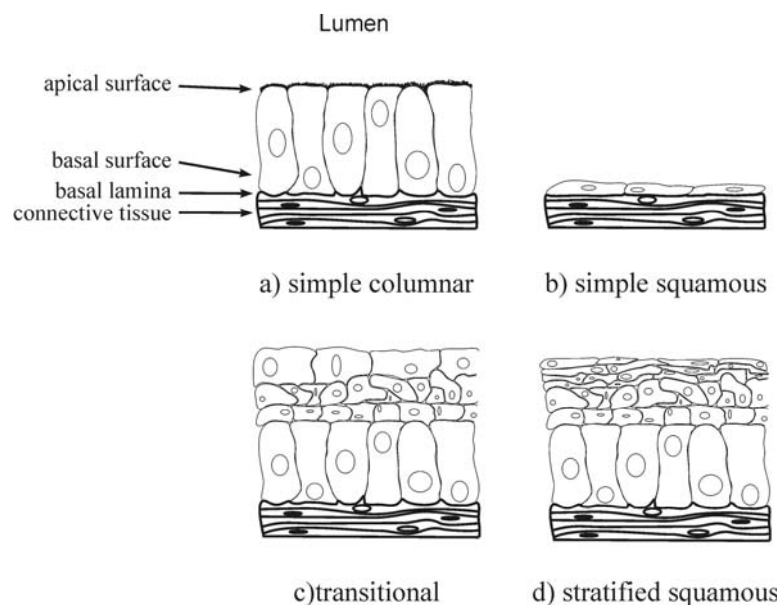


**Figure 4 Classification of epithelia**

According to figure 4 epithelia can be classified into four categories:

*Simple columnar* epithelia consist of elongated cells, including mucus-secreting cells (in the lining of the stomach and cervical tract) and absorptive cells (in the lining of the small intestine).

*Simple squamous* epithelia, composed of thin cells, line the blood vessels (endothelial cells/endothelium) and many body cavities.

*Transitional* epithelia, composed of several layers of cells with different shapes, line certain cavities subject to expansion and contraction (e.g., the urinary bladder).

*Stratified squamous* (nonkeratinized) epithelia line surfaces such as the mouth and vagina; these linings resist abrasion and generally do not participate in the absorption or secretion of materials into or out of the cavity.

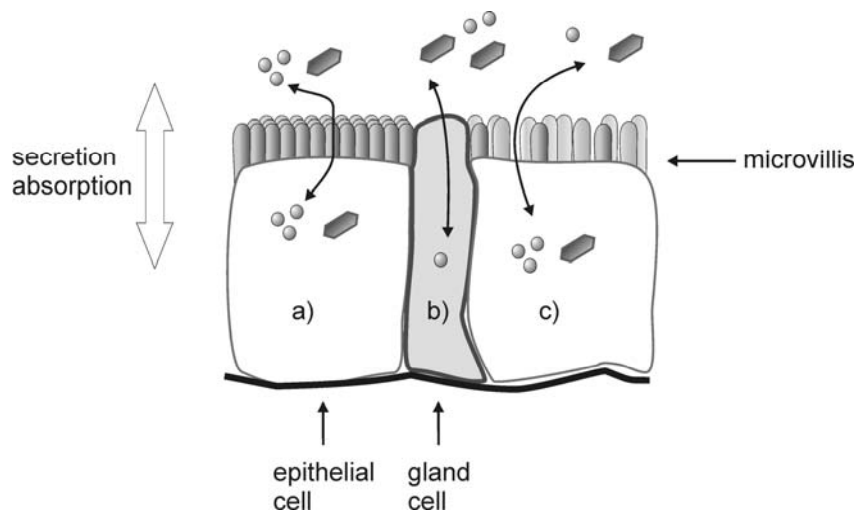


**Figure 5** Secretion and absorption can be either through microvillis (a), glands (b) or directly through the membrane (c)

Secretion and absorption of nutrients is carried through microvillis, glands or direct transmembrane communication as shown in figure 5. Microvillis are leaf-like formation lined over the outmost cell layers of most epithelia acting as a toll bridge between the lumen and the tissue. Glands are cells specialized for secretion of a specific substance or substances. In epithelia, glands are usually embedded, occurring as isolated cells containing the secretion, or as layer of cells surrounding interstitial space (secretory cavity or canal) into which secretion is discharged.

In conclusion, the epithelia are a diverse group of tissues which, with rare exceptions, cover or line all body surfaces. They protect and mediate absorption, secretion and communication; abilities that are essential for the physiological operation of the body's biological mechanisms.

### 2.3 Diffusion Pathways in Epithelial Tissues

Epithelial transport can be active or passive. Passive allows solute diffusion down its chemical concentration gradient spending no metabolic energy. It is achieved through random thermal motion of suspended or dissolved molecules moving from an area of higher to lower concentration. On the other hand, active is the transport mode that is not only independent, but may also operate against extreme concentration gradients fuelled by ATP<sup>1</sup> hydrolysis.

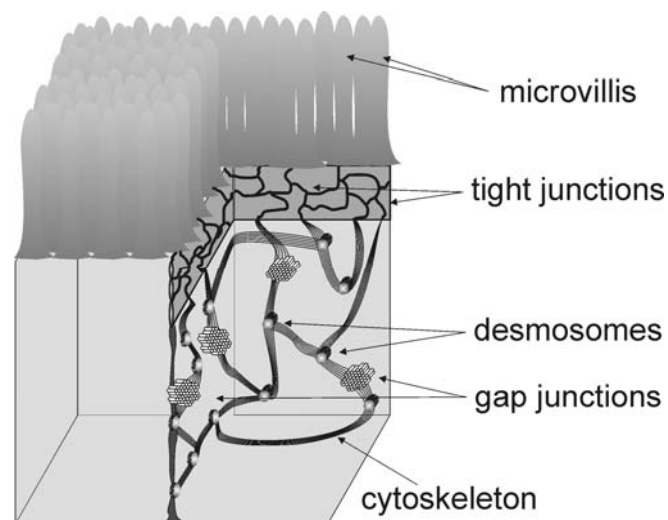


**Figure 6 The epithelial cell prime junctions**

Aforementioned, in order to function in an integrated manner, individual cells composing epithelia and other organized tissues must adhere to one another and to the surrounding extracellular matrix. Through this epithelia are able to control the movement of ions and small molecules between them. Adherence is established using certain types of protein structures called junctions. Prime junctions are the desmosomes, the tight and the gap junctions (figure 6).

Tight junctions and desmosomes assemble harmonically the cytoskeletons off nearby cells. The former clasp the apical surfaces of cells while the latter connect the rest of the cells' bodies. The gap junctions, on the other hand, are responsible for the interconnection of cells. They exchange nutrients and second messengers through neighbouring cytoplasm promoting intercellular communication [18].

---

<sup>1</sup> Adenosine 5'-triphosphate (ATP) is a multifunctional nucleotide that is most important in intracellular energy transfer. In this role, ATP transports chemical energy within cells for metabolism.

In general, these conformations play a critical role in controlling the movement of ions and small molecules in epithelia. During physiological circumstances, molecules penetrating epithelial barriers may diffuse, either actively or passively, via the transcellular (microvillus and/or cell's membrane), paracellular (tight junctions) or intercellular (gap junctions) pathway before they are consumed or canalized in the vasculature (figure 7).

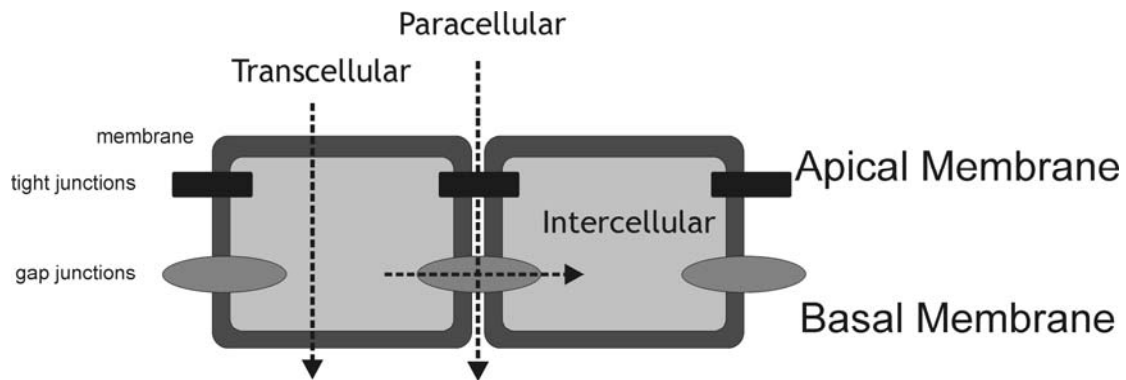


Figure 7 Transport pathways in epithelial tissues

### 2.3.1 Transcellular pathway

Transcellular is the pathway of solutes trafficking directly through the membrane into the cell's cytoplasm. It is classified in simple passive diffusion and protein mediated transport (passive or active) oftentimes abetted through microvillus [19]. This is the main absorptive pathway for epithelia that lack microvillus at the apical surface and all intra-extra lumen transport is managed through the uppermost membrane. Figure 8 depicts the classification of such mechanisms which will be shortly investigated.

#### 2.3.1.1 Cell membrane

The plasma membrane encloses the cell. It functions as a physical barrier, regulates the exchange with the environment, supports the communication between the cell and its environment and conduces to structural support. The cellular membrane is comprised of cholesterol, proteins and lipids which are positioned in a bilayeral mode as depicted in figure 9. These lipids, called

phospholipids, comprise of a glycerol backbone, two fatty acids and a phosphate group, having polar heads and non-polar tails. The phospholipid membrane is partitioned into two residues, namely the hydrophilic and hydrophobic. The former lies on the “outside” whereas the latter on the “inside” of the cytoplasm. These lipids are distributed unequally across the bilayer and their composition influences the physical properties of membranes.

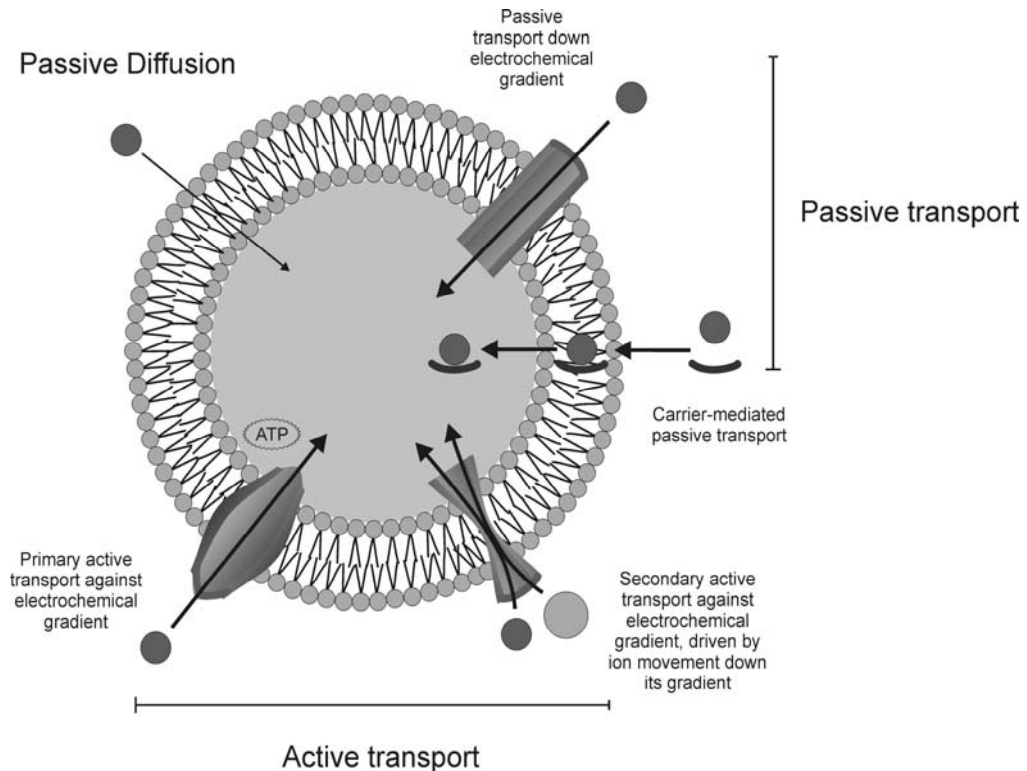


**Figure 8 Diffusion schemes through the membrane's lipid matrix**

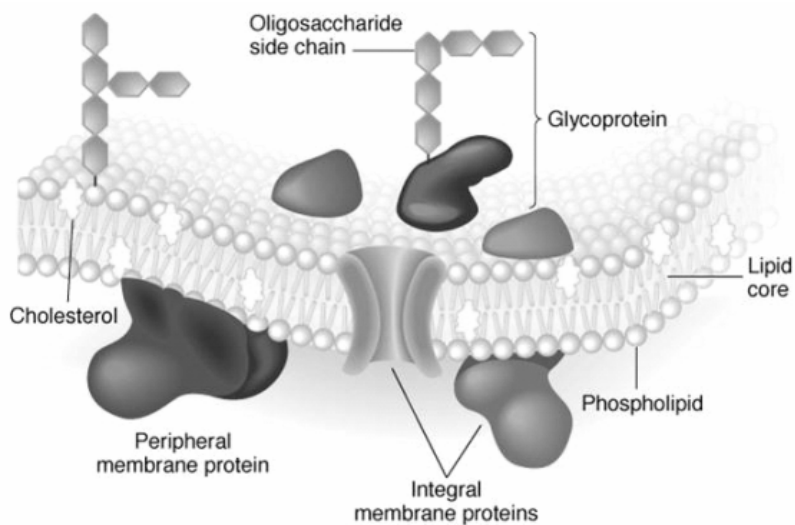


Figure 9 Composition of the cell's membrane

### 2.3.1.2 Simple passive diffusion

In simple passive diffusion solutes traverse solely and passively through the lipoidal matrix. As a rule, it is allowed only for a small amount of molecules such as gases and small uncharged solutes ( $O_2$ ,  $CO_2$ , acetic acid, etc.). *Fluidity* refers to the ease of motion of the phospholipid molecules in a membrane. Keeping in mind the membrane structure discussed earlier, its fluidity depends on four sectors; the phospholipid molecules, which are capable of moving freely with respect to each other, the degree of chemical saturation of the hydrocarbons in the lipid tails, the relative cholesterol content in the lipid bilayer and the temperature. On the other hand, the term *permeability* is used when referring to the passively diffusing molecule. It is proportional to the membrane's hydrophobicity and size, and concentration gradients between the intracellular and extracellular space [20].

The first to suggest that only the undissociated molecules are permeant through a lipid bilayer was Overton [20]. Since then, passive diffusion and modelling of the lipid bilayer has been the study of a variety of groups [21-26]. The prevailing solubility – diffusion model relates a given solute's permeability coefficient to its ability to dissolve into and then diffuse across the lipoidal membrane interior (figure 10) [25].

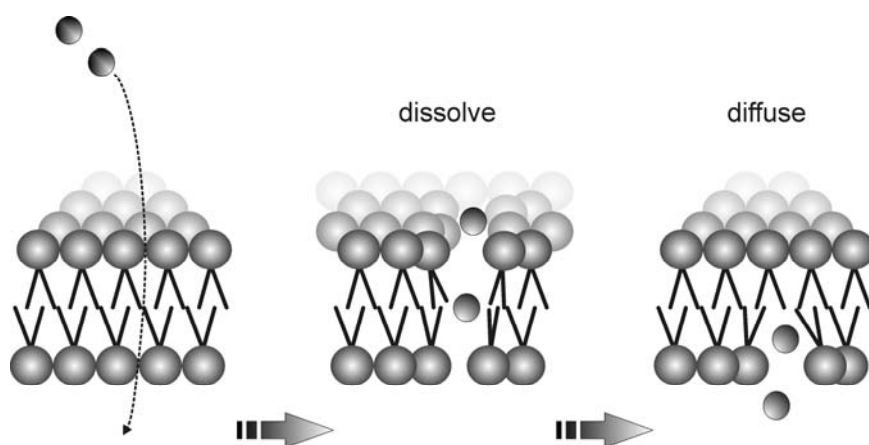
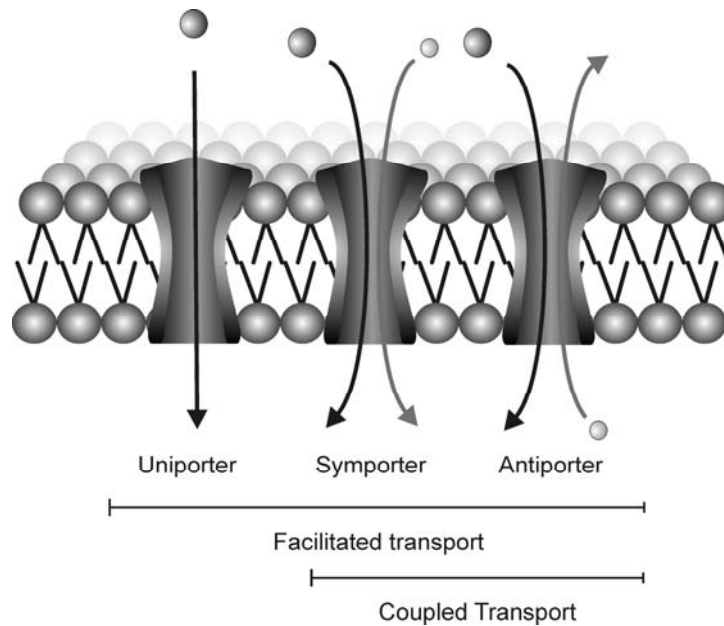


Figure 10 The dissolve-diffuse mechanism of passive membrane diffusion

However, this kind of modelling is oversimplified as it takes no consideration in the distribution of the lipids within the membrane, the temperature dependence, the pressure balance, lipoidal chain length, cholesterol concentration, partition coefficients etc [22, 27, 28]. Chain ordering which can be characterized by both segmental order parameters and bilayer surface density, is a major determinant of molecular transport across liquid-crystalline bilayers [22]. Thus, a correction of the solubility diffusion theory is brought on due to the misbalanced distribution of phospholipids across the liquid bilayer membrane [23]. Thereupon, the permeability coefficient is calculated by the equation:  $P_m = fP_0$ , where  $P_m$  is the observed permeability coefficient,  $P_0$  the coefficient predicted from bulk solubility-diffusion theory and  $f$  a constant.

### ***2.3.1.3 Protein mediated transport***

It is clear that the passive diffusion cannot describe the transcellular diffusion of molecules alone. By the time only small molecules have the ability of such diffusion it is essential to investigate the supplemental mechanisms that contribute in the solute trafficking between the intracellular and the extracellular space. That is the case; transmembrane transport proteins supply such a critical function. Membrane proteins protrude the lipoidal matrix implementing cellular communication with the external environment being responsible for a diversity of mechanisms [29].



**Figure 11 Transport proteins**

Transport proteins are either uniports (taking one solute type one way), symports (transport of one solute depends upon simultaneous carriage of another in the same direction) or antiports (carriage of one solute into the cell depends upon simultaneous transport of another out of the cell (figure 11)).

Transport proteins are also discerned in extrinsic and intrinsic. The former are peripheral membrane proteins that attach loosely to the polar regions of phospholipids, associate with the membrane's surface by electrostatic interactions and are easily removed from the membrane. The latter are integral membrane proteins tightly bound into the lipid bilayer, are difficult to remove from the membrane and can serve as transporters, membrane-linked enzymes, receptors or structural support. These intrinsic membrane proteins, mediate the passive or active transport of a solute. They appear either to traverse the membrane or be part of a structure which does. Reversible allosteric changes in a protein are probably responsible for the carriage, and for actively transported molecules these conformational changes are in part linked to ATP hydrolysis. Here it should be noted that all protein-mediated transported molecules demonstrate specificity, competition and saturation during their diffusion.

### 2.3.1.3.1 *Passive transport*

Passive membrane transport consists of facilitated diffusion and carrier mediated diffusion (uniport). Facilitated diffusion is the movement of molecules or water that depends on their electrochemical gradient through the hydrophilic passageways formed by channel proteins (figure 12a). Each channel protein transports only a single species of molecules or a single group of closely related molecules (e.g. ion channels). Therefore, selectivity is determined by the pore's size and/or charges lining the inside of the channel.

There exist two types of channel proteins that permit passive transport, the open and the gated channel proteins. The former spend most of time in an open state and are scarcely regulated. The latter spend most of time in a closed state and opening is induced by a conformational change such as voltage, chemical gradient or mechanical stress. Generally, protein subverted transport is limited by the degree of saturation of the carrier protein and the number of carrier proteins on the membrane.

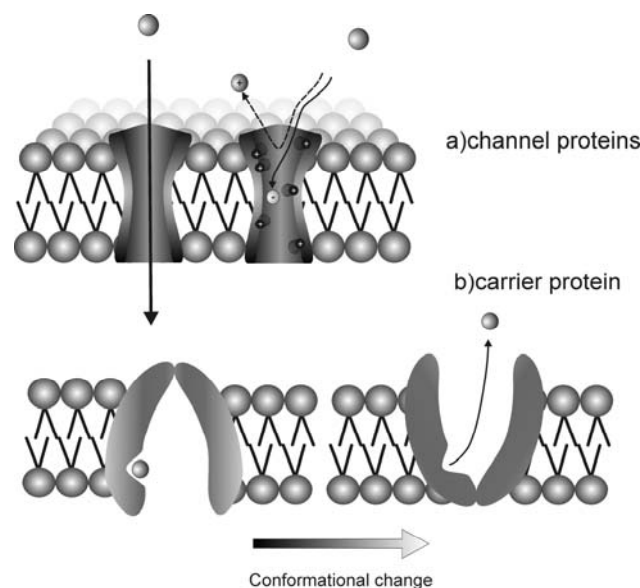


**Figure 12 Passive transport**

On the other hand, the carrier-mediated passive transport is a diffusion mode that uses a carrier molecule or protein (permease) to bind with the transported solute, assisting in its transport across cell membranes without being

permanently altered in the process (figure 12b) (i.e. ions bind specifically and reversibly).

### ***2.3.1.3.2 Active transport***

Active transport is of utmost importance as it keeps the cell under physiological conditions. The most important mechanism is the preservation of cytoplasmic composition in ions such as  $H^+$ ,  $Na^+$ ,  $Cl^-$ ,  $K^+$  and  $Ca^{+2}$  and the diffusion of macro-molecules that cannot diffuse passively. There are two types of active transport, the primary and the secondary active transport. Both move molecules against their concentration gradient through a channel protein, as in passive transport, and are blocked by specific inhibitors.

Primary active transport is the energy-dependent carriage that utilizes the ATP hydrolysis in opposition to chemical or electrochemical gradients (figure 13a). Transmembrane proteins, called ion pumps, exchange solutes between the endoplasmic and exoplasmic reticulum driven, initially, by electrical and osmotic gradients. The hydrolysis of ATP causes a conformational change in the carrier protein and then releases the substance on the other side of the membrane. Examples of primary active transporters are the  $Na^+K^+$ -ATPase (pump) that maintains gradient of  $Na^+$  and  $K^+$  across the cell membrane and is important for cell volume control, the  $Ca^{2+}$ -ATPase, the  $H^+$ -ATPase and the  $H^+K^+$ -ATPase.

On the other hand, secondary active transporters do not directly utilize ATP and energy to move molecules against their concentration gradient is derived from the potential energy stored in the concentration gradient (figure 13b). Secondary active transporters are the sodium and non-sodium dependent transporters, i.e. the sodium dependent symporters ( $Na^+$ -glucose,  $Na^+$ -amino acids,  $Na^+K^+2Cl^-$ ,  $Na^+$ -bile salts,  $Na^+$ -choline uptake,  $Na^+$ -neurotransmitter uptake) and antiporters ( $Na^+H^+$ ,  $Na^+Ca^{2+}$ , Nonsodium-dependent transporters) and the non-sodium dependent antiporters ( $HCO_3^-Cl^-$ ,  $H^+K^+$ ).

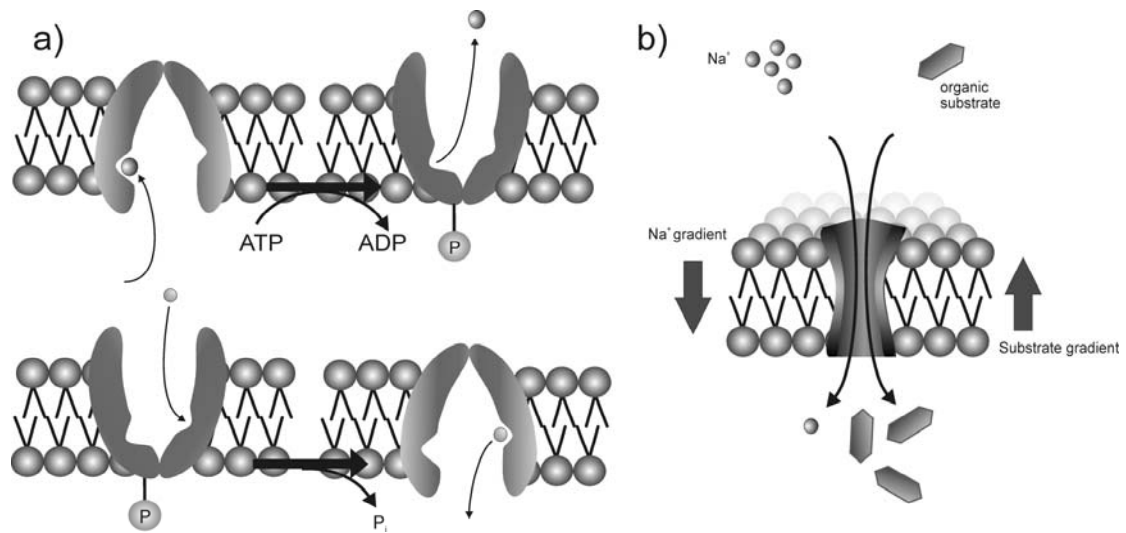


Figure 13 Primary (a) and secondary (b) active transport

### 2.3.2 Paracellular pathway

The paracellular pathway is delimited by the tight junctions and lipid membranes of adjacent epithelial cells of the latter interspace (figure 14). The principal integral proteins found in tight junctions are the adherin, occludin, claudin and cadherin. All, are bound to the cytoskeleton via actin and myosin, contributing in cellular kinetics [30]. They perform two vital functions: 1) they prevent the passage of molecules and ions through the interstitium and 2) they block the movement of integral membrane proteins between the apical and basolateral surfaces of the cell. Tight junctions are responsible for the maintenance of tissue's architecture and cohesiveness, besides desmosomes. They open and close under certain physiological stimuli [31, 32]. Therefore, the affiliation administered, acts as a gate which controls the diffusion along the paracellular pathway and also as a fence that produces a morphological boundary for lipids, keeping the tissue polarized [33-35].

Tight junctions comprise of a network of anastomosing strands, constructing small regions analogous to pores 4.9-7 Å in diameter (sometimes 15 Å) [35, 36] (figure 14). These pores are oriented parallel to the plasma membrane (tortuosity = 1) arranged, however, in an irregular network [35, 37, 38].

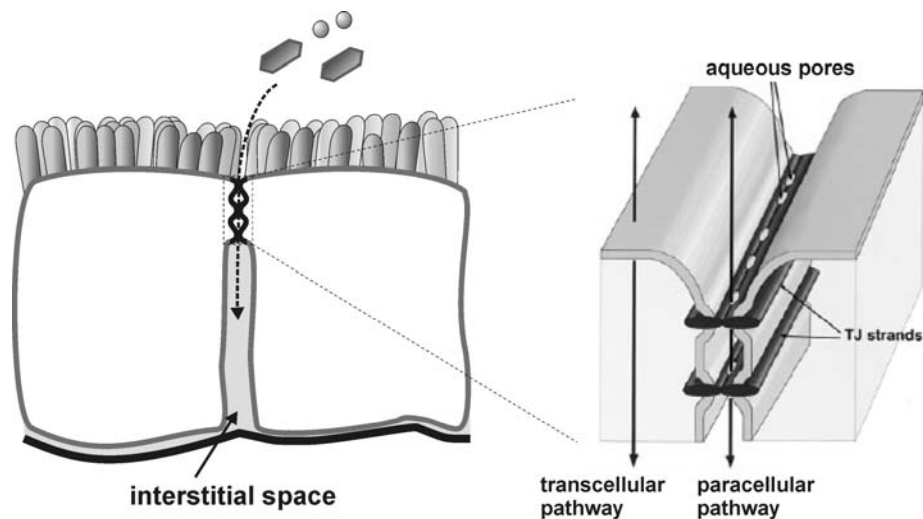


Figure 14 Epithelial tight junctions

Movement of fluid and solutes in the paracellular pathway has long been considered passive. Paracellular diffusion is mainly in response to transepithelial hydrostatic gradients or in compensation to ion or osmotic gradients created by active cellular ion transport [39]. Tight junctions have been found to share the biophysical properties of ion channels, including size and charge selectivity, dependence on ion concentration, pH, extracellular  $\text{Ca}^{+2}$ , as well as the presence of ionic competition [36-41].

The selectivity of the paracellular barrier varies from one epithelial tissue to another and different stimuli or manipulations can result in opposite effects on the permeability of ions and tracers. This type of tight junctional selectivity and restriction to paracellular diffusion of ions and hydrophilic non-ionic tracers is due to junctional potentials and concentration gradients.

In general, resistance is proportional to pore and solute size (mostly), number of strands (junctional tightness) and the probability of finding a pore in open or closed state [32, 38, 42]. However, a discrimination between cations and anions exists and resistance may vary by  $10^5$ -fold along the spectrum of the so-called tight to leaky epithelia. Besides, there is an abstruse paradox [32]. Assuming that junctional resistance is proportional to pore size the respective electrical should increase accordingly. Accordingly, the corresponding uncharged molecular flux should decrease. However there is a frequent junctional dissociation keeping this flux unaffected. Therefore, the barrier is

thought to be dynamic by the time electrical resistance can change without affecting flux of uncharged molecules [31].

Experiments on the subject revealed that the tight junction strands were occasionally broken and annealed [31]. That is the case; pore's diameter may change significantly according to environmental stimuli [43]. Adding up, specific measurements, *in vitro*, presented that luminal to subluminal movement rate remains constant for every hydrostatic condition whereas subluminal to luminal changes accordingly [39].

### 2.3.3 Intercellular pathway

Epithelial cells are known to be communicating directly between their cytoplasms sharing vital resources and signals. This intercellular pathway accommodates the direct communication between cytoplasms of neighbouring cell interiors via gap junctions. This allows cells to share nutrients, exchange information, grow and differentiate.

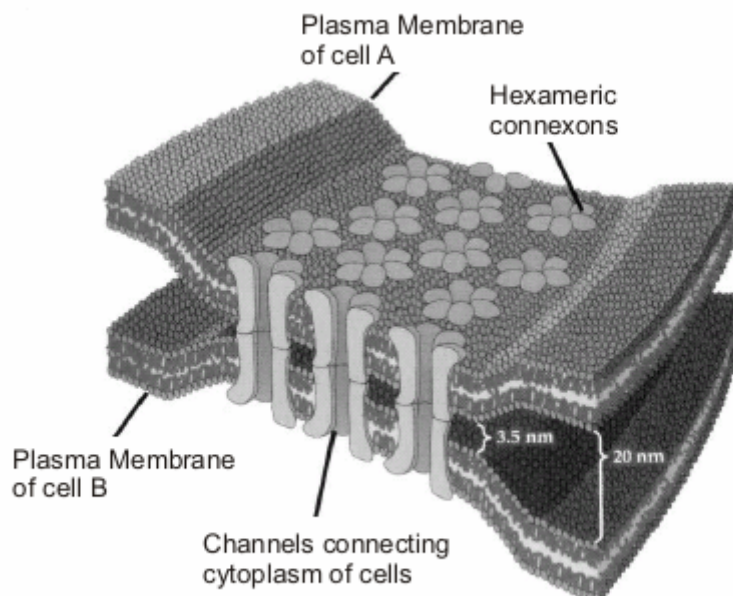


**Figure 15** The gap junction plaques consisting of several gap junction channels

Gap junction channels are leakproof formations and are located perpendicular to the membrane's axis, allowing structural continuity between adjacent cells

(figure 15) [18, 44]. They are formed by the protein family of connexins and are discerned by the protein's molecular weight [18, 45-49]. They are not stand alone intercellular passageways. A gap junction communication bus numerates approximately  $10^6$  channels. Connexins, formed at the Golgi apparatus, are transported through the cytoskeleton to gap junction plaques [48, 49]. There, numerous gap junctions are situated between adjacent cell membranes creating the gap junction bus.

Structural analysis of a gap junction revealed an 80-100Å in length protein junctional unit between adjacent cytoplasms with a 14-16Å hydrophilic pore diameter (they have water in their core). The size selectivity of these junctional units (in MW) ranges from 0,3 to approximately 1-1,5 KDa solutes and movement is granted through chemical or electrical potentials, allowing passive movement of ions and hydrophilic molecules [50, 51].

The intercellular pathway supports the integration of the metabolic activities of all cells in a tissue (metabolic cooperation) by allowing the direct passage of ions and small molecules from the cytosol of one cell to that of another [18, 46, 47]. Quantitative data [51-55] shows that passive electrodiffusion of ions and hydrophilic molecules at the gap junctions is a controversial subject. Permeability is not only proportional to solute and junction sizes, but also to the charges of either diffusion participants and the expression of connexins found. In contrast, qualitative data has not been established except for molecules with small MW for which the selectivity does not fluctuate significantly [53-55].

This structural and functional continuity of adjacent cells is uncoupled by cytoplasmic and junctional ionic composition, transjunctional voltage and phosphorylation. Gap junctions, just like ion channels are gated: they can undergo a reversible conformational change that closes or opens the channel in response to changes in the cell. Sensitivity (open or closed junctional pathway) emanates from intracellular calcium, calmodulin<sup>2</sup> and pH. The relation of gap junction permeability is linear and almost spontaneous with

---

<sup>2</sup> Calmodulin (CaM) is a ubiquitous, calcium-binding protein that can bind to and regulate a multitude of different protein targets, thereby affecting many different cellular functions, such as inflammation, metabolism, apoptosis, muscle contraction, intracellular movement, short-term and long-term memory, nerve growth and the immune response.

calcium concentration permutation, mediated by calmodulin's concentration. Dependence of gap junction permeability over pH fluctuation is modelled by the ball – and – chain model of voltage gating, with connexin's carboxyl terminal acting as the ball and the terminal tail as the chain (figure 16). In contrast, junctional conductance is indirectly related with pH, as intracellular rise of  $H^+$  may suggest increase in  $Ca^{+2}$  via cellular mechanisms. In vitro this mechanism exhibits a second time scale hysteresis with changes in internal pH. Thus, a cell with prolonged low pH, i.e. malfunction in pH regulation mechanisms, quits metabolic cooperation.

There have been many groups investigating the behaviour of gap junctions in response to pH fluctuations. In [56], it is also suggested that maintenance of low intracellular pH induces greater resistance and gap junctions tend to close with deficient pH regulation. Other experiments implied, that chemical gating triggers slow but complete gap junction closure, while voltage sensitive gating triggers fast but incomplete closure [57-59]. Furthermore, slow perfusion of acidification delivers greater junction resistance, whereas fast, lower. Anywise, the recovery of the junction's conductivity doesn't differ in rate.

All these findings further validate that acute acidification would provoke the gap junctions' closure. This seems to work as a protective mechanism, in order to avoid the possible spread of the potential impairment.

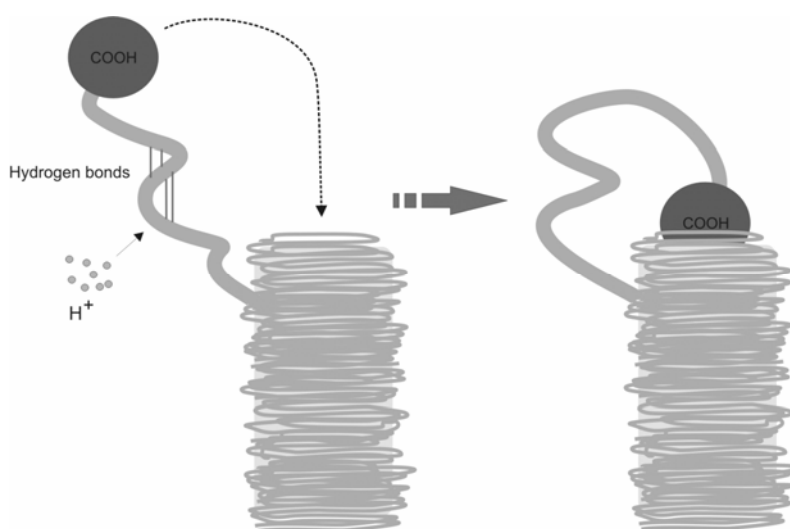


**Figure 16 The ball and chain gating procedure**

## 2.4 pH regulation

Tissue pH is physically regulated by biological and chemical mechanisms. Such are, as alluded to above, passive and active transport through cells, extrusion to the blood circulation system, metabolic cooperation through the gap junctions and physicochemical buffering. Intracellular pH maintenance near neutrality (7 – 7.5) is the foremost crucial activity of cell's outlasting. Responding to an acute acid load, the cell first recruits several, relatively rapid and reversible, short-term mechanisms that consume  $H^+$ , thereby minimizing the magnitude of the intracellular pH decrease. Later, pH slowly returns towards normal values as acid is extruded from the cell through ion pumps [60]. These mechanisms are classified as short and long term and are outlined below.

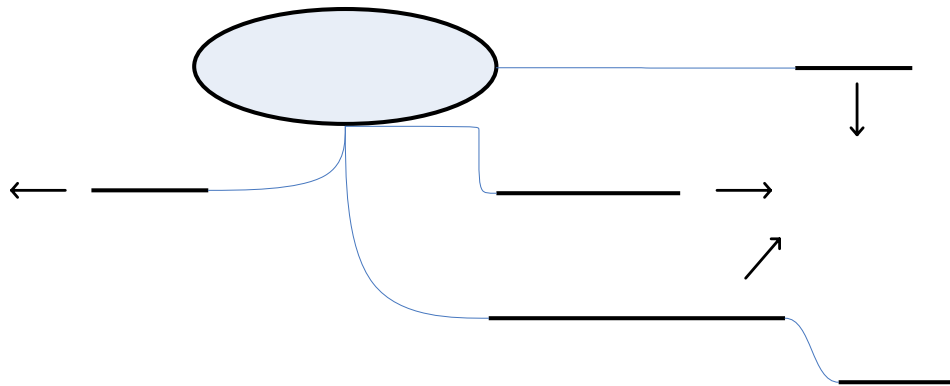


Figure 17 pH regulation procedures in response to acute acid loads

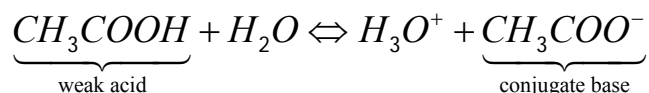
### 2.4.1 Short-term mechanisms

Following an acute acid load, the cell responds with the short-term mechanisms to buffer and consume protons. Ion consumption activates three main processes, namely: the physicochemical buffering, metabolic processing and organellar buffering [60].

Buffer is a solution containing a conjugate weak acid/weak base pair that is resistant to a change in pH when a strong acid or strong base is added. Weak are the acids that cannot completely donate their acidic protons to the solvent. Instead, most of the acid remains undissociated, with only a small fraction

In response to acid protons are removed

present as the conjugate base. The chemical reaction of weak acid (acetic acid) is:



At steady state (equilibrium) a numerical constant holds. This equilibrium constant for is called *acid dissociation constant* ( $K_a$ )<sup>3</sup>, and is written as  $K_a = [CH_3COO^-] \cdot [H_3O^+] / [CH_3COOH]$ . The magnitude of  $K_a$  provides information about the relative strength of a weak acid, with a smaller  $K_a$  corresponding to a weaker acid.

Thus, buffers are weak acids or bases that minimize shifts in pH by reacting with exogenous protons according to the equation  $M^n + H^+ \Leftrightarrow MH^{n+1}$  where,  $M^n$  is a weak base of valence  $n$  and  $MH^{n+1}$  is a weak acid of valence  $n+1$ . Thereinafter, some of the neutral products of the above chemical equation can be extruded from the cytoplasm passively either by transcellular or intercellular transport (mobile buffers) [51]. As the restoration of normal pH proceeds, buffers yield back  $H^+$  previously consumed and are thus restored to their initial state.

**Table 1 Potential buffering range**

pH	[Base/Conjugate Acid]	
$pK_a-3$	1/1000	
$pK_a-2$	1/100	
$pK_a-1$	1/10	Effective
$pK_a$	1	Buffer
$pK_a+1$	10/1	Range
$pK_a+2$	100/1	
$pK_a+3$	1000/1	

The buffering action is a consequence of the relationship between pH and the relative concentrations of the conjugate weak acid/weak base pair. In short,

<sup>3</sup> Acid dissociation constant is the equilibrium constant for a reaction in which an acid donates a proton to the solvent

buffering power or buffering capacity of a solution is the concentration of the protons which must be added to or removed from so as pH is altered by a unit [60].

Thorough examination of the table 1 reveals the potentiality of a buffer in the cytoplasm. When the drop (or rise) in pH exceeds the  $K_a$  of the weak acid (or base), acting as a buffer, then it is no longer effective. That is the case; cell's buffering capacity is proportional to the ratio of the concentrations of the buffer (weak acid or base) and the conjugate acid or base causing the pH drop (or rise).

The reactions involved in physicochemical buffering are ionic and thus reach completion in a fraction of second [60]. On the other hand, metabolic processing are somewhat slower than physicochemical (ionic) and are largely completed, within several seconds [59, 60]. In addition, cellular organelles, such as mitochondria, are in constant need of acid. As a result, - and due to the large surface/volume ratio of organelles - these proton sequestrations also contribute in limiting intracellular pH decrement [60].

It should be noted, however, that the short-term mechanisms offer only partial and temporal solution due to the limited cytoplasmic buffer concentration, metabolic processes and organelles. Owing to this adequate capacity to cope with acid loading, the central role in maintaining cytosolic pH is attributed to extruding mechanisms (cell pumps), which actively remove protons from the cytosol.

#### ***2.4.2 Long-term mechanisms***

Aforementioned, short-term mechanisms are incapable of coping thoroughly and exclusively with extreme acid loads. Therefore, acid consumption is further aided by active transport. Proton pumping or acid extrusion mechanisms are widely known to get involved in the cytosolic pH regulation, utilizing ATP. They are termed as long-term because they are slower than the buffering process. In general, the rate of active acid extrusion is low at normal state and enhanced gradually as intracellular pH or extracellular pH increases

[60, 61]. Even today, the exact mechanisms involved in cellular pH regulation are not clear. The fundamental mechanisms of active exchanging ions, according to stoichiometric models are (1)  $Na^+$  - dependent  $HCO_3^-/Cl^-$  exchanger, which is operational at nearly neutral intracellular pH ( $\approx 6.8 - 7.2$ ). (2) The  $Na^+$  - independent  $HCO_3^-/Cl^-$  exchanger and (3)  $Na^+$  -  $H^+$  exchanger (accounts for about 70% of total acid-extruding capacity), which is idle at neutral pH, becomes more operational as pH drops ( $\approx 6.38$ ) and is inactive at very low levels of pH [60-62].

# CHAPTER 3

## Background information for model development

### 3.1 Cervical Intraepithelial Neoplasia

The cervix is the portion of the uterus attached to the top of vagina (figure 18). Generally, the cervix is covered by two epithelial tissue types, namely: the columnar epithelium and the stratified squamous epithelium. The former is a single layer cell structure typically found in the cervical canal while the latter consists of several cell layers with cell morphology transitionally converted from cuboidal to squamous cells at the apical surface. Somewhere on the cervix the two cell types meet at a place called Squamo-Columnar Junction (SCJ). During the woman's life span, columnar epithelium is converted progressively to squamous and for this reason SCJ is often called Transformation Zone (TZ). CIN tends to form in the vicinity of the TZ.

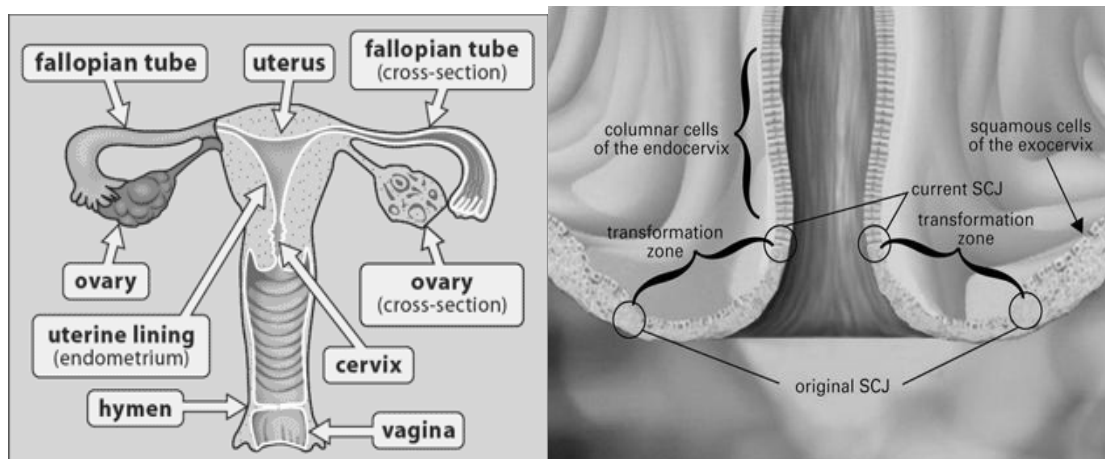
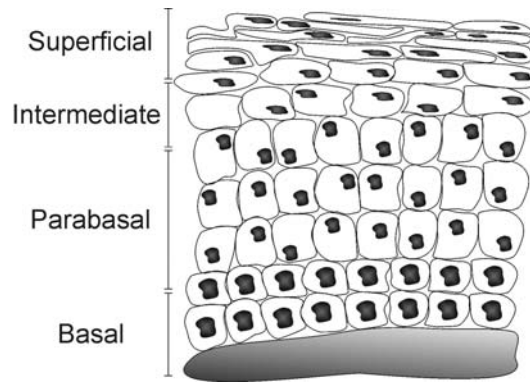


Figure 18 The cervix

Keeping pace with general epithelial structure, cervical cells are firmly adjoined via desmosomes, tight junctions and gap junctions consisting of several layers. The layers of the squamous epithelium are subdivided into a number of different classes: basal, parabasal, intermediate and superficial (figure 19).



**Figure 19 Cervical Epithelial Layers**

### ***3.2 Structure of normal and abnormal cervical epithelia***

CIN is a continuous spectrum of change, whereby the epithelium may become progressively more abnormal in appearance, or neoplastic. Moreover, neoplasia development is strongly associated with the loss of differentiation and stratification resulting in tissue homogenization throughout its thickness, in terms of both cell size distribution and shape. The size of cells is reduced, while the nucleus size increases, resulting in an increase of both nuclear-to-cytoplasmic ratio (nuclear density) and extracellular space [63]. In normal tissue, the rate of cell production and proliferation is well controlled, whereas in tumors control mechanisms are disrupted and cells may grow at an unusually fast rate, or undergo unusual differentiation processes.

Figure 20 illustrates the basic structure of the cervical epithelium together with the structural changes provoked during the progress of the disease. Viral genomes, that manifest high-risk HPV types, are maintained as episomes in the basal layer, with viral gene expression being tightly controlled as the infected cells move towards the epithelial surface [64]. There are no quantitative descriptors for the CIN grades and thus histological diagnosis is highly subjective. Generally, the CIN histological grading roughly correlates with the proportion of the total epithelial thickness affected by neoplasia. For instance, tissue diagnosed as typical of CIN I will be normal throughout the upper two-thirds of its thickness, but enlarged nuclei may be visible in the lower third. The lower two-thirds of CIN II epithelium may appear abnormal,

whereas in the case of the CIN III, abnormal nuclei and cell structures may be present throughout the entire cross-section of the epithelium.

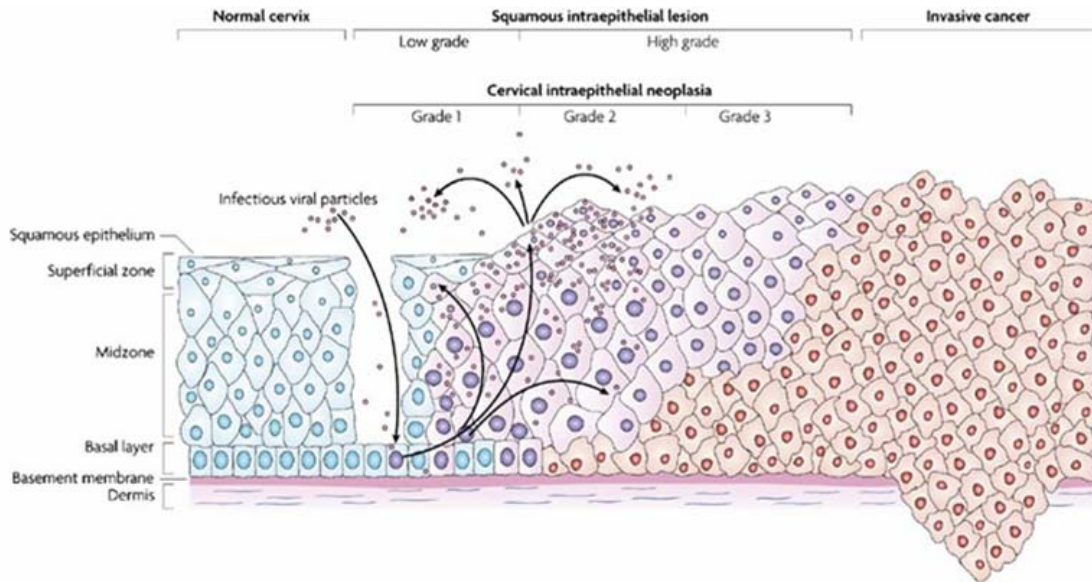


Figure 20 The structure of the cervical epithelium in normal and progressive CIN and Invasion

### 3.3 Transport phenomena in normal and abnormal cervical epithelia

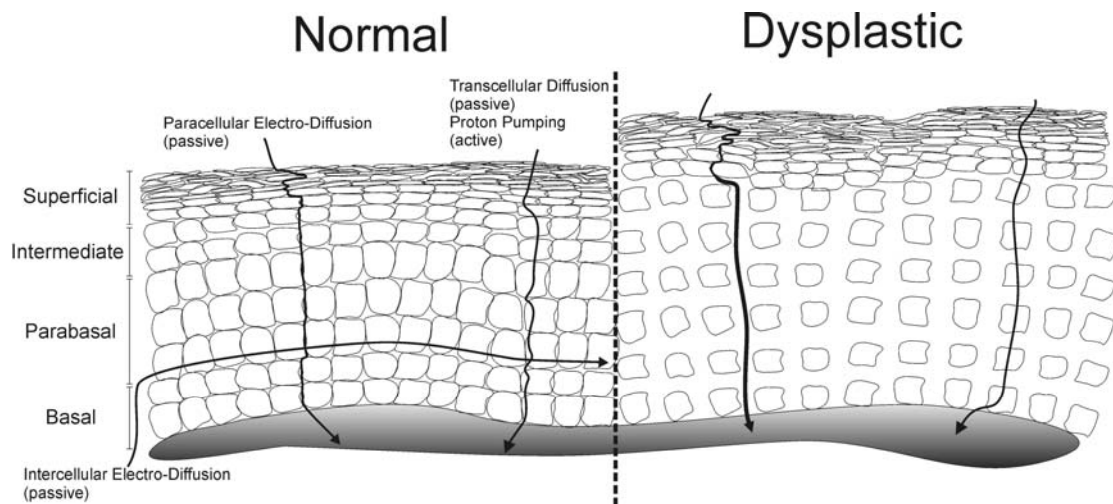


Figure 21 Diffusion pathways in normal and abnormal cervical epithelia

The cervical epithelium, where CIN develops, is aglandular and villus free. Secretion and absorption are managed by the transcellular and paracellular

pathway only. Vaginal mucus secretion is delivered through the paracellular pathway to the lumen which produces openings on the apical surface like pores [39]. Withal, nutrient absorption is carried through both the paracellular route and the direct transmembrane communication of the apical cell layers with the cervical lumen. Moreover, communication through the gap junctions is operational and diffusion is feasible in all cell layers. Therefore, molecules penetrating the cervical epithelium may travel through the transcellular, paracellular or intercellular pathway, either passively or actively according to the previous chapter (figure 21).

### ***3.3.1 Gap Junctions***

In the cervical epithelium there are three main types of connexins present, Cx26, Cx30 and mainly Cx43 [50, 65, 66]. Immunofluorescence staining and phosphorylation methods revealed the localization of connexins inside the cervical epithelium layers. Particular studies for Cx43 showed that this protein is conformal to the ball -and- chain model proposed in the previous chapter and that it exhibits chemical gating with acidification [57, 58, 67, 68].

Recent studies have shown a direct relation between gap junctions, connexins, cervical neoplasia and the HPV virus [50, 65, 66]. Comparing normal and neoplastic specimens, authors argued that cervical carcinoma is starkly related to the gap junctional pathway deficiency and connexin aberrant localization during carcinogenesis and tumor growth. In [65], authors correlated normal and CIN affected epithelium using connexin phosphorylation. Gap junction evanescence was also governed to be the offspring of HPV virus in both [50, 65] and that the situation, is due to reduced expression rather than localization in cytoplasm. Finally, in [66] aberrant localization of connexins was specifically examined for various epithelial cancer models. As the authors suggested, gap junctional intracellular communication can be found either among cancer (even deficiently) or normal cells. However, irregular cytoplasmic localization of connexins is due to cancer stage (possibly by cadherin inexpression) which is a general phenomenon of carcinogenesis. Accordingly, connexins may play a role in

promoting carcinogenesis by the time tumor, in contrast with normal, cells communicate in an extremely difficult manner.

In conclusion, gap junctions control the intercellular cervical epithelial transport pathway, integrating metabolic activities of all cells in the tissue. However, a remarkable reduction of the cell-to-cell cross talking and metabolic cooperation is associated with the development of neoplasia.

### ***3.3.2 Tight Junctions***

The expression<sup>4</sup> level of proteins that mediate adhesion at the tight junctions and desmosomes directly associates with the degree of differentiation of cancer cells [69]. There is an obvious correlation between protein downregulation and the junction inactivation. Surprisingly, the later can also be provoked by upregulation of the former. Both circumstances play a major role in malignant transformation and metastasis. In the cervical squamous epithelium and during carcinogenesis, expression of such proteins (claudins and cadherin) tends to increase [70]. Thereby, cervical tumors exhibit leaky biological barriers [71]. As a result, tight junctions decrease and desmosomes ease off during CIN [30, 32, 34, 63, 72].

Particular interesting attempts have been made to adjoin regular tight junctional behaviour and gap junctions [73]. Argument on the matter is brought on because of the hemeostatic purpose of gap junctions and their maintenance feature of general tissue's functions. It has been shown that the gap junction pathway inactivation influences the tight junction complex accordingly [74]. On top, as alluded to above, gap junctions are inexpressed or aberrantly localized in cervical cancer cells [65, 75]. Thus, paracellular permeability is indirectly influenced by the lack of intercellular communication and metabolic cooperation in the cervical dysplastic epithelium.

Because of the importance of the pathway, many groups have measured with different methods junctional conductance and permeability of different markers and ions [36, 38, 39, 76-78]. Interestingly, experiments on the

---

<sup>4</sup> *Protein expression*: the ability of a protein to operate properly, according to its physiology

cultured cervical epithelium characterized the degree of paracellular permeability as relatively high [77]. Others, indicated that tight junctional permeability can be mediated indirectly and directly by extracellular pH and  $Ca^{+2}$  respectively [38, 39, 41]. These conclusions further validate that, as in most tumors, during CIN tight junctions malfunction. Thereupon, the extracellular environment becomes spacious, allowing greater diffusivity to ions and molecules.

### ***3.3.3 Tumor pH***

It's a common trend that tumor cells live in a lower extracellular pH, than normal cells, while the intracellular pH is almost the same in both cases [79, 80]. One obvious hypothesis to explain the low extracellular pH in solid tumors is the production of lactic acid under anaerobic conditions, and the hydrolysis of ATP in an energy-deficient environment (2 to 15 times more than normal ones) [60-62, 80-84]. Anaerobic glycolysis leads to the formation of 2 mol of lactic acid and 2 mol of ATP for each mole of glucose utilized. Because lactic acid has a low dissociation constant, it is dissociated into a lactate anion and a proton at physiological pH. However, even if the production of protons by this mechanism is probably the major cause of acidity in tumors, additional pathways may also lead to acid production.

In cervical neoplastic cells, pH regulation is expected to be remarkably less efficient than in normal cells due to the absence of gap junctions (as described above) and to the associated lack of metabolic cooperation. Thereupon, in order the cell to keep its alkaline pH an increase in ATP production is required to fuel proton pumps and eventually increase the extrusion rates. This request for greater ATP turnover is granted by the increased glycolysis and it is documented that tumor cells not only maintain proton extrusion rates, but acid utilization, by short-term mechanisms, is also equal to that of normal ones [80, 85]. As a result, cervical tumor cells are extruding ions in their micro-environment, which becomes acidic preserving their neutral intracellular pH.

Here, it should be noted that acidic extracellular environment is maintained for longer time periods due to the disorganized vasculature, or to poor lymphatic drainage or elevated interstitial pressure observed in tumors. Furthermore, extracellular pH is lower as we get further from blood vessels [61, 84]. In fact the extrusion rate of excess waste ( $H^+$  clearance) to the blood is very slow. Therefore, a reversed pH gradient between the extracellular and the intracellular space of tumors cells is constantly maintained.

### ***3.4 Interpretation of the temporal characteristics of the AW phenomenon - model assumptions***

Biomarkers are chemical substances that have the ability to react with tissue material and induce, selectively, transient alterations in the optical properties of the component(s) in issue. The visual inspection with acetic acid of cervical cancer (VIA) is used as a test of primary screening or an adjunctive test of cytology. The agent-tissue interaction in normal tissues produce minimal reflected glare while in neoplastic produce temporal tissue whitening. Luminance, as measured by the diffuse reflected light, maximizes within the first 1-2 min and decays over several minutes thereafter (figure 22).

Practically, the method dictates the application of acetic acid to the cervix exterior and then visualizing the biochemical reaction on it (figure 23). It can be done under incandescent light with or without magnification producing a low intensity chemiluminescent light. This chemiluminescent light allows the physician to have a subjective interpretation of the epithelial condition *in vivo*. Here, we attempt to interpret the kinetics of acetic acid that penetrates a cervical neoplastic tissue and correlate them with the transient phenomenon.

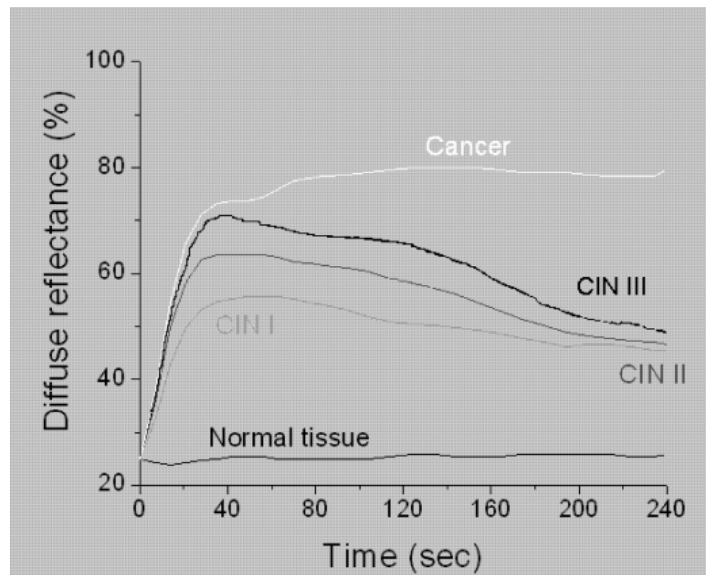
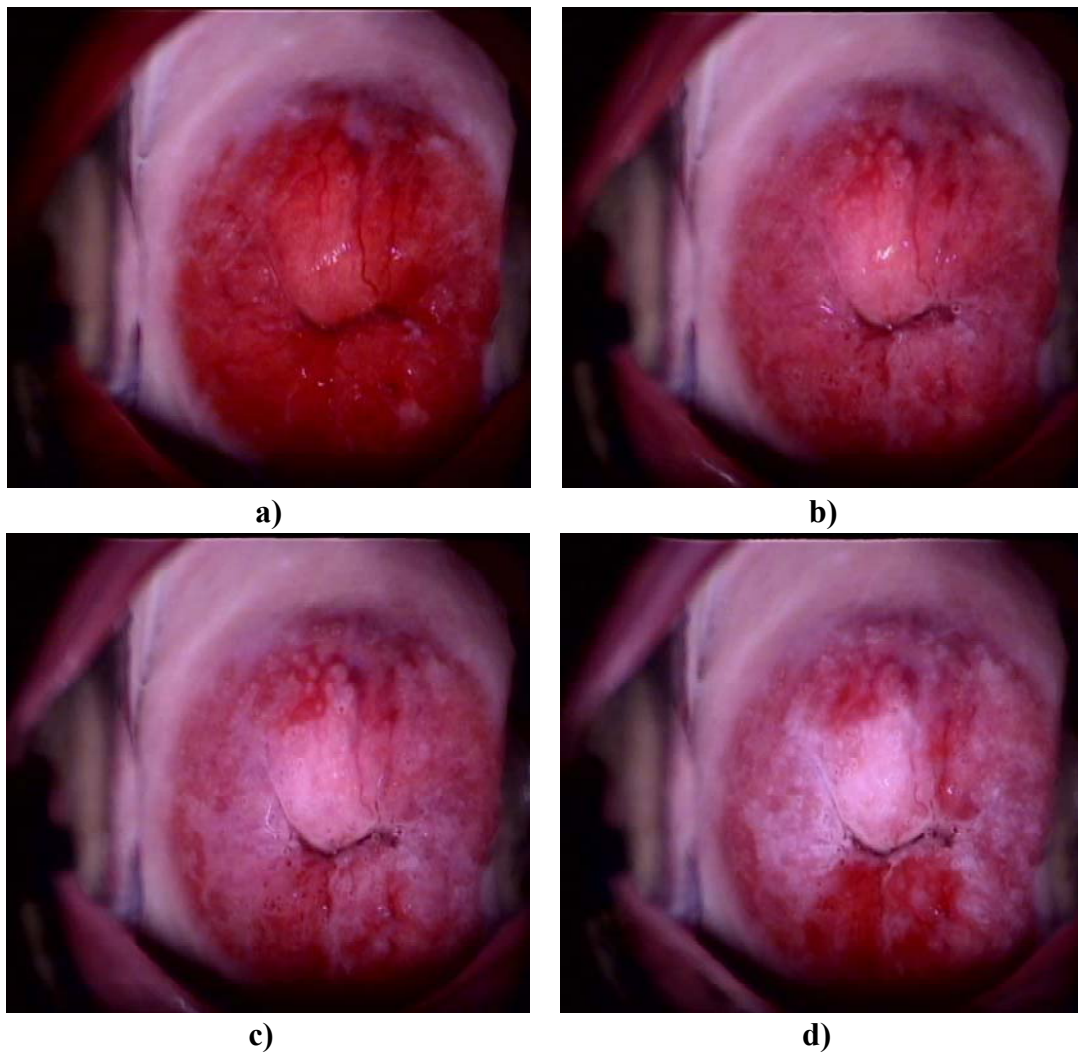


Figure 22 Intensity of the backscattered light as measured in normal and CIN tissues





e)

**Figure 23** Time sequence of images from a cervix with biopsy confirmed CIN III. The images were taken (a) immediately after application of acetic acid, (b) 20 s after, (c) 60 s after, (d) 80 s after, (e) 90 sec after.

### ***3.5 Transport pathways of acetic acid in normal and abnormal epithelia***

As discussed earlier, the extracellular pH ( $\text{pH}_{\text{ECS}}$ ) in tumors is lower, as compared with normal cells, while the intracellular pH ( $\text{pH}_{\text{ICS}}$ ) is almost the same in both cases.

Assuming a topical application of acetic acid (AA) dilute solution onto the surface of the cervical epithelium, the acid molecules will enter to the extracellular space, where they will be partially disassociated to hydrogen ( $\text{H}^+$ ) and acetate ( $\text{AC}^-$ ) ions. For a weak electrolyte, such as AA with  $\text{pK}_a^{37\text{C}}=5.1$ , the amount of disassociation depends heavily on the extracellular buffering capacity, which is determined by the  $\text{pH}_{\text{ECS}}$ . At normal epithelium  $\text{pH}_{\text{ECS}}=7.3$ , while in tumors  $\text{pH}_{\text{ECS}}=6.8$ . At both normal and tumorous epithelia the  $\text{pH}_{\text{ICS}}$  is maintained at neutral levels (7.3-7.1) [60-62, 80-84].

As mentioned in the previous chapter, buffering capacity is the extent of acid load a solution can bare without altering its initial pH. By the time the intracellular and the extracellular space in the cervical epithelium are buffered, we can apply the Henderson and Hasselbalch (HH) equation for buffered solutions in order to find the extent of AA ionization.

In normal epithelium:

$$pH_{ECS} = pK_a + \log \frac{C_{Ac^-}^{ECS}}{C_{AA}^{ECS}} \Leftrightarrow \frac{C_{Ac^-}^{ECS}}{C_{AA}^{ECS}} = 10^{pH_{ECS} - pK_a} \stackrel{pH_e=7.3}{pK_a=5.1} = 160 \Leftrightarrow C_{Ac^-}^{ECS} = 160 \cdot C_{AA}^{ECS}$$

$$pH_{ICS} = pK_a + \log \frac{C_{Ac^-}^{ICS}}{C_{AA}^{ICS}} \Leftrightarrow \frac{C_{Ac^-}^{ICS}}{C_{AA}^{ICS}} = 10^{pH_{ICS} - pK_a} \stackrel{pH_e=7.5}{pK_a=5.1} = 251 \Leftrightarrow C_{Ac^-}^{ICS} = 251 \cdot C_{AA}^{ICS}$$

while in a dysplastic epithelium:  $C_{Ac^-}^{ECS} \cong 50 \cdot C_{AA}^{ECS}$  and  $C_{Ac^-}^{ICS} \cong 100 \cdot C_{AA}^{ICS}$ . These figures indicate that:

- In the vicinity of the neoplastic cell (extracellularly), AA ionization will be less pronounced.
- The concentration of unionized AA molecules is higher extracellularly, in both normal and dysplastic tissue.
- The concentration of unionized AA molecules, extracellularly, is higher in dysplastic tissue than normal one.

Provided that electrolytes can passively diffuse through the cell membrane only in their unionized form, it is reasonably expected that the amount of the unionized AA permeating the cell membrane to be higher in neoplastic cells, as compared to the normal ones. The relative intracellular and extracellular concentration of the unionized AA ( $C_{ICS}$ ,  $C_{ECS}$  respectively) is given by the formula:

$$C_{ICS}/C_{ECS} = \left(1 + 10^{pH_{ICS} - pK_a}\right) / \left(1 + 10^{pH_{ECS} - pK_a}\right) \quad (1)$$

By substituting the above mentioned pH values to equation (1), it yields to  $C_{ICS}/C_{ECS} \cong 1.6$  for normal epithelium and to  $C_{ICS}/C_{ECS} \cong 2.5$  for the neoplastic tissue. These results indicate that a greater amount of AA is accumulated into the intracellular space of the neoplastic cells. In addition, it should be noted that the application of AA further lowers the  $pH_{ECS}$ , decreasing the buffering capacity of the extracellular space, thus favouring the inwards flux of the unionized molecules.

## Acetic Acid ionization in normal and dysplastic ECS and ICS

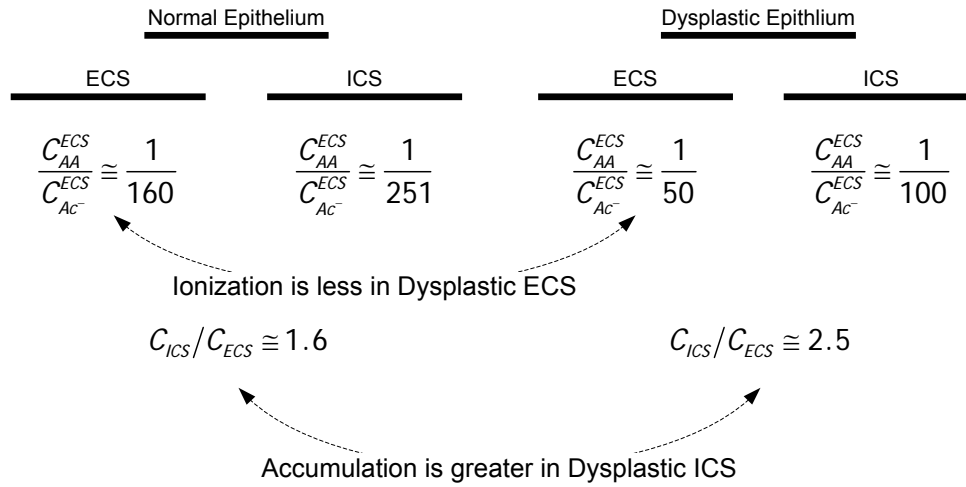


**Figure 24** The less the pH the less the ionization of acetic acid

Besides the lower  $pH_{ECS}$ , careful analysis of the epithelial biophysics suggests that the previously discussed differences in the intracellular-to-extracellular volume ratio, between normal and neoplastic epithelium, should be an additional factor determining the inwards flux of the unionized AA. The structure of the normal cervical squamous epithelium dictates that the intracellular space at the utmost layers, gradually aggrandizes in volume, while the extracellular space falls away [63]. As a result, the hydraulic pressure applied from the intracellular space overcomes the pressure of the extracellular space, thus minimizing the inward passive diffusion flux in normal epithelial cells. In contrast, in neoplastic epithelial cells, the aforementioned volume ratio is reversed, further favoring the inwards flux of AA.

Let us assume a CIN II epithelium with its upper 1/3 part occupied by normal cells and with its lower 2/3 occupied by neoplastic cells. The administered AA will first encounter the normal cell layers and it will be transmitted across the epithelium following either the transcellular and/or the paracellular pathway. It is reasonably expected that the first AA molecules entering the uppermost epithelial layer will be disseminated to the underlying normal layers though the well functioning gap junctions, thus enabling metabolic cooperation. As the AA influx continues the acidic load exceeds a certain level, the gap junctions are closing in order to protect the underlying layers from this high acidic load that

could irreversibly damage them [18, 51, 55, 57]. It is therefore argued that in high acidic load conditions, which are the case for 3%-5% AA, the dominant transport pathway should be the paracellular one. In fact, it has been found that the intracellular acidification by AA opens the tight junctions to facilitate paracellular diffusion. Intracellular acidification causes an increase in intracellular calcium ( $\text{Ca}^{+2}$ ) of epithelial cells [57]. Elevation in the concentration of  $\text{Ca}^{+2}$  leads subsequently to myosin light-chain phosphorylation of the apical cytoskeleton, where tight junction proteins dock [86]. Provided that tight junctions are dynamic epithelial barriers, the latter mechanism has been proved to produce cytoskeletal contraction in epithelial cells which, in turn, opens the tight junction barriers, creating macromolecular gaps between them [31, 32, 35, 87].

By entering the extracellular space of the normal cells, AA is disassociated remarkably and together with the unionized molecules are transmitted to the underlying normal layers through the tight junctions. Recall here that both molecules and ions cannot penetrate the cell membrane in normal epithelium due to charge and to small extracellular space, respectively. The size of the AA molecule is 3 Å, which is smaller than the tight junction's pore, even at its native state, and therefore it is expected the transmission to be almost unobstructed with  $\text{H}^+$  travelling faster due to its unitary size. Upon reaching the extracellular space of the first neoplastic layer, the AA ions recombine, due to the acidic environment, and a fraction of the AA molecules diffuses passively to the intracellular space. Transmembrane diffusion is now facilitated by the large extracellular volume, which is a characteristic of the neoplastic cells (figure 25).

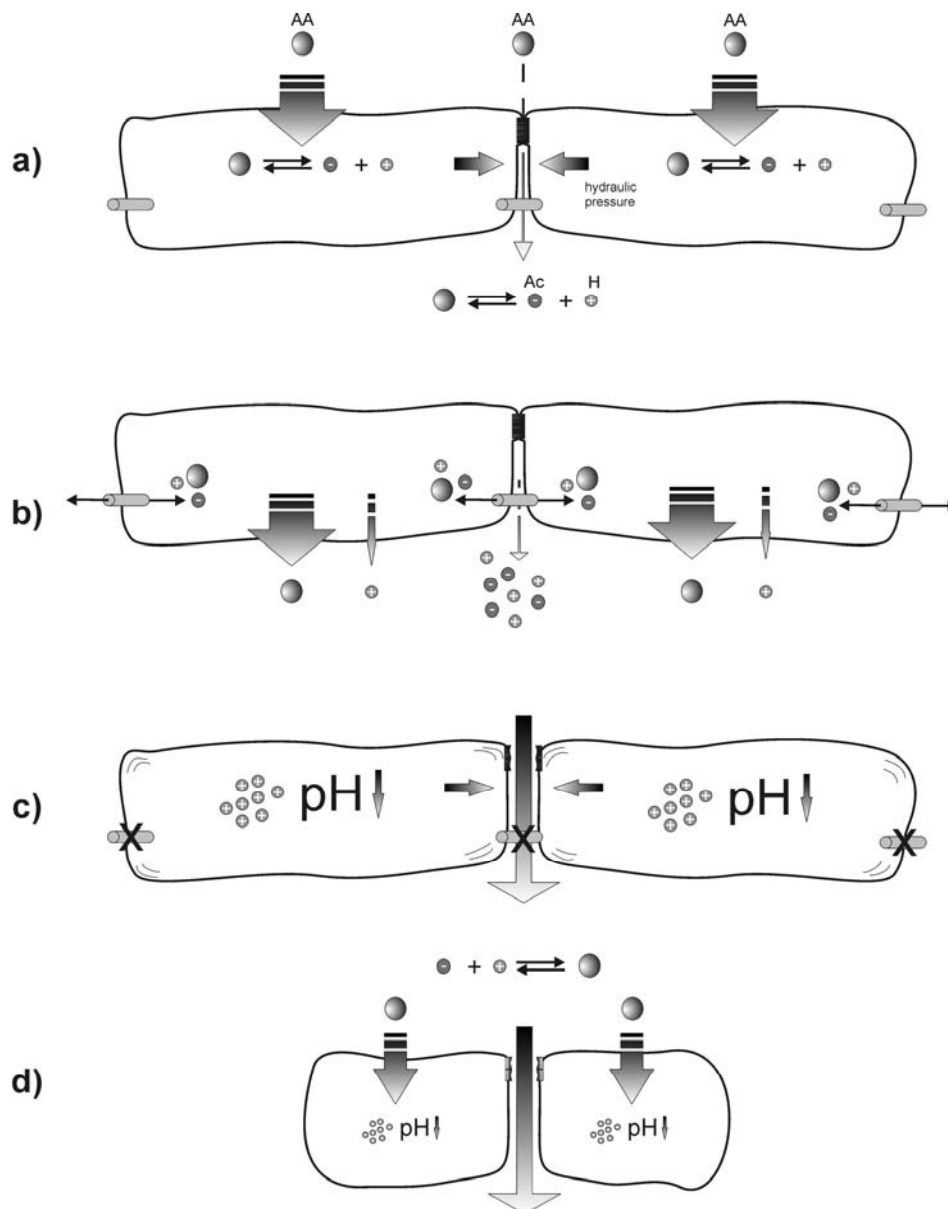


**Figure 25** a) AA enters the ICS and ECS via the transcellular and paracellular pathway respectively and ionizes. b) AA and protons are extruded through the membrane to the ECS. Both AA and ions permeate the intercellular pathway and through the gap junctions to adjacent cytoplasms (metabolic cooperation). c) The intracellular pH drop closes gap junctions and causes cytoskeletal contracts that open the paracellular pathway. d) Reaching the ECS of a neoplastic cell, pH is dropped, ions recombine and AA enters the ICS

Due to the almost neutral  $pH_{ICS}$ , the intruded AA molecules are ionized, thereby causing a pH fall. The absence of gap junctions and metabolic cooperation, due to the isolation of the neoplastic cells, implies that they have to cope with the high acidic load on their own, by triggering its pH regulating mechanisms. In contrast to what happens in the extracellular space, the

buffering capacity of the cell is almost the same in normal and pathologic conditions. The intracellular acidic load, however, exceeds cell's buffering capacity and thus slow mechanisms such as the ion pumps are activated. The rate of the pH regulation through the ion pumps depends on the intracellular pH drop [60, 80, 85, 88-90]. The confronted acidic load creates a pH gradient between the intracellular and the extracellular space, which generates a low transmembrane conductance for the acetate ion ( $\text{Ac}^-$ ). As a result, AA dissociation products are constantly consumed (physicochemical buffering) or are outdriven (active proton pumping and passive electrodiffusion) from the intracellular space. Therefore, there is a constant intracellular depletion of the AA that maintains a concentration gradient, which favours its up-take from cells.

The AA molecules and ions that did not manage to pass the cell membranes, when travelling across the epithelium, together with the ones that are extruded by the cell continue to travel across the abnormal epithelium, through the loose tight junctions, interacting with the cells as describe above. Finally, they reach the stroma, where they drain to the blood circulation and to the lymphatic system and the epithelium restores its original state.

### ***3.7 Correlation between epithelial transport kinetics of acetic acid and dynamic scattering characteristics of the AW phenomenon***

Experiments presented in [91] have shown that dicarboxylic acids such as lactic acid is not producing AW phenomenon. This explains why although lactic acid is produced constantly in neoplastic cells, no native AW effect is observed. The same study demonstrated that sodium acetate did not produce any AW effect either. Both observations indicate that AW effect is not associated with the acetate ions. It is therefore reasonable to suggest that the AW effect is associated with either the intracellular concentration of the unionized AA or with the  $\text{H}^+$  concentration (pH). It is well known that the latter can provoke conformational changes in cellular components, such as protein denaturation, fixation and cross-linking, which can in turn cause a local variation in the refractive index and consequently an alteration in the light

scattering characteristics. This can explain the alterations in the scattering properties of the abnormal epithelium, observed as AW phenomenon. Confocal and phase contrast microscopy [15, 16] in cell cultures have both demonstrated that the AW phenomenon is developed in the nucleus of the cell, indicating that the above mentioned conformational changes refer to nucleic components. The determination of the actual nucleic components comprising the biological origins of the AW phenomenon lies outside the scope of this thesis and it is a subject of our on-going research in the field. Nevertheless, the reversible nature of the AW effect indicates that the associated biological processes should also be reversible after AA removal from the cell. It is well known however, that reversible biological processes, such as protein denaturation, fixation and cross-linking provoked by weak acids, are very fast following the concentration changes of the latter. For example, proteins restore their native structure spontaneously and within a ns/ $\mu$ s time scale after denaturant's removal [17]. Provided that the AW effect lasts for more than 4min, we reasonably suggest that the phenomenon's dynamics is not determined by the intrinsic time characteristics of the conformational changes, but from the dynamic characteristics of the change causing factor instead, which is the intracellular proton concentration dynamics. Subject to the amount of correlation of the latter with the macroscopic light scattering properties of the tissue, the quantitative assessment of the AW phenomenon could provide a means for the in vivo assessment of functional alterations associated with the development of the neoplasia. Moreover, it is expected that the intracellular AA concentration dynamics at each epithelial layer to be affected by the cell packing and the nuclear density of the entire epithelium. Depending on the validity of these hypotheses it could be possible to assess both microstructure and functionality of cervical epithelium, in vivo, by measuring and modelling the macroscopic AW dynamic scattering characteristics. It is expected that besides the intracellular proton concentration, the AW scattering characteristics are also affected by the concentration of nuclear components that are subjected to conformational changes in the presence of  $H^+$ . Such a component may be the nucleoprotein, the concentration of which is increasing with the neoplasia grade. Nevertheless, we initially assume that the AW

kinetics is largely determined by the  $pH_{ICS}$ , while the concentration of nucleic AW scattering centers is expected to affect the static scattering intensity. The model output ( $pH_{ICS}$ ) will be compared with the experimental data and the validity of the aforementioned assumptions will be assessed and discussed.

# Chapter 4

## Compartmental modelling of the cervical epithelium

### 4.1 Introduction

As discussed in the previous section, the cervical epithelium can be described as a multilayered epithelium that changes both structurally and functionally during CIN. It is reasonably assumed that each individual cell constitutes a two-compartmental system. The first compartment associates with the cell itself (intracellular) and the second compartment with the corresponding extracellular space (extracellular) both considered buffered, well-stirred and kinetically homogeneous. Adopting a uniform distribution of cells in a dysplastic layer and keeping in mind that CIN progression is proportional to the number of layers; we model mathematically a stack of two-compartmental cell systems, the exact number of which arises from the layers appointed by a given CIN grade (figure 26).

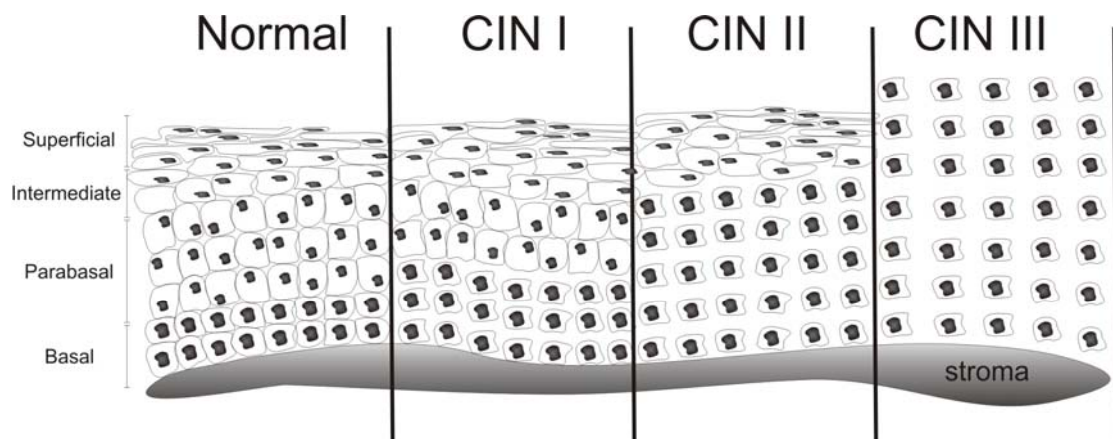


Figure 26 Structural changes during CIN development as a stack of dysplastic cell layers.

As depicted in figure 27a, mass interchange among the intracellular (*ICS*) and extracellular (*ECS*) compartments is carried out by passive diffusion through

the cell's membrane ( $m$ ) and active proton pumping ( $p$ ). Communication between the two-compartmental systems ( $layers$ ) is performed by passive electro-osmotic diffusion, via the tight junction membrane ( $tj$ ), at the apical and bottom regions of each ECS, while after passing the last layer, molecules diffuse to the stroma ( $s$ ). In figure 27b, a more elaborate analysis of a two-compartmental layer system is drawn depicting solute fluxes ( $J$ ). Based on previous analysis, Acetic Acid (AA), acetate ion ( $Ac^-$ ) and protons ( $H^+$ ) enter ( $in$ ) the ECS of the  $i$ -th layer, after passing through the tight junctions ( $J_{AA_i}^{tj, in}, J_{Ac_i^-}^{tj, in}, J_{H_i^+}^{tj, in}$ ). Here, AA is instantly dissociated ( $J_{ion}$ ), depending on the extracellular pH ( $pH_{ECS}$ ) and buffering consumption capacity ( $b_{ECS}$ ). Afterwards, the unionized AA readily and passively permeates the cell's membrane. The unionized flux ( $J_{AA_i}^m$ ) depends on the concentration gradients ( $\Delta C_i = C_{AA_i}^{ECS} - C_{AA_i}^{ICS}$ ). In nearly neutral ICS environment the consecutive AA dissociation is extensive. Due to pH gradients between the ICS and ECS, a low constant field transmembrane conductance is generated that permits  $Ac^-$  diffusion ( $J_{Ac_i^-}^m$ ) while, encore, the flux direction depends on the potential's sign. The  $pH_{ICS}$  drop, (or elevation of  $H^+$  ICS concentration ( $C_{H_i^+}^{ICS}$ )), which is considered to be linked with the acetowhitening phenomenon, is then regulated by physicochemical buffering ( $\beta$ ) and proton pumping ( $J^p$ ) only, given the absence of gap junctions ( $J_S^{gj}$ ) in neoplastic cells. On the other hand, the unionized AA of the ECS that did not enter the ICS lessens as it is outdriven to the next layer. In parallel the cellular pumps are activated extruding AA from ICS to ECS, and the intracellular pH is restored to its normal level. Molecules and ions existing in the ECS together with the ones extruded by the cell are transported to the next dysplastic layers ( $J_{AA_i}^{tj, out}, J_{Ac_i^-}^{tj, out}, J_{H_i^+}^{tj, out}$ ). After experiencing similar biological processes, when travelling across the epithelial layers, AA is consumed mainly due to the buffering and the remaining amount (if any) is finally removed from the epithelium after reaching the stroma ( $J_{AA_i}^V, J_{Ac_i^-}^V, J_{H_i^+}^V$ ).

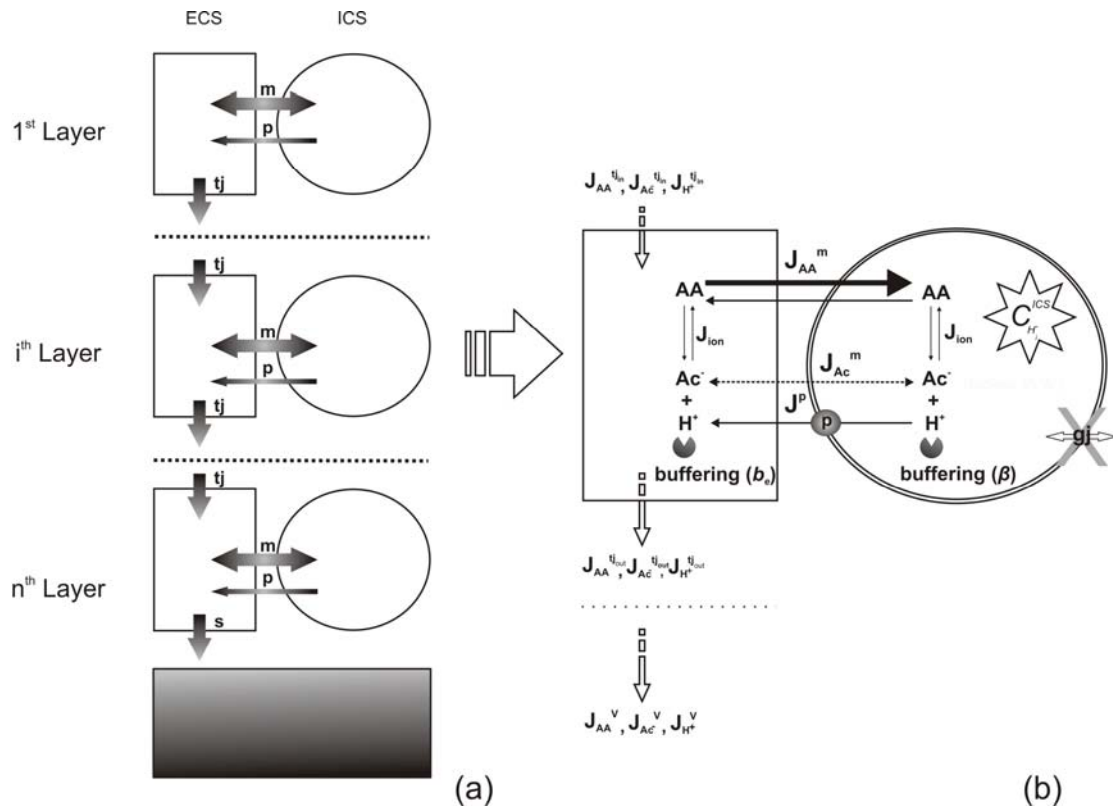


Figure27 (a) Epithelial compartments and transport fluxes (b) The two-compartment cell model and transport fluxes

## 4.2 Model Formulation

### 4.2.1 Estimation of epithelial dysplastic layers and of the number of the corresponding compartments ( $n$ )

It has been found [63] that the average cervical epithelial depth is 360 $\mu$ m. Supposing that all sections (basal, parabasal, intermediate, and superficial) cover equal areas, it follows that the height of each one is 360/4=90  $\mu$ m. The total number of epithelial layers for each CIN grade is estimated by the following relationship:

$$n = \sum_{i=1}^4 \frac{90}{h_i} \quad (2)$$

where  $n$  is the total number of layers and  $h_i$  is the cell height for each epithelial section. Thus the total number of dysplastic layers at the squamous cervical epithelium, in different CIN grades, is estimated using (2) and cell morphological values obtained from table 2 as follows:

$$n_{CIN_1} = 90/13 \cong 7,$$

$$n_{CIN_2} = 90/13 + 90/15 \cong 13 \text{ and}$$

$$n_{CIN_3} = 90/13 + 90/16 + 90/16 + 90/14 \cong 7.$$

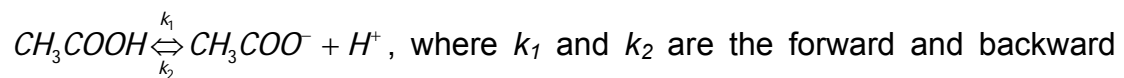
**Table 2** Cervical cell dimensions as measured in [63]

Tissue type	Length (μm)	Height (μm)	Calculated n:c volume ratio
<i>Normal</i>	66 ± 9.2	14 ± 4.8	0.01
<i>Normal</i>	52 ± 10	14 ± 4.7	0.01
<i>Normal</i>	31 ± 6.0	17 ± 5.1	0.03
<i>Normal</i>	16 ± 3.2	15 ± 5.0	0.19
<i>CIN I</i>	46 ± 10	14 ± 1.3	0.01
<i>CIN I</i>	41 ± 9.4	14 ± 2.4	0.01
<i>CIN I</i>	25 ± 5.0	16 ± 3.8	0.04
<i>CIN I</i>	12 ± 4.2	13 ± 2.2	0.21
<i>CIN II</i>	38 ± 7.1	15 ± 2.3	0.02
<i>CIN II</i>	25 ± 7.1	17 ± 4.1	0.04
<i>CIN II</i>	18 ± 5.0	15 ± 2.5	0.17
<i>CIN II</i>	12 ± 1.6	13 ± 1.7	0.33
<i>CIN III</i>	20 ± 5.5	13 ± 3.2	0.14
<i>CIN III</i>	18 ± 5.9	16 ± 1.8	0.15
<i>CIN III</i>	15 ± 3.6	16 ± 1.5	0.20
<i>CIN III</i>	13 ± 2.3	14 ± 2.4	0.28

These values determine the number of the two-compartment systems that compose the epithelial model for each CIN grade and comprise model inputs for specifying a neoplasia grade to be analyzed.

#### 4.2.2 Acetic acid ionization ( $J_{ion}$ )

AA dissociates according to the chemical equation



dissociation rates. According to the mass action law, the AA ionization rate is

$J_{ion} = -k_1 C_{AA}(t) + k_2 C_{Ac^-}(t) C_{H^+}(t)$ , where  $C(t)$  is the solute concentration at a given time. Because of the acute nature of AA ionization we consider that AA is constantly at chemical equilibrium. Thus, in steady state ( $J_{ion} = 0$ ) the following relationship holds:

$$K_a = k_1/k_2 = C_{Ac^-}(t)C_{H^+}(t)/C_{AA}(t), \quad (3)$$

where  $K_a$  is the AA dissociation constant.

#### 4.2.3 Concentration change rates by acetic acid passive diffusion through the cell membrane and tight junction ( $J_{AA}^m, J_{AA}^j$ )

The flux of particles in the positive x-direction,  $J(x,t)$ , is proportional to the spatial gradient of particle concentration  $c(x,t)$ ,

$$J(x, t) = -D \frac{\partial c(x, t)}{\partial x}, \quad (4)$$

where  $D$  is the diffusion coefficient or diffusivity and is independent of the units used for the number of diffusing particles. Under the condition that the flux is constant over a given surface area  $A$  and the concentration is constant over a volume  $V$ , equation (4) is reduced to:

$$J = -\frac{V dc}{A dt} \quad (5)$$

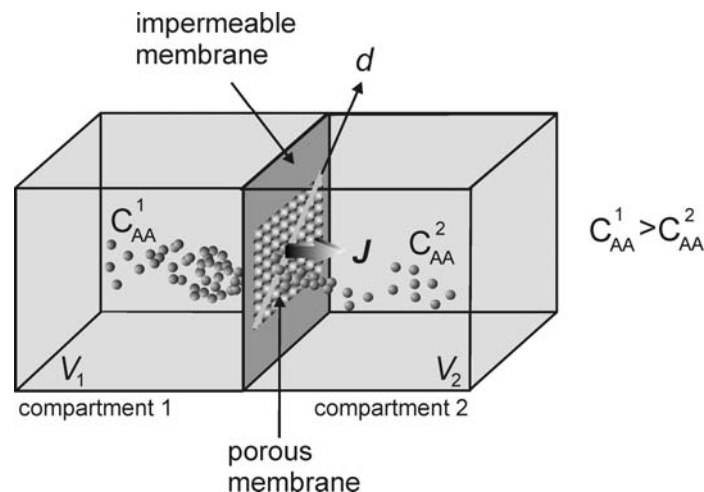


**Figure 28 Two-compartment steady state passive diffusion through a porous membrane**

Assuming that AA kinetics is in equilibrium at all times, steady state (ss) passive diffusion (figure 28) between two compartments with volumes  $V_1, V_2$  separated by a porous membrane ( $p_m$ ) of area  $A_{pm}$  is governed by Fick's Law of membrane diffusion [92]:

$$\begin{aligned} J_{AA}^{pm_{1 \rightarrow 2}} &= -Dk_s/d \cdot \dot{C}_{AA}^1 \stackrel{ss}{=} P_{AA}^{pm} (C_{AA}^1 - C_{AA}^2) \Leftrightarrow, \\ \Leftrightarrow -\dot{C}_{AA}^1 &= \rho_1 P_{AA}^{pm} (C_{AA}^1 - C_{AA}^2) \end{aligned} \quad (6)$$

where  $D$  is the AA diffusion coefficient,  $k_s$  the AA oil:water partition coefficient,  $d$  the pore length,  $P_{AA}^{pm}$  the AA permeability through the porous membrane and  $\rho_1$  the area:volume ratio ( $A_{pm}/V_1$ ). From (4) the AA concentration change rates due to cell membrane diffusion in the ICS and ECS are given by the formulas:

$$\dot{C}_{AA_i}^{ICS} = -\rho_{ICS} J_{AA_i}^m = \rho_{ICS} P_{AA}^m (C_{AA_i}^{ECS} - C_{AA_i}^{ICS}) \quad (7)$$

$$\dot{C}_{AA_i}^{ECS} = -\rho_{ECS} J_{AA_i}^m = \rho_{ECS} P_{AA}^m (C_{AA_i}^{ICS} - C_{AA_i}^{ECS}) \quad (8)$$

where  $\rho_{ICS}$ ,  $\rho_{ECS}$  are the area:volume ratios of the intracellular and extracellular space and  $P_{AA}^m$  the AA's membrane permeability.

Generally, if the dimensions of pores are sufficiently small, the diffusion coefficient in a pore is less than that in free solution. Hence, such diffusion is called hindered diffusion. Provided that the dimensions of a tight junction pore varies within the range of (4.9-7 Å) and that the molecular dimension of AA is similar size (3 Å), its apparent diffusion coefficient is much lower than in bulk solution. Using the Renkin equation [93] we can describe the permeability of such a hindered diffusion process as follows:

$$P_{AA}^H = N\pi r^2 D_{AA}^{bulk} F(a/r)/d \cdot (1 - a/r^2)/(1 - a_w/r^2), \quad (9)$$

where  $P_{AA}^H$  is the AA hindered permeability,  $N$  the number of pores,  $D_{AA}^{bulk}$  the diffusion coefficient of AA in bulk solution,  $d$  the pore length,  $a_w$  the water molecule diameter and  $F(a/r) \approx 1 - 2.1044(a/r) + 2.089(a/r)^3 - 0.948(a/r)^5$  is the hindered drag coefficient between AA and tight junction paries.

For the  $i$ -th layer, the AA concentration change rate due to tight junction diffusion between two layers is:

$$\dot{C}_{AA_j}^{ECS} = \rho_{ECS} \left( J_{AA_j}^{tj_{in}} - J_{AA_j}^{tj_{out}} \right) = \rho_{ECS} P_{AA}^H \left( C_{AA_{j-1}}^{ECS} - 2C_{AA_j}^{ECS} + C_{AA_{j+1}}^{ECS} \right), \quad (10)$$

where  $C_{AA_{j-1}}^{ECS}$ ,  $C_{AA_j}^{ECS}$ ,  $C_{AA_{j+1}}^{ECS}$  denote the previous, current and next layer concentrations and  $P_{AA}^H$  is the hindered AA permeability through the tight junctions.

#### 4.2.4 Concentration change rates of ionic diffusions ( $J_{H^+}^{ij}$ , $J_{Ac^-}^{ij}$ , $J_{Ac^-}^{ij}$ )

Ions apart from chemical gradients also diffuse due to electrical potentials. Ion diffusion is described by the Nerst-Planck [92] equation of electrodiffusion:

$$J_s^{el} = \underbrace{-D_s \frac{dC_s}{dx}}_{diffusion} - \underbrace{\frac{z_s F}{RT} D_s C_s \frac{d\psi}{dx}}_{drift}, \quad (11)$$

where  $z$  is the valence,  $F$  the Faraday's constant,  $R$  gas constant,  $T$  the temperature,  $S$  the diffusing ion and  $d\psi/dx$  the electrical field's intensity. Considering that the electrical field between the two sides of a membrane is constant ( $\Delta V$ ), the Goldman-Hodgkin-Katz [94] equation of electrodiffusion yields:

$$J_S^{I \rightarrow II} = \frac{z_s F \Delta V}{RT} P_S \frac{C_S^I - C_S^{II} e^{z_s F \Delta V / RT}}{1 - e^{z_s F \Delta V / RT}} \Leftrightarrow \dot{C}_S^{II} = \rho J_S^{I \rightarrow II}, \quad (12)$$

where  $z$  is the valence,  $F$  the Faraday's constant,  $R$  gas constant,  $T$  the temperature, index  $S$  denotes the diffusing ion ( $H^+$  or  $Ac^-$ ),  $\rho$  is the area:volume ratio of diffusing compartment and  $C^I$ ,  $C^{II}$  are the concentrations of compartment  $I$  and  $II$ , respectively (fluxes from  $I$  to  $II$  are positive). Even though there is discrimination of cations over anions in tight junction pores, we

adopt that both charged ions come under the same channel resistance while, in addition,  $\text{Ac}^-$  diffusion is considered hindered due to its molecular dimensions [32]. Using (9) we describe  $\text{H}^+$  and  $\text{Ac}^-$  concentration change rates from the inward (*in*) and outward (*out*) extracellular tight junction electrodiffusion fluxes under the hindered diffusion condition, using the general formula:

$$\begin{aligned} \dot{C}_{S_{ij}^i}^{ECS} &= \rho_{tj} \left( J_s^{tj_{in}^i} - J_s^{tj_{out}^i} \right) = \\ &= \rho_{tj} \frac{z_s F \Delta V_{tj}}{RT} P_s^H \left( \frac{C_s^{i-1} - C_s^i e^{z_s F \Delta V_{tj} / RT}}{1 - e^{z_s F \Delta V_{tj} / RT}} - \frac{C_s^i - C_s^{i+1} e^{z_s F \Delta V / RT}}{1 - e^{z_s F \Delta V / RT}} \right) \end{aligned} \quad (13)$$

We can reasonably assume that similar formulation applies to the passive diffusion of ions through the cell membrane. In that case, the  $\text{Ac}^-$  concentration change rates in the ICS and ECS due to membrane electrodiffusion are given by the system:

$$\dot{C}_{\text{Ac}^-}^{ICS} = \rho_{ICS} J_{\text{Ac}^-}^m = \rho_{ICS} \frac{z_{\text{Ac}^-} F \Delta V_m}{RT} P_{\text{Ac}^-}^m \frac{C_{\text{Ac}^-}^{ECS} - C_{\text{Ac}^-}^{ICS} e^{z_{\text{Ac}^-} F \Delta V_m / RT}}{1 - e^{z_{\text{Ac}^-} F \Delta V_m / RT}} \quad (14)$$

$$\dot{C}_{\text{Ac}^-}^{ECS} = \rho_{ECS} J_{\text{Ac}^-}^m = \rho_{ECS} \frac{z_{\text{Ac}^-} F \Delta V_m}{RT} P_{\text{Ac}^-}^m \frac{C_{\text{Ac}^-}^{ICS} - C_{\text{Ac}^-}^{ECS} e^{z_{\text{Ac}^-} F \Delta V_m / RT}}{1 - e^{z_{\text{Ac}^-} F \Delta V_m / RT}} \quad (15)$$

The fraction ( $\alpha$ ) of the total unionized AA ( $C_{AA_T}^{ICS}$ ) is given by the formula:  $\alpha = C_{\text{H}^+}^{ICS} / (C_{\text{H}^+}^{ICS} + K_a)$ . We can therefore reduce the number of variables in (1.12) by substituting the intracellular  $\text{Ac}^-$  concentration ( $C_{\text{Ac}^-}^{ICS}$ ) with

$$C_{\text{Ac}^-}^{ICS} = (1 - \alpha) C_{AA_T}^{ICS}.$$

#### 4.2.5 Active Proton and Vasculature Flux ( $J_{H^+}^p, J_{AA}^v, J_{Ac^-}^v, J_{H^+}^v$ )

AA extrusion from the cells and stroma diffusion are unidirectional fluxes. Both are proportional to the concentration of the native diffusing solute and its perfusion rate through the membrane. In the simple possible circumstance, both fluxes can be described by the equation  $J = kC_s$ , where  $k$  is a proportionality constant that has units of permeability (cm/s) and  $C_s$  the concentration of transported solute [92]. Therefore, concentration change rates by a generic pump  $\dot{C}_{H^+p}$  and stroma diffusion  $\dot{C}_{Sv}^{ECS}$  will be described by the equations:

$$\dot{C}_{H^+p} = \rho_p J_{H^+}^p = k_p C_{H^+}^{ICS} \quad (16)$$

$$\dot{C}_{Sv}^{ECS} = \rho_v J_S^v = k_v C_S^{ECS} \quad (17)$$

where  $k_p, k_v$  are the proportionality constants described earlier,  $\rho_p$  and  $\rho_v$  are the area:volume ratio of pump and stroma respectively and  $S$  the diffusing solutes (AA,  $Ac^-$ ,  $H^+$ ).

#### 4.3 The model differential equation system

As it has been stated in chapter 3, the AW dynamic characteristics are expected to be largely proportional with the  $pH_{ICS}$  dynamics. For this reason, the model equations are developed with the purpose of providing the latter as the model's output. Following [90], the time characteristics of the  $pH_{ICS}$  ( $\dot{C}_{H^+i}^{ICS}$ ) and of the total AA ( $\dot{C}_{AAi}^{ICS}$ ) concentration at the  $i$ -th layer is governed by the following differential system:

$$\dot{C}_{H^+i}^{ICS} = -\frac{\ln 10}{\beta} \frac{C_{H^+i}^{ICS}}{\rho_{ICS}} \left( (1 - a_i) J_{AAi}^m - a_i J_{Ac^-i}^m \right) - J_{H^+}^p \quad (18)$$

$$\dot{C}_{AA_i}^{ICS} = \rho_{ICS} J_{AA_i}^m + \rho_{ICS} J_{Ac_i}^m \quad (19)$$

where  $\ln 10^{C_{H^+}^{ICS}}$  is the pH to  $H^+$  concentration conversion factor,  $\rho_{ICS}$  is the cell area:volume ratio ( $A_{cell}/V_{cell}$ ) and  $\beta$  is the intracellular buffering power of a solution, mathematically defined as  $\beta = -dC_{H^+}^{ICS}/dpH_{ICS}$  [60, 90]. The corresponding differential system for the ECS, as depicted in (fig. 2b), is:

$$\dot{C}_{AA_i}^{ECS} = \rho_{tj} \left( J_{AA_i}^{tj_{in}} - J_{AA_i}^{tj_{out}} \right) + \rho_{ECS} J_{AA_i}^m + J_{ion} \quad (20)$$

$$\dot{C}_{Ac_i}^{ECS} = \rho_{tj} \left( J_{Ac_i}^{tj_{in}} - J_{Ac_i}^{tj_{out}} \right) + \rho_{ECS} J_{Ac_i}^m - J_{ion} \quad (21)$$

$$b_{ECS} \dot{C}_{H_i^+}^{ECS} = \rho_{tj} \left( J_{H_i^+}^{tj_{in}} - J_{H_i^+}^{tj_{out}} \right) + J_{H_i^+}^p - J_{ion} \quad (22)$$

where  $\rho_{ECS}$  and  $\rho_{tj}$  are the ECS and tight junction area:volume ratio respectively and  $b_{ecs}$  is a proportionality constant defined by the fraction the ionized over the non-consumed protons in the ECS. For the last layer, the terms  $\rho_{tj} J_{AA}^{tj_{out}}$ ,  $\rho_{tj} J_{Ac}^{tj_{out}}$  and  $\rho_{tj} J_{H^+}^{tj_{out}}$  are substituted with the terms  $k_V J_{AA}^V$ ,  $k_V J_{Ac}^V$  and  $k_V J_{H^+}^V$  respectively.

#### 4.4 Model approximation

The accurate model consists of five nonlinear differential equations. This induces augmented computational cost. For example, the acetic acid action in a twenty-layer dysplastic epithelium needs differential equations to be mathematically represented. Thus, in order the computational cost to be reduced, without losing arithmetical accuracy, it would be desirable a simplified model to be obtained. A more strict observation in the parameters of the model reveals that the kinetic processes involved in the acetowhitening effect can be separated in two parts: fast and slow processes. For example

acetic acid dissociation is a very rapid process, while the proton extrusion takes place slowly. Several mathematical techniques are used to simplify a differential system which includes fast and slow kinetic steps. In the present modelling, the method of Rapid Equilibrium Approximation (REA) is used. An analytical description and the application of this technique in the proposed model can be found in Appendix.

By setting  $X_i = C_{AA_i}^{ECS} + C_{Ac_i^-}^{ECS}$  and  $Y_i = C_{H_i^+}^{ECS} - C_{Ac_i^-}^{ECS}$  the differentiated form of the former equals with the sum of (17) and (18), while the differentiated form of the latter equals with the subtraction of (18) from (19). Then the reduced system is:

$$\dot{X}_i = \rho_{tj} \left( J_{AA_i}^{tj_{in}} - J_{AA_i}^{tj_{out}} \right) + \rho_{ECS} J_{AA_i}^m + \rho_{tj} \left( J_{Ac_i^-}^{tj_{in}} - J_{Ac_i^-}^{tj_{out}} \right) + \rho_{ECS} J_{Ac_i^-}^m \quad (23)$$

$$\dot{Y}_i = \rho_{tj} \left( J_{H_i^+}^{tj_{in}} - J_{H_i^+}^{tj_{out}} \right) + J_{H_i^+}^p - \rho_{tj} \left( J_{Ac_i^-}^{tj_{in}} - J_{Ac_i^-}^{tj_{out}} \right) - \rho_{ECS} J_{Ac_i^-}^m \quad (24)$$

Using equation (3), solute concentrations can then be calculated by the equations:

$$C_{AA_i}^{ECS} = \frac{(2X_i - Y_i + K_a b_{ECS}) - \sqrt{(Y_i + K_a b_{ECS})^2 + 4X_i K_a b_{ECS}}}{2} \quad (25)$$

$$C_{Ac_i^-}^{ECS} = X_i - C_{AA_i}^{ECS} \quad (26)$$

$$C_{H_i^+}^{ECS} = \frac{X_i + Y_i - C_{AA_i}^{ECS}}{b_{ECS}} \quad (27)$$

Equations (18), (19), (23), (24) comprise now the approximated model differential equations, which will be used for the modelling of epithelial transport phenomena.

#### 4.5 Model parameters

The number of dysplastic layers comprise the model input variable, while  $C_{H^+}^{ICS}$  is the model's output. Table 3 summarizes the parameters of the proposed model and their corresponding values as found in literature. Since the neoplastic portion of the epithelium tends to homogenize, we adopt that the ICS volume ( $V_{ICS}$ ) and cell's membrane area ( $A_{ICS}$ ) remain constant, while ECS volume ( $V_{ECS}$ ) increases as CIN progresses. Abnormal cells are cubical, with volume  $(15\mu\text{m})^3 = 3375\mu\text{m}^3$  and their corresponding  $V_{ECS}$  has minimum value  $15\mu\text{m} \times 15\mu\text{m} \times 0.4\mu\text{m} = 90\mu\text{m}^3$  [71]. The abnormal cell membrane area is approximately  $225\mu\text{m}^2$ . In addition, physiological tight junctions of squamous epithelia are documented to extend in a typical area of  $0.45\mu\text{m}^2$  [31, 95]. However, this value may be varied, remarkably along the spectrum of the so-called tight to leaky epithelia according to measurements on tight junction resistance [32, 37, 38, 41]. Since the epithelial  $V_{ECS}$  and  $A_{tj}$  are increasing with the number of abnormal cells ( $n$ ), we have selected to express the former as function of the latter, in order to avoid having multiple interdependent variables as model inputs. This function is empirical and has been determined experimentally.

**Table 3 Model parameter values**

Parameter	Value	Unit
$\text{pH}_{ECS}$	7.2	-
$\text{pH}_{ICS}$	6.8	-
ICS volume ( $V_{ICS}$ )	3375	$\mu\text{m}^3$
ECS volume ( $V_{ECS}$ )	90	$\mu\text{m}^3$
Cell area ( $A_{\text{cell}}$ )	225	$\mu\text{m}^2$
TJ area ( $A_{tj}$ )	0.45	$\mu\text{m}^2$
$P_{AA}^m$	70	$\mu\text{m}/\text{s}$
$P_{Ac}^m$	67	$\text{pm}/\text{s}$
$P_{AA}^{tj}$	0.97	$\mu\text{m}/\text{s}$

$P_{Ac}^{tj}$	1.1	$\mu\text{m/s}$
$P_H^{tj}$	25	$\mu\text{m/s}$
Intracellular buffering ( $\beta$ )	-10 – -50	mM
Pumping rate ( $k_p$ )	50 – 150	$\mu\text{M/s}$
$\Delta V_m, \Delta V_{tj}$	-50	mV
AA ionization constant at 37°C ( $K_a$ )	$10^{-5.1}$	-
F	$9.648 \times 10^4$	$\text{C}\cdot\text{mol}^{-1}$
R	8.314	$\text{J}\cdot\text{mol}^{-1}\text{K}^{-1}$
T	310	K
$Z_{Ac}$	-1	-
$Z_H$	1	-

According to literature AA and  $Ac^-$  permeability through lipid biomembranes are approximately  $70\mu\text{m/s}$  and  $67\text{pm/s}$ , respectively [22, 96, 97]. As described earlier, tight junction diffusion permeabilities of AA and  $Ac^-$  are approximated using the Renkin equation (17). Their hindered permeabilities were fitted with values of  $0.97\mu\text{m/s}$  and  $1.1\mu\text{m/s}$  respectively, with reference to mannitol's permeability (MW=182Da) which has been found to be  $2.2 \times 10^{-7}\text{m/s}$  in cervical epithelium cultures [77]. Diffusion of  $H^+$  through tight junction is considered to be, unobstructed by the channel pores, due to its unitary MW. However, due to the ECS buffering, channel resistance and race conditions with the other molecules, we attributed a value of  $25\mu\text{m/s}$  according to  $H^+$  mobility in buffered solutions [98]. Furthermore, as discussed earlier the  $\text{pH}_{ICS}$  and  $\text{pH}_{ECS}$  are found on the alkaline and acidic side in most tumors respectively. In current model we use an average of the values found in literature:  $\text{pH}_{ICS}=7.2$  and  $\text{pH}_{ECS}=6.8$ , [61, 62, 81-84]. In addition, ICS buffering capacity ( $\beta$ ), lies in the range -10mM, -50mM for various cell models, while pumping rate ( $k_p$ ) ranges 50-150 $\mu\text{M/s}$  [60-62, 98-100]. Electrical potentials ( $\Delta V$ ) in cell membrane and in tight junctions are almost independent from pH gradients and therefore its not expected to be affected by the neoplasia grade [60, 90]. We adopt the value of -50mV as being consistent with the literature [60, 90]. Unfortunately, there is no quantitative information available in the literature, regarding the outflow to the cervical subjacent tissue ( $k_v$ ), and extracellular buffering proportionality constant ( $b_{ECS}$ ). Nevertheless, due to the fact that AA is in general consumed before reaching the stroma (see in discussion), and to the fact that the acid extrusion flux in stroma is not

affected by the neoplasia grade ( $k_V$ ) is treated as a constant with an arbitrary value determined by the fitting of the experimental data [84]. The same applies to the ( $b_{ECS}$ ), since in all neoplasia grades the  $pH_{ECS}$  remains constant, as discussed earlier.

# Chapter 5

## Simulation results

Solution of the proposed mathematic model was brought on using The MathWorks Matlab™ software. Defining a system of kinetic functions in terms of time ( $t$ ), concentration ( $C$ ) and its rate of change ( $dC/dt$ ) and including the initial condition vector we can utilize a numerical solver to get the system's solution. Keeping in mind that the acetate ions do not participate in the acetowhitening phenomenon, we used the Matlab™ *ode15s* function, which is a multi-step numerical solver for stiff equation systems, in order to find the time characteristics of the AA and H<sup>+</sup> epithelial kinetics in terms of concentration profiles during 0-250 seconds. We run the model with different input vectors and collected a series of graphs that will be analyzed here.

### *5.1 Multistage CIN*

In section 4.2.1, the epithelial dysplastic layers during neoplasia were predicted. Setting the number of layers ( $n$ ) according to the neoplasia grade ( $n=7$  for CIN I,  $n=15$  for CIN II and  $n=25$  for CIN III) we can depict the concentration profiles of AA and H<sup>+</sup> in the total dysplastic region.

Figures 29a and b clearly demonstrate the differences on the concentration kinetics during different CIN stages. During CIN, initial slopes become smoother increasing simultaneously their peak values. These peaks are almost doubled in time and value comparing CIN I and CIN II, a manifestation that does not appear between CIN II and CIN III. During CIN I both the intracellular AA and H<sup>+</sup> concentration rise and reach their peak values in less than a minute. Thereinafter, however, intracellular H<sup>+</sup> clearance commences earlier than that of AA in all neoplastic grades. Comparing the decay courses of CIN I, protons appear to follow an exponential attenuation and AA a rather linear one. In addition, after 250 seconds, proton concentration reaches almost a quarter of its peak value, while, in contrast, only half of the peak AA

molecules are conserved. These important observations acknowledge the cell's antecedence in pH regulation regardless the pH's fluctuation origin.

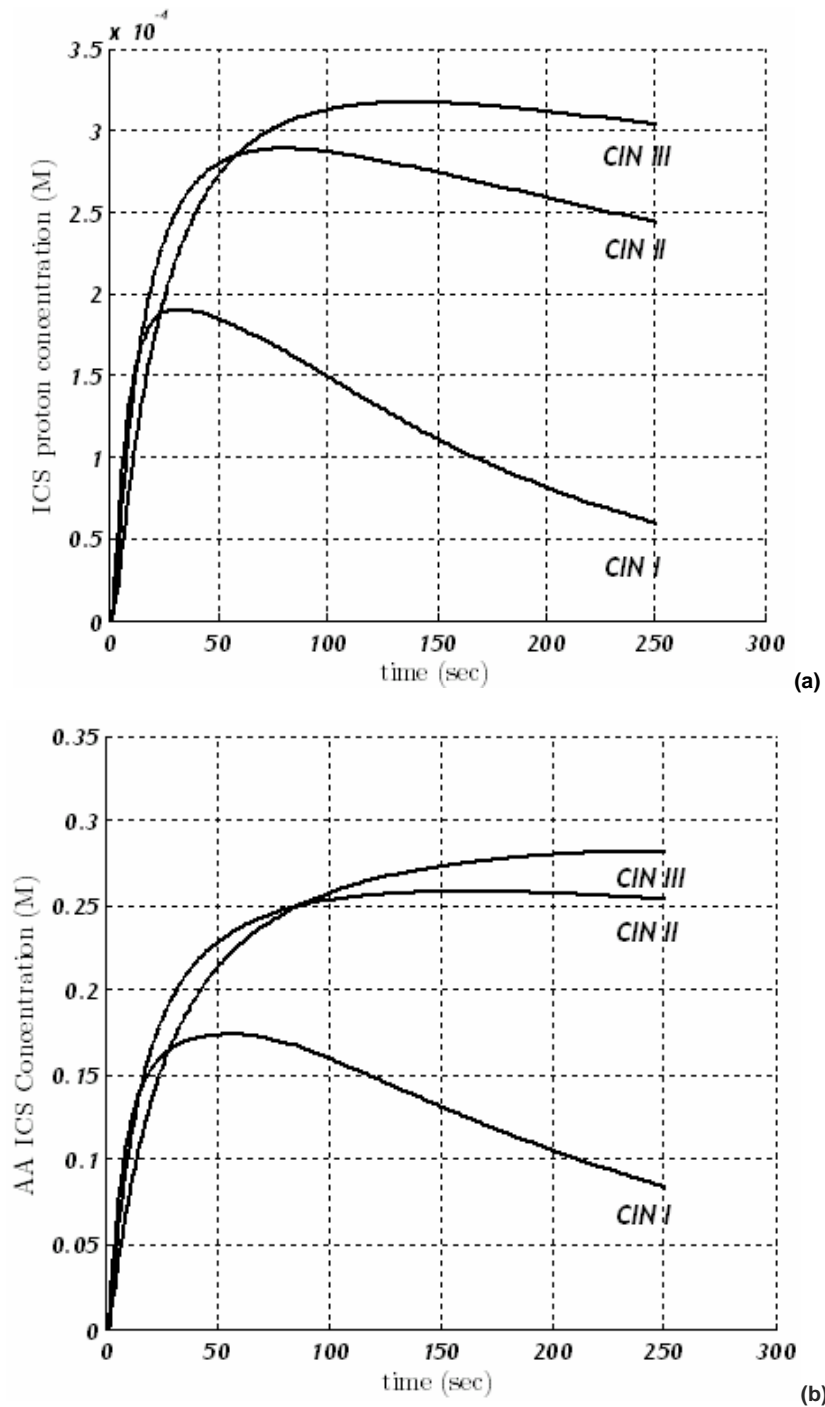


**Figure 29** Intracellular concentration profiles of (a)  $H^+$  and (b) AA in the total epithelial dysplastic layers

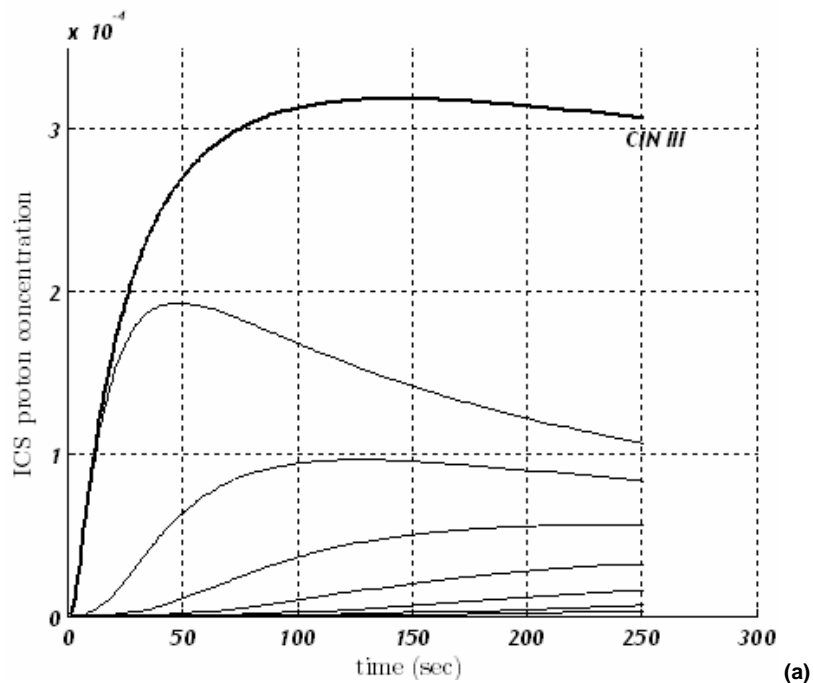
In conclusion, there is an apparent analogy between the concentration profiles of both AA and  $H^+$  evidencing the discrepancy found in literature about the origin of acetowhitening. However, both profiles suggest that intracellular

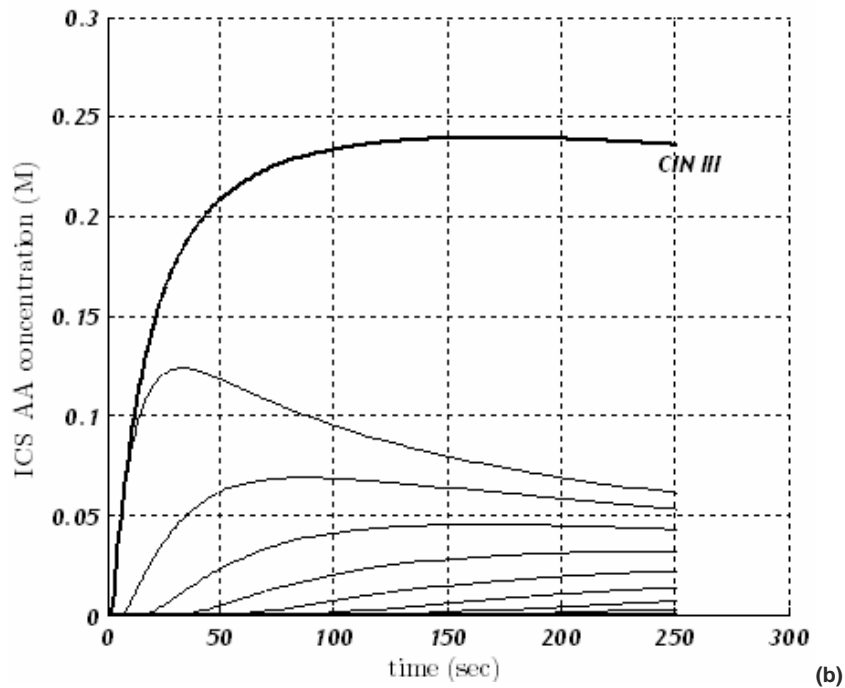
solute preservation is proportional to the severity of dysplasia the extent of which (peak values) is also governed by the number of dysplastic layers.

### 5.2 The diffusion routes

The most critical diffusion pathway from those mentioned in chapter 3 is the paracellular one. Indeed, the outmost structural changes of the cervical epithelium during CIN are the tight junction relaxation, the cellular amassing and the interstitial enlargement. These three factors directly influence the paracellular solute diffusion, which in our case are the AA and its ionization products, the  $Ac^-$  and  $H^+$ .

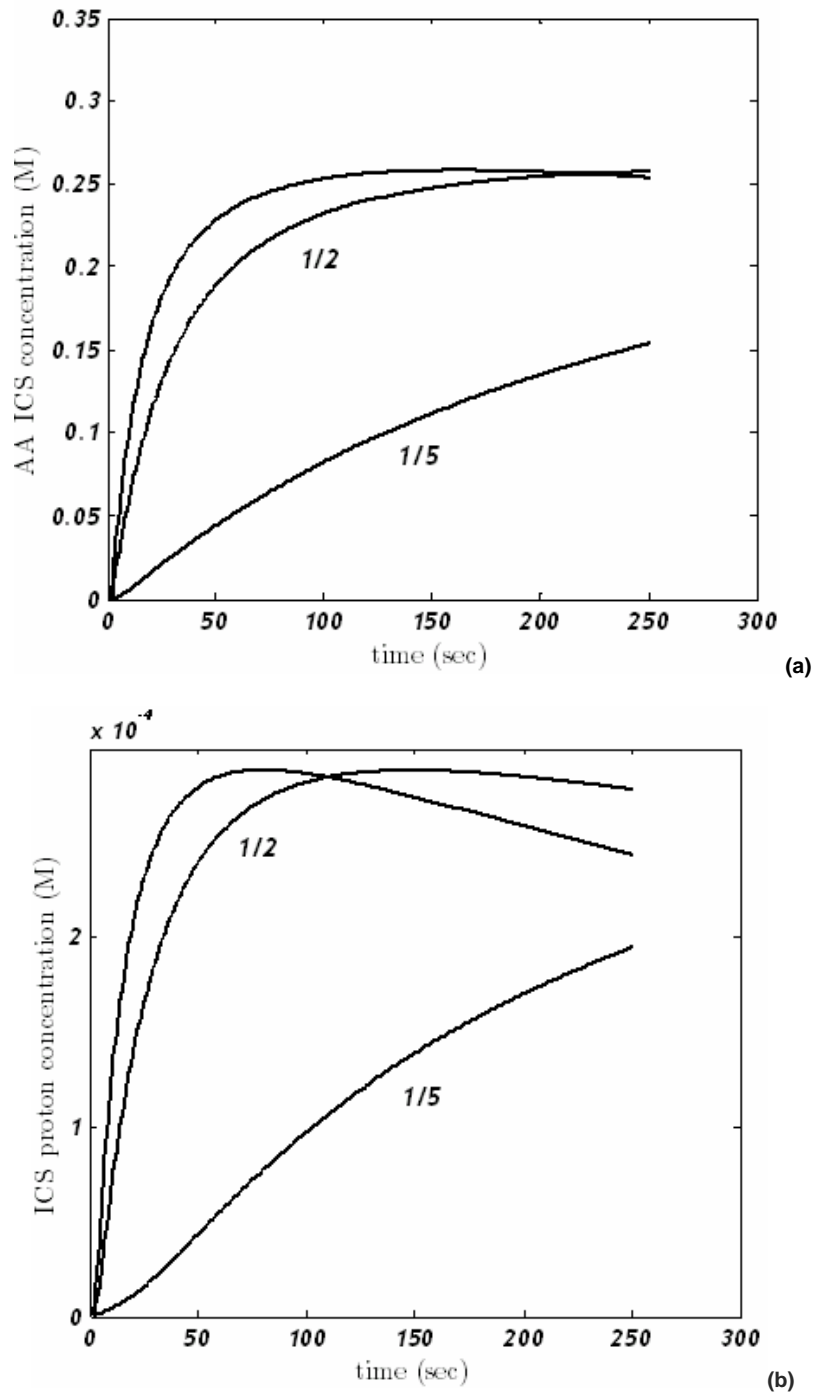
The fact that the intracellular transmembrane diffusion of AA is almost instantaneous due to high membrane permeability, suggests that the paracellular route governs the solute kinetics through the entire epithelium. Figures 30a and b depict the solute concentration profiles in the entire epithelium (bold line) and in each layer independently (soft lines). It is clear that the total intracellular concentration is provided by the upper dysplastic layers and is evidenced that the paracellular route prevents the rapid diffusion of molecules from one layer to the other. In fact, in the first 8-10 layers almost all initial solute mass is distributed in the ICS of these dysplastic layers.





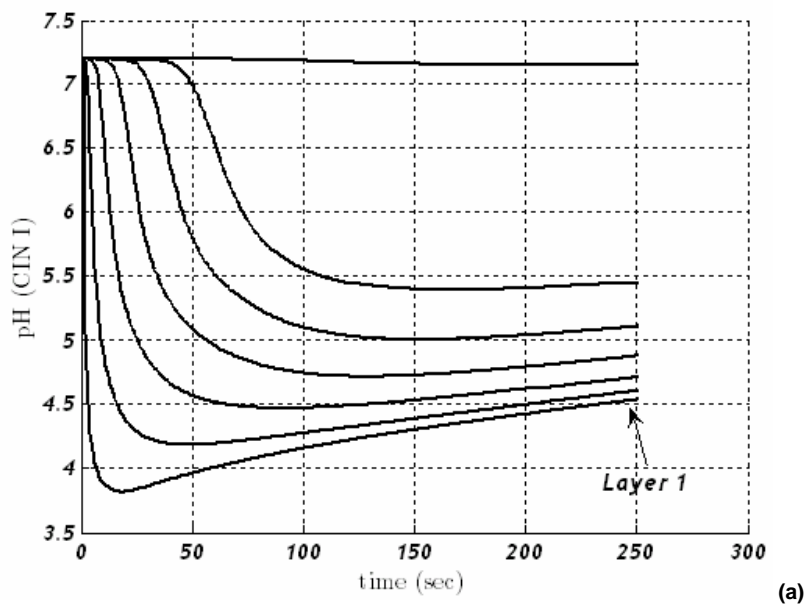
**Figure 30** Concentration profiles of (a) protons and (b) in the entire epithelium (bold line) and in each layer independently (soft lines)

Therewithal, figures 31a and b show the significant influence of the paracellular diffusion in the intracellular concentrations of both protons and AA. Noticing that the peak values are constant we conclude that the paracellular route is able to slow down the overall kinetical process shifting the concentration profiles in time. If the diffusion rate is the half of the initial one, the total intracellular concentration rises smoothly and commences to relax after 300 seconds. This is not the case when more effective changes occur. The differentiation is obvious if the diffusion rate is 1/5 of the initial which has a sigmoidal profile (figure 31b) suggesting that only a small portion of dysplastic layers and their respective intracellular spaces have accumulated the solutes.



**Figure 31 Dropping the paracellular diffusion rate and the effect on (a) ICS proton concentration and (b) ICS AA concentration**

Figures 32a,b and c show the pH profiles during CIN I, II III in the first epithelial layers. CIN III shows the smoothest and greatest intracellular pH drop followed by a longer relaxation time than CIN I and II. That is the case; intracellular acidic conditions are stronger and maintained for a longer time period as CIN progresses.



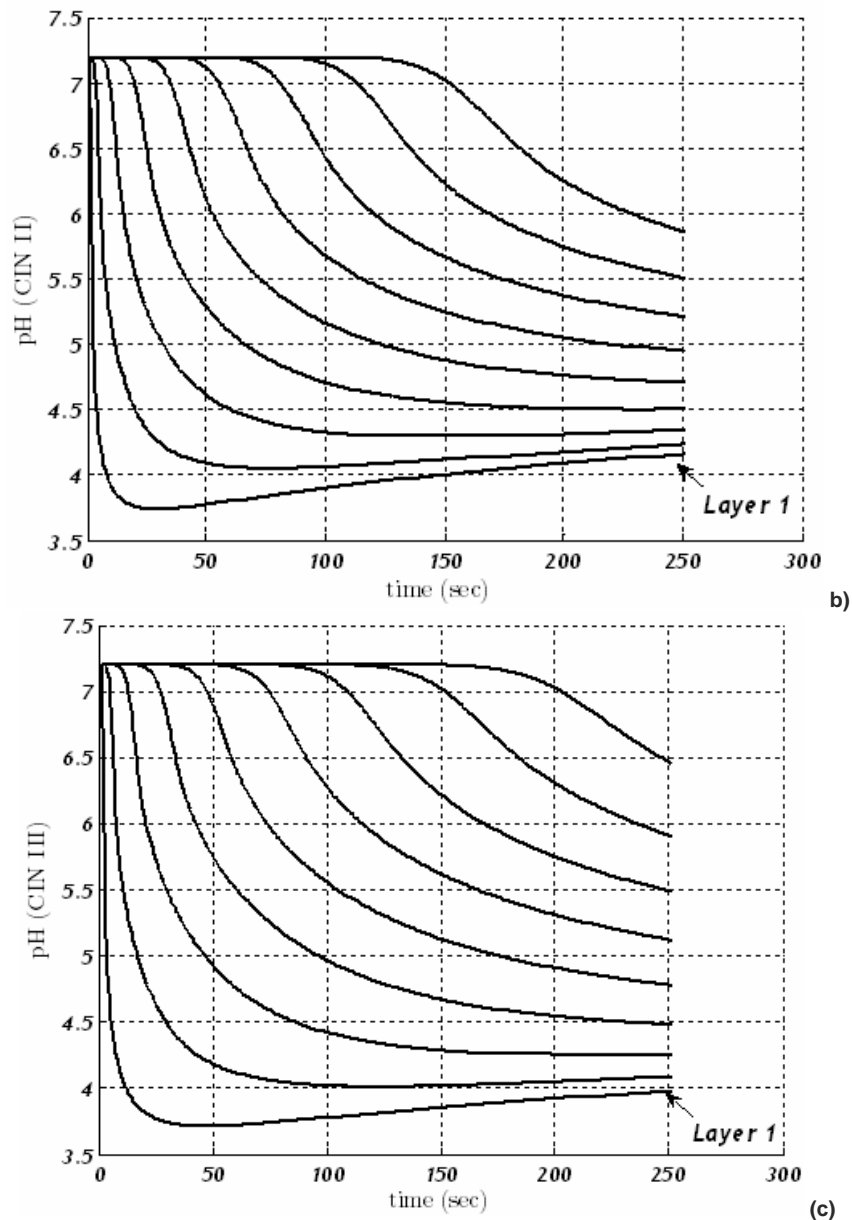


**Figure 32 pH profiles in (a) CIN I (b) CIN II and (b) CIN III**

A rather interesting observation is that, during CIN I, the last layer shows a small and insignificant pH drop. This is due to the fact that the dysplastic layers are few and close to the vasculature which accumulates greatly extracellular solutes. This situation, however, does not apply in more severe dysplasia, when the first dysplastic layers lay afar from the basement epithelial membrane. Due to the paracellular diffusion rate molecules cannot reach the lower layers of the epithelium and are consumed in the upper ones. Hence, the diffusion to the underlying tissue cannot potentially affect the intracellular AA diffusion in CIN grades II and III.

Therefore, it is clear that the diffusion pathways govern the solute kinetics as expected. If the acetowhitening phenomenon is to be linked with either the AA or proton concentration, the paracellular diffusion rate is its time-scale regulation factor. The faster the rate the faster the concentration peaks are reached. In addition, the diffusion to the underlying tissues would influence the phenomenon's time course; however the paracellular diffusion rate limits its potential.

### *5.3 The buffering effect*

The prime Acellular mechanism in coping with acute acid loads is the physicochemical buffering. Buffering tends to diminish intracellular pH changes. Unfortunately, we cannot fully demonstrate the buffering effect by the time little is known over the buffer species inhabiting the ICS and ECS of the cervical transformation zone. Qualitatively, we attempt to demonstrate the correlation among the concentration of AA and protons having neoplasia grade II as a reference. However, the fact that the buffering effect is expected to be the same in all dysplastic layers suggests that it will have no effect on the differentiation between different CIN grades.

Figures 33a and b demonstrate the relation of the intracellular buffering in both solute concentrations. Equations (18) and (19) suggest the direct effect of buffering on intracellular proton concentration and indirect on AA. The prospective concentration attenuation during intracellular buffering strengthening reveals the inverse proportionality between the biological elements. Proton's concentration profile exhibits, however, an abrupt peak fall in the ICS followed by a slow relaxation time. AA, in contrast, does not fluctuate significantly showing analogue rise and fall slope. This less profound effect can be attributed to the indirect relation of AA and buffering through ionization.

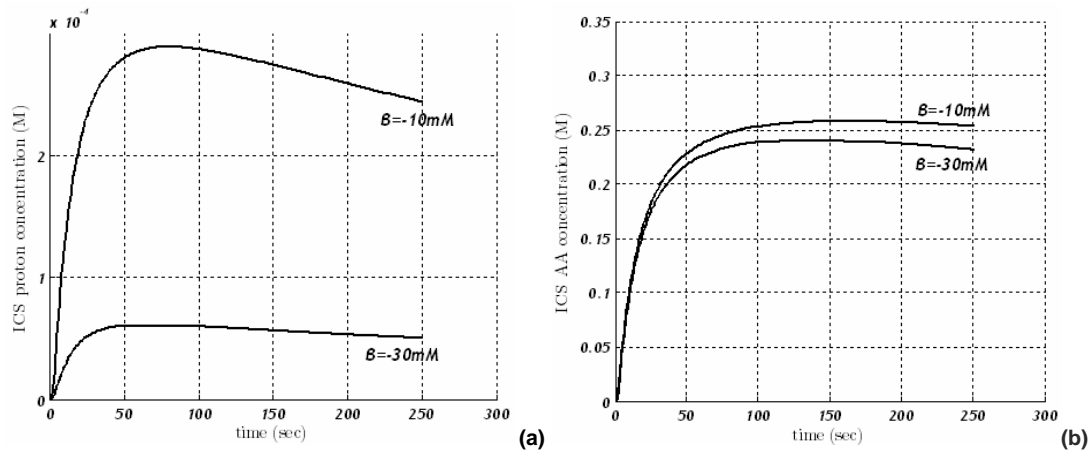


**Figure 33 The ICS buffering effect on (a) protons and (b) AA intracellular concentrations**

On the other hand, there is a different relation between the fraction the ionized over the non-consumed protons in the ECS and the intracellular concentrations. As expected, both concentration profiles that are depicted in figures 34a and b show a parallel attenuation. This evidences that by the time less AA exists in the ECS, less AA intrudes the ICS and therefore less ionization (or pH drop).

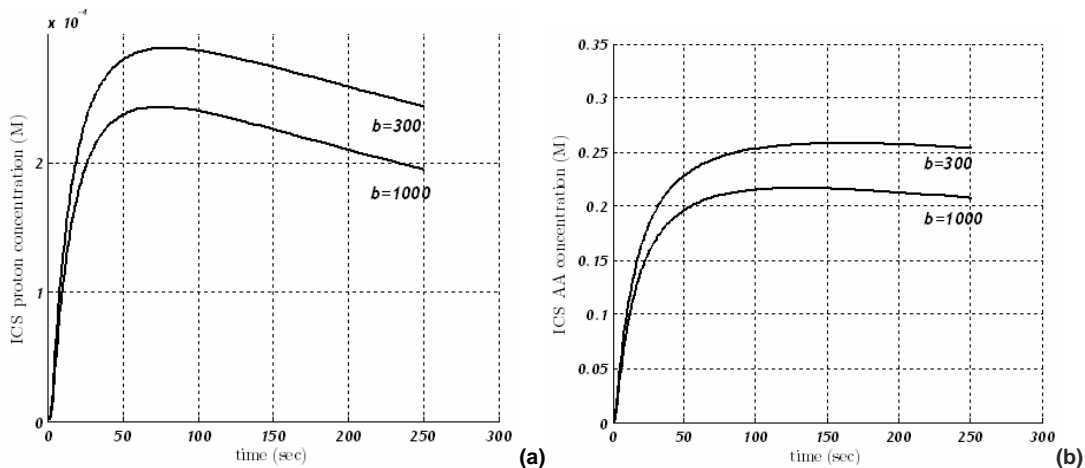


**Figure 34 The ECS buffering effect on (a) protons and (b) AA intracellular concentrations**

### 5.4 Initial concentration

The most obvious influential factor on intracellular solute concentrations is the initial AA concentration. Aforementioned, physicians use topical application of acetic acid solution 3% or 5% v.v. in order to highlight dysplastic regions. Figures 35a and b depict the modified concentration profiles using CIN II

grade as a reference. Both graphs depict an analogue elevation in solute concentrations proportional to the initial AA concentration rise. Thus, the more the initial AA concentration is, the greater the intracellular concentrations of AA and protons become.

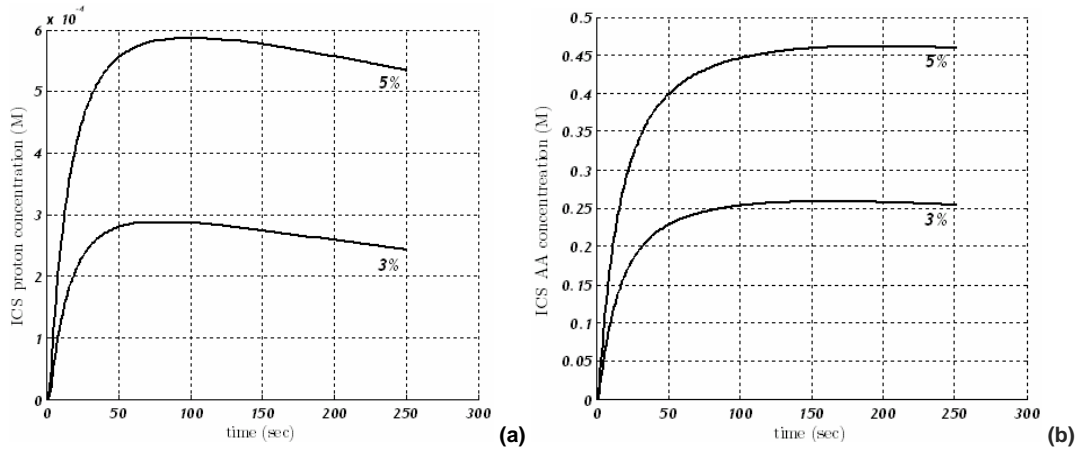


**Figure 35** The effect of the initial AA concentration on (a) protons and (b) AA intracellular concentrations

## Chapter 6

### Model validation and Discussion

#### *6.1 Experimental set-up*

An imaging device capable of measuring the AW kinetics for every image pixel has been developed [10]. The device integrates an optical imaging head supported by a mechanical basis, which includes weight counter balancing and space translating mechanisms. The basis allows for the easy manual positioning of the optical imaging head to obtain a sharp image of the tissue and includes mechanical and electromagnetic brakes that are manually activated through a trigger, once the optimum field-of-view has been achieved. In order to maintain approximately the same field-of-view throughout the entire examination procedure, the optical imaging head is detachably connected through a mechanical shaft attached to a vaginal speculum. Once the latter has been inserted into the vagina, its blades are opened to enable the visualization and the imaging of the cervix of the uterus. Tissue imaging is performed with the aid of a 35 mm lens, coupled with a 1024X768, 8bit/channel color CCD camera. The camera is interfaced with a dual core microprocessor computer unit, through a fire-wire (IEEE-1394) cable. The optical imaging head further comprises a white Light Emission Diode (LED), coupled with light collimating and focusing optics for uniform tissue illumination. A pair of polarizers, one disposed at the imaging and one at the illumination pathways having their polarization axes perpendicular with each other, is employed for the cutting-off of the surface reflection originating from the air-tissue interface and of the glare originating from the mucus. The optical head has been configured to capture images from a 23mm X 20mm tissue area, including the entire transformation zone of the cervix. Assuming an average 35 $\mu$ m cell diameter and given the aforementioned sensor's spatial resolution, it can be easily calculated that the back-scattered light intensity recorded by a given pixel, corresponds approximately to the area occupied by a single cell. Technical evaluation shows that the sensor has a substantially linear response across its entire dynamic range. In order to ensure device

independent and reproducible imaging, systems calibration is performed using  $\text{Ba}_2\text{SO}_4$  calibration plate, with unity reflectance across the visible spectral range (figure 36).

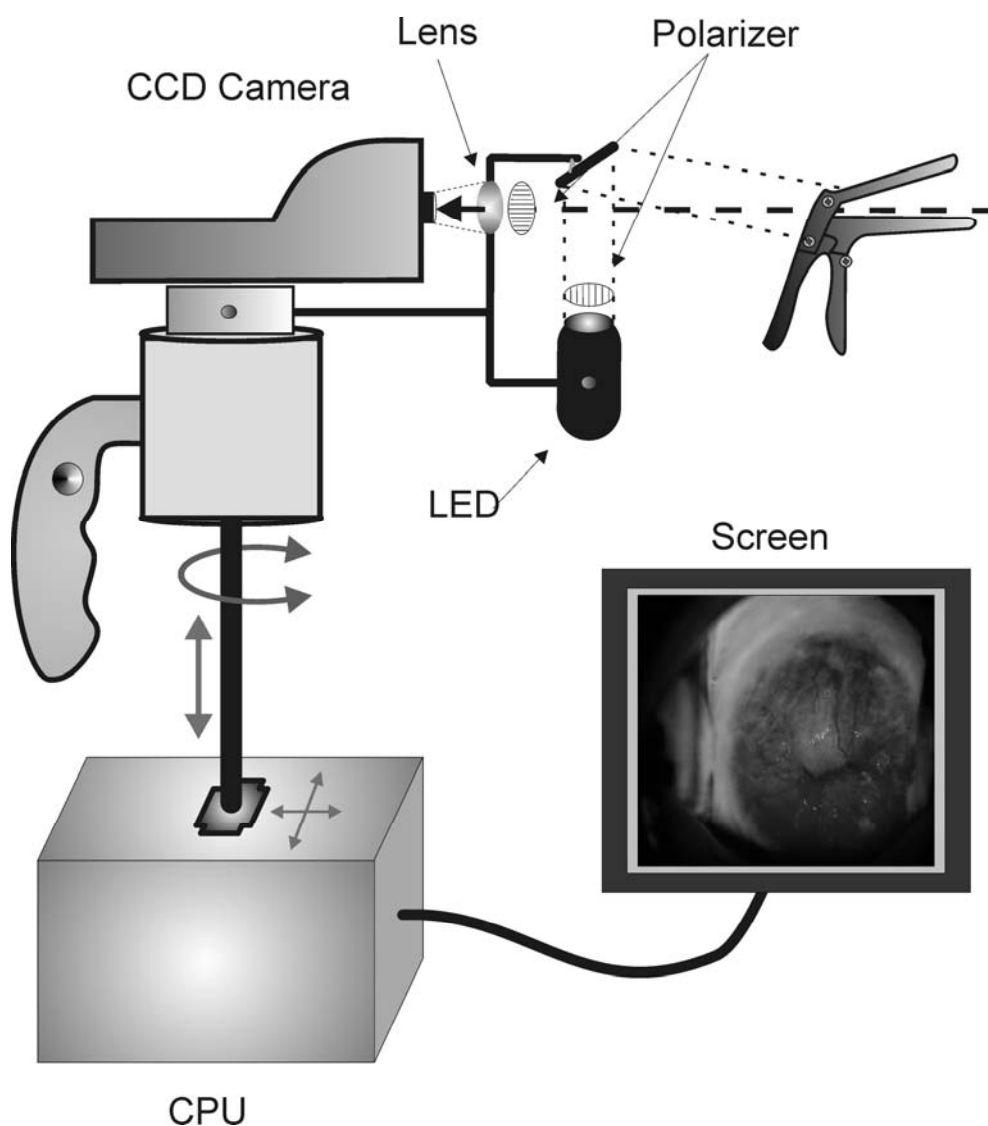


Figure 36 Experimental setup

The initiation of the image capturing procedure is triggered by an AA applicator in order to ensure synchronization between them. The AA applicator is a nozzle connected with a syringe, which has been pre-filled with a 2 ml AA solution 3% (0.5M). A reference image is captured before the application of the AA solution, which is followed by an automatic image capturing of images during the evolution of the AW phenomenon, with a frequency one image every 5 s and for a 240 s total acquisition time. The latter have been determined as the optimum ones for recording the AW

phenomenon. The captured images are aligned automatically, using an embedded image registration algorithm, in order to compensate for both image translations and deformations, provoked by tissue contractions and patient's micromovements respectively. From the captured image stack and particularly from their green channel, Diffuse Reflectance (DR) curves are calculated for every image pixel, expressing the temporal characteristics of the AW phenomenon. The green channel has been selected since it provides greater than the other channels dynamic range and S/N ratio for the monitoring of the latter [10]. From the obtained curves a series of parameters can be calculated such as time integral, DR peak value (DRmax) etc. A pseudocolor map is then generated, with different colors representing different parameter values, allowing for the direct visualization of the spatial distribution of calculated parameters expressing the AW effect kinetics. The generated map is overlaid onto the real-time displayed color image of the cervix for guiding biopsy sampling. Histological results are compared with the parameter values, corresponding to the biopsied tissue area, thus enabling their direct comparison of parameter values with histological classification, thus enabling the evaluation of the diagnostic value of the derived dynamic optical parameters.

## ***6.2 Clinical data***

We present selective results obtained from clinical feasibility tests performed before the phase II clinical trial, as a preparatory phase [13]. All patients signed an informed consent and the measurements have been approved by the hospitals' ethics committee. The results that will be presented below have been obtained from 30 women with low grade and 30 with high grade lesions referred to the colposcopy clinic as having an abnormal pap-test. From patients examined with the imaging device described above, biopsy samples were obtained from tissue areas corresponding to pseudocolors indicating the presence of AW effect. The biopsy samples were submitted for histological assessment.

### 6.3 Model Validation

Figure 37(a) illustrates a color image of a high grade CIN lesion, captured with cross polarizers. The elimination of the surface reflection enables the clear visualization of the stroma vasculature through the transparent epithelium.

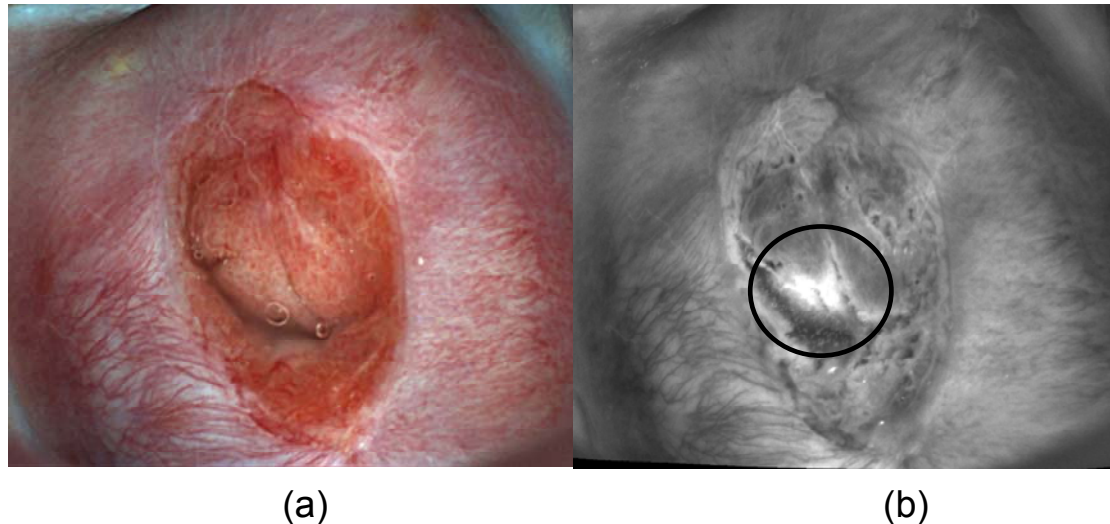
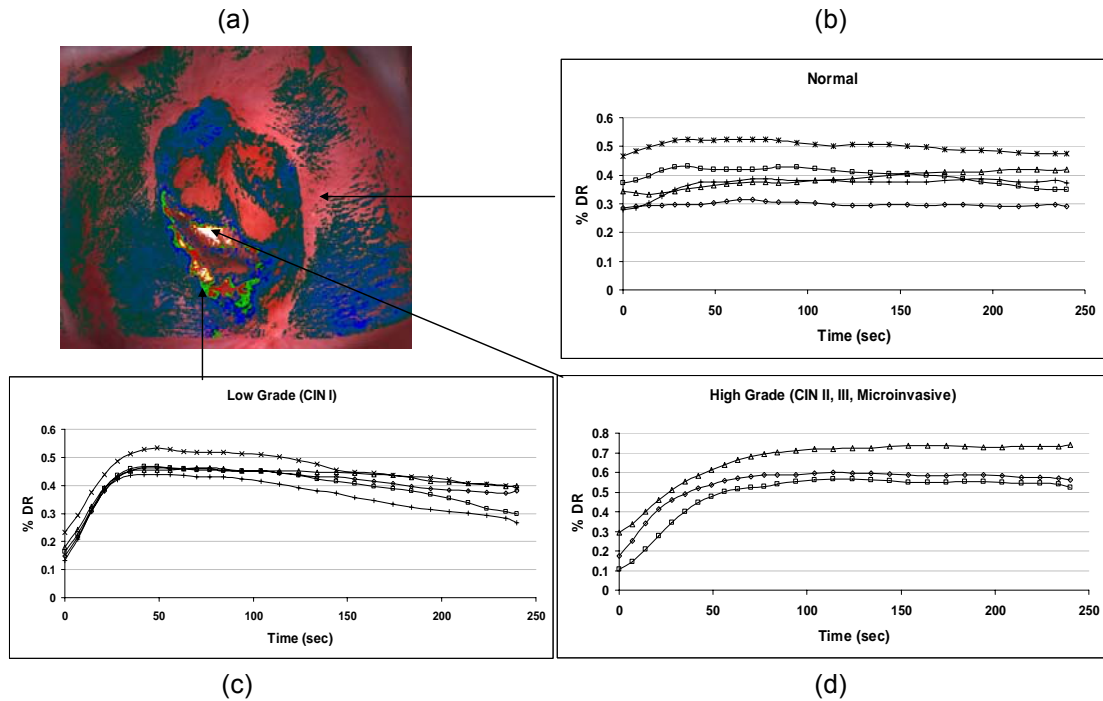


**Figure 37 (a) Polarized image of a cervix with high grade cervical neoplasia  
(b) Spectral image of the same cervix ( $550\pm 20\text{nm}$ ) computed at 90sec time point after the application of acetic acid solution 3%. The circle surrounds the acetowhitening area**

Figure 37(b) illustrates the green channel image of the same tissue, captured 90 sec after the application of 2ml AA 3%. It is clearly seen that the epithelial area surrounded by the circle has become opaque due to the alterations in its scattering properties provoked by the application of AA solution. Figure 38(a) illustrates a pseudocolor map with different (pseudo) colors representing different AW degree and dynamics. The parameter employed to express the latter is the DR time integral taken over the 0-240s.

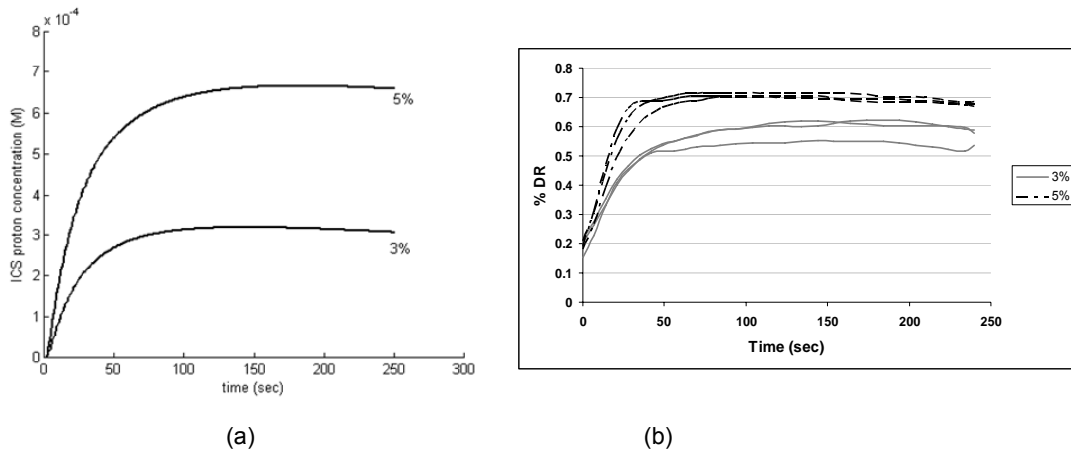
Figures 38(b),(c) and (d) depict the unfitted (raw) DR vs. time curves corresponding to normal low grade and high grade lesions. Low integral values are represented with no color or blue, medium values are represented with green-red and high integral values are represented with yellow-white. For the purpose of model evaluation we have selected to test the validity of its predictions in two main conditions: a) In different AA concentrations, b) in different CIN grades. The first condition has been selected since we expect that by altering the concentration of the administered AA the intracellular

proton concentration will alter proportionally. In addition, it is widely known that both 3% and 5% concentrations are used in clinical practice and that in the 5% case, more intense AW effect is produced.



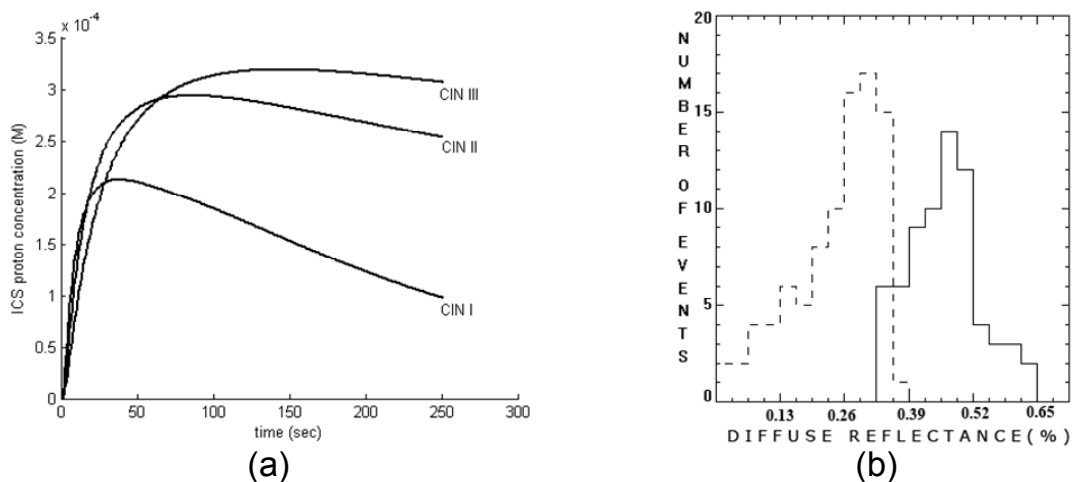
**Figure 38(a) The acetowhitening map pseudocolor image overlaid onto the color image of the cervix the DR vs. time curves of**  
**(b) normal epithelium (no color in map)**  
**(c) low grade epithelium (green color in map) and**  
**(d) high grade epithelium (white color in the map)**

Figure 39(a) depicts the intracellular concentration vs. time curves corresponding to 5% and 3% AA concentration as they are predicted by the model. Figure 39(b) illustrates the experimental DR vs. time curves obtained from the same high grade lesion at 3% and 5% AA concentrations. Each curve corresponds to different pixels within the same area. It is clearly seen that both intracellular peak proton concentrations and DR peak values are increasing with the concentration of AA. In addition, the slopes before the maximum of both model predicted and experimental curves become steeper as the concentration increases.



**Figure 39 (a)** The intracellular concentration (M) vs. time curves for 5% and 3% acetic acid as predicted by the model  
**(b)** Experimental DR vs. time curves obtained from the same patient at 5% and 3% acetic acid concentrations

The substantially proportional alteration of both peak values and slopes with the concentration of the administered AA can be reasonably attributed to increased concentration gradients between the model compartments. This strongly suggests that the model provides valid predictions for the epithelial transport phenomena, which in term are correlated with the functional status of the tissue. Moreover, it is clearly seen that the AW phenomenon, as depicted in figure 39(b), follows the dynamics of the intracellular proton concentration 39(a). This confirms the validity of the original assumption that the AW effect characteristics are mainly determined by the epithelial transport phenomena.



**Figure 40 (a)** Intracellular concentration vs. time curves corresponding to CIN I, CIN II and CIN III as predicted by the model. The peak concentration values are proportional with the CIN grade.  
**(b)** The normalized DR peak AW values distribution corresponding to 30 low grade (dashed line) and 30 high grade (solid line) CIN grade

Model validation in different CIN grades was performed using histology as reference. Histological assessment of CIN is largely based on the estimation of the nuclear density in epithelial sections. In other words, histological assessment provides a reasonable means for testing the model's performance in predicting the number of layers with high nuclear density. Figure 40(a) depicts the intercellular proton concentration vs. time curves using as model input the epithelial layers corresponding to CIN I, CIN II and CIN III. It is clearly seen that mainly the peak values and the absolute values of the slopes after the peak are increasing with CIN grade. Figure 40(b) illustrates the distribution of the peak DR values corresponding to 30 low (dashed line) and 30 high grade (solid line) cases. Peak AW values have been normalized to the DR value of the tissue before the application of the AA solution. As it is also depicted in figs. 38(b,c), the AW peak values are also increasing with the CIN grade. The fact that the CIN grade has a similar effect to both intracellular proton concentration and AW dynamics further confirms the validity of the original hypothesis that the former is largely determining the latter. The increase of the scattering intensity with the CIN grade is attributed to the fact that the higher the grade the greater the number of abnormal epithelial layers and consequently the greater the total intracellular proton volume in the epithelium at a given time point. By increasing the total intracellular volume of the protons in the total abnormal epithelium, the volume of the proteins subjected to conformational changes is expected to increase accordingly. This implies that the alteration of the refractive index will occur in a greater number of cell nuclei, which in turn will increase back scattering cross section of the epithelial tissue. The demonstrated correlation between the AW dynamics and the nuclear density of the epithelium indicates that the solution of the inverse problem is possible. By fitting the experimental data with functions derived from the developed model, the model inputs (i.e. abnormal cell layers) would become outputs, providing parameters that are directly related with the structural and functional status of the epithelium. It is worth noticing that with the 1024x768 image sensor used in this study, such parameters can be calculated for 786432 area points, with each point corresponding approximately to a single epithelial cell column.

Besides the high spatial resolution, the developed model is also capable of providing information across the third (vertical) direction of the epithelium. Figure 41 displays the intracellular proton concentration vs. time curves corresponding to a CIN III lesion and to its constituting layers. As it can be seen, the proton intracellular concentration falls remarkably across the epithelium and becomes almost zero at the first 10 layers.

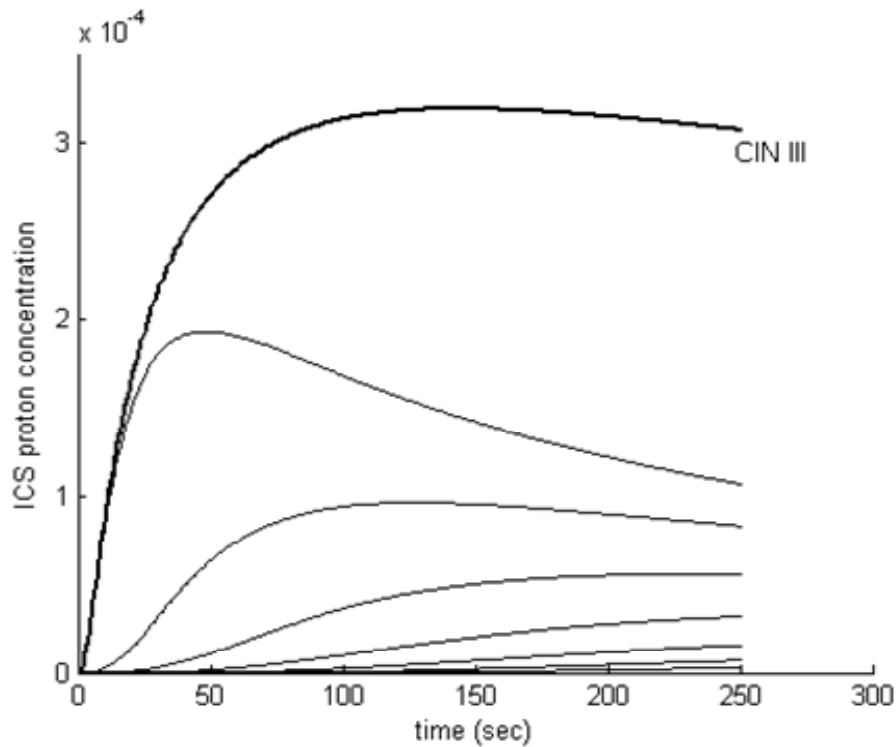


**Figure 41** Model predicted ICS proton concentration vs. time curves corresponds to both CIN III lesions and to its constituting epithelial layers. Intracellular concentration drops fast within the upper 10 layers.

Due to this fact, it seems that in high grade cases, AA is consumed in the epithelium totally, never reaching the stroma. This finding is in full agreement with finding obtained with Transmission Electron Microscopy (TEM) of the AW epithelium [101]. On the other hand this observation would eventually set a natural barrier in the method's ability to discriminate CIN II from CIN III. This is because in both cases the numbers of neoplastic layers are more than ten and consequently it is expected to have similar AW pattern. Nevertheless, according to current clinical guidelines, lesion's management decision-making is based on the discrimination between high and low grade CIN, which is clearly possible with this approach. This fact is further supported by the results obtained in the phase II clinical trial [13] where the quantitative

assessment of the AW dynamic characteristics succeeded to discriminate objectively low from high grade lesions with high sensitivity and specificity.

In normal and non-CIN lesions the model predicts a very low, but non-zero intracellular proton concentration. This could explain the low intensity AW signal observed in most of these cases. However, the modelling of the non-CIN lesions goes beyond the scope of this thesis comprising a subject of our ongoing research. Another subject of our current research is the modelling of the scattering properties of the epithelium. As it can be seen in fig. 5, the change in AA concentration from 3% to 5% almost doubles the intracellular proton concentration. The same change affects less drastically the experimental curves (fig 5(b)). This is attributed to the fact that the scattering of the uppermost layers filters backwards the photons originating from the scattering of the lower layer, thus reducing the photon flux reaching the sensor. The accurate solution of the inverse problem requires the compensation for this inter-layer photon loss and we are currently working on this subject.

## CONCLUSION – FUTURE WORK

Cervical neoplasia is the third most common cancer and in developing countries the leading cause of death among women. Throughout the years, methods and instrumentation have been brought on for the early detection and identification of cancer curable precursor (CIN) targeting the highest range of sensitivity and specificity. Nowadays, non-invasive techniques are of particular interest. The imaging techniques developed provide a great motivation to new innovative diagnostic methods. Such screening programs undergo, however, several limitations preventing their practical adoption. The presentation of a novel hyperspectral imaging system that utilizes a timeworn, but well defined, technique used by practitioners has triggered the investigation of the strong correlation between its measured dynamic data and the precancerous lesions of different neoplasia stage. This technique is known as acetowhitening and involves the interaction of a chemical substance (acetic acid) with the dysplastic regions of the cervical epithelium.

In the current thesis we tried to investigate the structural and functional characteristics of the cervical stratified epithelium that are involved in this physicochemical procedure. By developing a mathematical biophysical model, based on qualitative and quantitative knowledge, we attempted to specify the time characteristics of the chemical solutes involved in the process. Concession of the inability to encapsulate the current model with specific quantitative data resulted in the application of parametrical values. Such adoption was investigated by the existing qualitative data presented in literature.

After completing such a task we attempted to understand and extract the biophysical processes involved in the acetowhitening effect and correlate them with the actual simulation results. Such an arbitrary molecular imaging led us to the distinction of several functional and structural characteristics that are responsible for the phenomenon at hand. We have demonstrated that the dynamic characteristics of the AW phenomenon are largely determined by the intracellular proton concentration kinetics. We have also demonstrated that the latter is affected by both microstructural and functional alterations

occurring in the epithelium during the development of cervical neoplasia. The observed correlation between the dynamic scattering characteristics of the AW effect and the structural and functional characteristics of the epithelium enables the assessment of the latter *in-vivo* and non-invasively. This highlights the potential of the developed method and imaging technology in replacing traditional colposcopes and in improving colposcopic performance in terms of both diagnostic and biopsy sampling accuracy.

The validation process presented here may be on a qualitative basis, depicts, however, the biophysical assessment of the acetowhitening kinetics. In the future, more precise parameter values can be introduced in order to get more accurate system identification, i.e. the determination of the model in terms of its structure and the values of its parameters. Even if the parametrical values presented in this compartmental model are realistic, especially the structural ones, a more elaborate work on the subject can always be applied.

Moreover, it is essential to investigate other acetowhitening agents in order to establish a greater understanding on the agent-tissue interaction and the potential globalization of the proposed model. In addition, model optimization also instructs the identification of *in-vivo* tissue scattering characteristics. Over and above, the identification of the nucleoproteins that get involved in the agent-tissue interaction must be provided. This would appoint us with the refractive indexes of every dysplastic epithelial layer which will guide us to adopt a more precise opto-biophysical and biochemical model. The determination of such characteristics and their application to the model are prerequisite for the solution of the inverse problem. Upon fitting the accurate inverse problem, we will be able to retain user-independent, quantitative information for neoplasia grade *in-vivo*, which would establish a more reliable and cost-effective alternative screening tool for the early detection and prevention of cervical neoplasia.

## References

- [1] J. Ferlay, et al., "GLOBOCAN 2002: Cancer Incidence, Mortality and Prevalence Worldwide version 2.0," in *IARC CancerBase*, IARC Press, Lyon, 2004.
- [2] C. P. Crum, D. W. Abbott, and B. J. Quade, "Cervical Cancer Screening: From the Papanicolaou Smear to the Vaccine Era," *Journal of Clinical Oncology*, vol. 21, pp. 224-230, 2003.
- [3] M. Schiffman and P. E. Castle, "The promise of global cervical-cancer prevention," *New England Journal of Medicine*, vol. 353, pp. 2101-2104, 2005.
- [4] D. G. Ferris, et al., "Colposcopy quality control: establishing colposcopy criterion standards for the National Cancer Institute ALTS trial using cervigrams.," *Journal of Lower Genital Tract Disease*, vol. 2, pp. 195-203, 1998.
- [5] S. F. Wu, L. Meng, S. X. Wang, and D. Ma, "A comparison of four screening methods for cervical neoplasia," *International Journal of Gynecology & Obstetrics*, vol. 91, pp. 189-193, 2005.
- [6] R. Sankaranarayanan, et al., "A critical assessment of screening methods for cervical neoplasia," *International Journal of Gynecology & Obstetrics*, vol. 89, pp. S4-S12, 2005.
- [7] E. H. Hopman, F. J. Voorhorst, P. Kenemans, C. Meyer, and T. J. M. Helmerhorst, "Observer Agreement on Interpreting Colposcopic Images of Cin," *Gynecologic Oncology*, vol. 58, pp. 206-209, 1995.
- [8] D. Solomon, M. Schiffman, R. Tarone, E. E. Partridge, L. Kilgore, S. Hester, J. L. Walker, G. A. Johnson, A. Yadack, R. S. Guido, K. McIntyre-Seltman, R. P. Edwards, J. Gruss, N. B. Kiviat, L. Koutsky, C. Mao, J. M. Haug, D. Ferris, J. T. Cox, L. Burke, C. M. Wheeler, C. Peyton-Goodall, M. M. Manos, R. J. Kurman, D. L. Rosenthal, M. E. Sherman, M. H. Stoler, D. M. Harper, J. Rosenthal, M. Dunn, J. Quarantillo, D. Robinson, A. T. Lorincz, and L. Rich, "A randomized trial on the management of low-grade squamous intraepithelial lesion cytology interpretations," *American Journal of Obstetrics and Gynecology*, vol. 188, pp. 1393-1400, 2003.
- [9] C. Balas, A. Dimoka, E. Orfanoudaki, and E. Koumandakis, "In vivo assessment of acetic acid-cervical tissue interaction using quantitative imaging of back-scattered light: Its potential use for the in vivo cervical cancer detection grading and mapping," *SPIE-Optical Biopsies and Microscopic Techniques*, vol. 3568, pp. 31-37, 1998.
- [10] C. Balas, "A Novel Optical Imaging Method for the Early Detection, Quantitative Grading, and Mapping of Cancerous and Precancerous Lesions of Cervix.," *IEEE Transactions in Biomedical Engineering*, vol. 48, pp. 96-104, 2001.
- [11] I. M. Stefanaki, A. D. Tosca, G. C. Themelis, E. M. Vazgiouraki, D. N. Dokianakis, J. G. Panayiotidis, D. A. Spandidos, and C. J. Balas, "In vivo detection of human papilloma virus-induced lesions of anogenital area after application of acetic acid: a novel and accurate approach to a trivial method," *Journal of Photochemistry and Photobiology B-Biology*, vol. 65, pp. 115-121, 2001.
- [12] C. J. Balas, G. C. Themelis, E. P. Prokopakis, I. Orfanoudaki, E. Koumantakis, and E. S. Helidonis, "In vivo detection and staging of epithelial dysplasias and malignancies based on the quantitative assessment of acetic acid-tissue interaction kinetics," *Journal of Photochemistry and Photobiology B-Biology*, vol. 53, pp. 153-157, 1999.
- [13] P. Soutter, E. Diakomanolis, D. Lyons, S. G. Maghami, T. Ajala, D. Haidopoulos, D. Doublis, C. Kalpaktsoglou, G. Sakellaropoulos, S. Soliman, K. Perryman, V. Hird, C. Simos, Y. Skiadas, H. Kavagiou, and B. C., presented at the *British International Congress of Obstetrics & Gynaecology London Jul. 4-6 2007*.
- [14] R. Sankaranarayanan, P. O. Esmay, R. Rajkumar, R. Muwonge, R. Swaminathan, S. Shanthakumari, J.-M. Fayette, and J. Cherian, "Effect of visual screening on cervical cancer incidence and mortality in Tamil Nadu, India: a cluster-randomised trial," *Lancet*, vol. 370, pp. 398-406, 2007.
- [15] R. A. Drezek, T. Collier, C. K. Brookner, A. Malpica, R. Lotan, R. R. Richards-Kortum, and M. Follen, "Laser scanning confocal microscopy of cervical tissue

- before and after application of acetic acid," *American Journal of Obstetrics and Gynecology*, vol. 182, pp. 1135-1139, 2000.
- [16] T. T. Wu, J. Y. Qu, T. H. Cheung, S. F. Yim, and Y. F. Wong, "Study of dynamic process of acetic acid induced-whitening in epithelial tissues at cellular level," *Optics Express*, vol. 13, pp. 4963-4973, 2005.
- [17] A. V. Finkelstein and O. V. Galzitskaya, "Physics of protein folding," *Physics of Life Reviews*, vol. 1, 2004.
- [18] W. R. Loewenstein, "Junctional Intercellular Communication and the Control of Growth," *Biochimica et Biophysica Acta*, pp. 1-65, 1979.
- [19] H. Lodish, A. Berk, P. Matsudaira, C. A. Kaiser, M. Krieger, M. P. Scott, S. L. Zipursky, and J. Darnell, "Integrating Cells into Tissues," in *Molecular Cell Biology*, 5th ed., New York, W.H. Freeman and Company, vol. 6, pp. 197-231, 2004.
- [20] E. Overton, "Über die osmotischen eigenshaften der lebenden pflanzen und tierzellen," *Vierteljahrschr. Naturforsch. Ges. Zurich*, vol. 40, pp. 159 - 201, 1895.
- [21] T.-X. Xiang and B. D. Anderson, "Influence of Chain Ordering on the Selectivity of Dipalmitoylphosphatidylcholine Bilayer Membranes for Permeant Size and Shape," *Biophysical Journal* vol. 75 pp. 2658-2671, 1998.
- [22] T.-X. Xiang and B. D. Anderson, "Permeability of Acetic Acid Across Gel and Liquid-Crystalline Lipid Bilayers Conforms to Free-Surface-Area Theory," *Biophysical Journal* vol. 72, pp. 223-237, 1997.
- [23] T.-X. Xiang and B. D. Anderson, "Phospholipid surface density determines the partitioning and permeability of acetic acid in DMPC : Cholesterol Bilayers.," *Journal of Membrane Biology*, vol. 148, pp. 157 - 167, 1995.
- [24] E. Orbach and A. Finkelstein., "The nonelectrolyte permeability of planar lipid bilayer membranes," *J. Gen. Physiol.*, vol. 75, pp. 427-436, 1980.
- [25] A. Finkelstein, "Water and nonelectrolyte permeability of lipid bilayer membranes," *J. Gen. Physiol.*, vol. 68, pp. 127-135, 1976.
- [26] R. C. Bean, W. C. Shepherd, and H. Chan., "Permeability of lipid bilayer membranes to organic solutes," *J. Gen. Physiol.*, vol. 52, pp. 495-508, 1968.
- [27] S. Mitragotri, M. E. Johnson, D. Blankschtein, and R. Langer, "An Analysis of the Size Selectivity of Solute Partitioning, Diffusion, and Permeation across Lipid Bilayers," *Biophysical Journal* vol. 77, pp. 1268-1283, 1999.
- [28] D. Bemporad, C. Luttmann, and J. W. Essex, "Computer Simulation of Small Molecule Permeation across a Lipid Bilayer: Dependence on Bilayer Properties and Solute Volume, Size, and Cross-Sectional Area," *Biophysical Journal*, vol. 87, pp. 1-13, 2004.
- [29] S. Singer and G. L. Nicholson, "The fluid mosaic model of the cell membranes," *Science*, vol. 172, pp. 720-730, 1972.
- [30] C. Tselepis, M. Chidgey, A. North, and D. Garrod, "Desmosomal adhesion inhibits invasive behavior," *Cell Biology*, vol. 95, pp. 8064-8069, 1998.
- [31] H. Sasaki, C. Matsui, K. Furuse, Y. Mimori-Kiyosue, M. Furuse, and S. Tsukita, "Dynamic behavior of paired claudin strands within apposing plasma membranes," *Proceedings of the National Academy of Sciences of the United States of America*, vol. 100, pp. 3971-3976, 2003.
- [32] C. M. Van Itallie and J. M. Anderson, "Claudins and epithelial paracellular transport," *Annual Review of Physiology*, vol. 68, pp. 403-429, 2006.
- [33] K. Matter and M. Balda, "Functional analysis of tight junctions," *Methods*, vol. 30, pp. 228-234, 2003.
- [34] M. Mori, N. Sawada, Y. Kokai, and M. Satoh, "Role of tight junctions in the occurrence of cancer invasion and metastasis," *Medical Electron Microscopy*, vol. 32, pp. 193-198, 1999.
- [35] C. M. Van Itallie and J. M. Anderson, "The molecular physiology of tight junction pores," *Physiology*, vol. 19, pp. 331-338, 2004.
- [36] V. W. Tang and D. A. Goodenough, "Paracellular Ion Channel at the Tight Junction," *Biophysical Journal*, vol. 84 pp. 1660-1673, 2003.
- [37] V. Wong and D. A. Goodenough, "Paracellular Channels!," *Science, New Series*, vol. 285, pp. 62, 1999.
- [38] P. Claude, "Morphological Factors Influencing Transepithelial Permeability" A Model for the Resistance of the Zonula Occludens," *Journal of Membrane Biology*, vol. 39, pp. 219-232, 1978.

- [39] G. I. Gorodeski, M. F. Romero, U. Hopfer, E. Rorke, W. H. Utian, and R. L. Eckert, "The Cultured Human Cervical Epithelium: A New Model for Studying Paracellular Transport," *Society of Gynecologic Investigation*, vol. 3, pp. 267-280, 1996.
- [40] A. Martinez-Palomo and D. Erlij, "Structure of tight junctions in epithelia with different permeability," *Cell Biology* vol. 72, pp. 4487-4491, 1975.
- [41] N. N. Salama, N. D. Eddingtona, and A. Fasano, "Tight junction modulation and its relationship to drug delivery," *Advanced Drug Delivery Reviews*, vol. 58, pp. 15-28, 2006.
- [42] J. L. Madara, "Regulation of the movement of solutes across tight junctions," *Annual Review of Physiology*, vol. 60, pp. 143-59, 1998.
- [43] A. Nusrat, J. R. Turner, and J. L. Madara, "Molecular physiology and pathophysiology of tight junctions IV. Regulation of tight junctions by extracellular stimuli: nutrients, cytokines, and immune cells," *American Journal of Physiology-Gastrointestinal and Liver Physiology*, vol. 279, pp. G851-G857, 2000.
- [44] M. V. L. Bennett, M. E. Spew, and D. C. Spray, "Permeability of Gap Junctions Between Embryonic Cells of Fundulus: A Reevaluation," *Developmental Biology* vol. 65, pp. 114-125 1978.
- [45] A. Salameha and S. Dheinb, "Pharmacology of Gap junctions. New pharmacological targets for treatment of arrhythmia, seizure and cancer?," *Biochimica et Biophysica Acta*, vol. 1719 pp. 36 - 58, 2005.
- [46] R. Dermietzel, T. K. Hwang, and D. S. Spray, "The Gap Junction Family - Structure, Function and Chemistry," *Anatomy and Embryology*, vol. 182, pp. 517-528, 1990.
- [47] W. H. Evans and P. E. M. Martin, "Gap junctions: structure and function (Review)," *Molecular Membrane Biology*, vol. 19, pp. 121-136, 2002.
- [48] L. S. Musil and D. A. Goodenough, "Biochemical Analysis of Connexin43 Intracellular Transport, Phosphorylation, and Assembly into Gap Junctional Plaques," *The Journal of Cell Biology* vol. 115, pp. 1357-1374, 1991.
- [49] L. S. Musil and D. A. Goodenough, "Multisubunit Assembly of an Integral Plasma Membrane Channel Protein, Gap Junction Connexin43, Occurs after Exit from the ER," *Cell*, vol. 74, pp. 1065-1077, 1993.
- [50] T. Aasen, S. V. Graham, M. Edward, and M. B. Hodgins, "The relationship between connexins, gap junctions, tissue architecture and tumor invasion, as studied in a novel in vitro model of HPV-16-associated cervical cancer progression," *Oncogene*, vol. 22, pp. 6025-6036, 2003.
- [51] P. Swietach and R. D. Vaughan-Jones, "Novel method for measuring junctional proton permeation in isolated ventricular myocyte cell pairs," *AJP Heart and Circulatory Physiology*, vol. 287, pp. 2352-2363, 2004.
- [52] T. M. Suchyna, J. M. Nitsche, M. Chilton, A. L. Harris, R. D. Veenstra, and B. J. Nicholson, "Different tonic selectivities for connexins 26 and 32 produce rectifying gap junction channels," *Biophysical Journal*, vol. 77, pp. 2968-2987, 1999.
- [53] F. L. Cao, R. Eckert, C. Elfgang, J. M. Nitsche, S. A. Snyder, D. F. Hulser, K. Willecke, and B. J. Nicholson, "A quantitative analysis of connexin-specific permeability differences of gap junctions expressed in HeLa transfectants and *Xenopus* oocytes," *Journal of Cell Science*, vol. 111, pp. 31-43, 1998.
- [54] B. J. Nicholson, P. A. Weber, F. Cao, H. C. Chang, P. Lampe, and G. Goldberg, "The molecular basis of selective permeability of connexins is complex and includes both size and charge," *Brazilian Journal of Medical and Biological Research*, vol. 33, pp. 369-378, 2000.
- [55] P. A. Weber, H.-C. Chang, K. E. Spaeth, J. M. Nitsche, and B. J. Nicholson, "The Permeability of Gap Junction Channels to Probes of Different Size Is Dependent on Connexin Composition and Permeant-Pore Affinities," *Biophysical Journal Volume*, vol. 87, pp. 958-973, 2004.
- [56] C. Peracchia, "Increase in Gap Junction Resistance with Acidification in Crayfish Septate Axons Is Closely Related to Changes in Intracellular Calcium But Not Hydrogen Ion Concentration," *Membrane Biology*, pp. 75-92, 1990.
- [57] C. Peracchia, "Chemical gating of gap junction channels Roles of calcium, pH and calmodulin," *Biochimica et Biophysica Acta*, vol. 1662, pp. 61-80, 2004.
- [58] J. F. Ek-Vitorin, G. Calero, G. E. Morley, W. Coombs, S. M. Taffet, and M. Delmar, "pH Regulation of Connexin43: Molecular Analysis of the Gating Particle," *Biophysical Journal*, vol. 71 pp. 1273-1284, 1996.

- [59] E. B. Trexler, F. F. Bukauskas, M. V. L. Bennett, T. A. Bargiello, and V. K. Verselis, "Rapid and direct effects of pH on connexins revealed by the connexin46 hemichannel preparation," *Journal of General Physiology*, vol. 113, pp. 721-742, 1999.
- [60] A. Roos and W. F. Boron, "Intracellular pH," *Physiology Reviews*, vol. 61, pp. 296-434, 1981.
- [61] A. H. Lee and I. F. Tannock, "Heterogeneity of intracellular pH and of Mechanisms That Regulate Intracellular pH in Populations of Cultured Cells," *Cancer Res.*, vol. 58, pp. 1901-1908, 1998.
- [62] J. M. Boyer and I. F. Tannock, "Regulation of Intracellular pH in Tumor Cell Lines: Influence of Microenvironmental Conditions," *Cancer Res.*, vol. 52, pp. 4441-4447, 1992.
- [63] D. C. Walker, B. H. Brown, A. D. Blackett, J. Tidy, and R. H. Smallwood, "A study of the morphological parameters of cervical squamous epithelium," *Physiological Measurements*, vol. 24 pp. 1-15, 2003.
- [64] J. Doorbar, "Molecular biology of human papillomavirus infection and cervical cancer," *Clinical Science*, vol. 175, pp. 1110-1113, 2006.
- [65] I. Steinhoff, K. Leykauf, U. Bleyl, M. Du`rst, and A. Alonsob, "Phosphorylation of the gap junction protein Connexin43 in CIN III lesions and cervical carcinomas," *Cancer Letters* vol. 235 pp. 291-297, 2006.
- [66] S. C. Marc Mesnil , Jose´-Luis Avanzo , Maria-Lucia Zaidan-Dagli "Defective gap junctional intercellular communication in the carcinogenic process," *Biochimica et Biophysica Acta* vol. 1719, pp. 125 - 145, 2005.
- [67] G. E. Morley, S. M. Taffet, and M. Delmar, "Intramolecular Interactions Mediate pH Regulation of Connexin43 Channels," *Biophysical Journal*, vol. 70, pp. 1294-1302, 1996.
- [68] K. T. Davis, N. Prentice, V. L. Gay, and S. A. Murray, "Gap junction proteins and cell-cell communication in the three functional zones of the adrenal gland," *Journal of Endocrinology*, vol. 173, pp. 13-21, 2002.
- [69] I. J. Latorre, K. K. Frese, and R. T. Javier, "Tight Junction Proteins and Cancer," *In Tight Junctions, Springer US ed.*, pp. 116-134, 2006.
- [70] G. Sobel, C. Paska, I. Szabo, A. Kiss, A. Kadar, and Z. Schaff, "Increased expression of claudins in cervical squamous intraepithelial neoplasia and invasive carcinoma," *Human Pathology*, vol. 36, pp. 162-169, 2005.
- [71] D. C. Walker, B. H. Brown, R. H. Smallwood, D. R. Hose, and D. M. Jones, "Modelled current distribution in cervical squamous tissue," *Physiological Measurement*, vol. 23, pp. 159-168, 2002.
- [72] S. Hirohashi, "Inactivation of the E-Cadherin-Mediated Cell Adhesion System in Human Cancers," *American Journal of Pathology*, vol. 153, pp. 333-339, 1998.
- [73] J. J. Eckerta, A. McCalluma, A. Mearsa, M. G. Rumsby, I. T. Cameronb, and T. P. Fleming, "Relative contribution of cell contact pattern, specific PKC isoforms and gap junctional communication in tight junction assembly in the mouse early embryo," *Developmental Biology*, vol. 288, pp. 234-247, 2005.
- [74] J. J. Eckert, A. McCallum, A. Mears, M. G. Rumsby, I. T. Cameron, and T. P. Fleming, "Relative contribution of cell contact pattern, specific PKC isoforms and gap junctional communication in tight junction assembly in the mouse early embryo," *Developmental Biology*, vol. 288, pp. 234-247, 2005.
- [75] T. Aasen, S. V. Graham, M. Edward, and M. B. Hodgins, "Reduced expression of multiple gap junction proteins is a feature of cervical dysplasia," *Molecular Cancer*, vol. 4, pp. art. no.-31, 2005.
- [76] O. Lacombe, J. Woodley, C. Solleux, J.-M. Delbos, C. Boursier-Neyret, and G. Houin, "Localisation of drug permeability along the rat small intestine, using markers of the paracellular, transcellular and some transporter routes," *European Journal of Pharmaceutical Sciences*, vol. 23, pp. 385-391, 2004.
- [77] G. I. Gorodeski, M. F. Romero, U. Hopfer, E. Rorke, W. H. Utian, and R. L. Eckert, "Human uterine cervical epithelial cells grown on permeable support - a new model for the study of differentiation," *Differentiation Ontogeny, Neoplasia and Differentiation Therapy*, vol. 56, pp. 107-118, 1994.
- [78] S. G. Schultz and R. A. Frizzell, "Ionic Permeability of Epithelial Tissues," *Biochimica Et Biophysica Acta*, vol. 443, pp. 181-189, 1976.

- [79] I. F. Tannock and D. Rotin, "Acid pH in tumors and its potential for therapeutic exploitation," *Cancer Research*, vol. 49, pp. 4373-4384, 1989.
- [80] S. D. Webb, J. A. Sherratt, and R. G. Fish, "Mathematical Modelling of Tumour Acidity: Regulation of Intracellular pH," *J. theor. Biol.*, vol. 196, pp. 237-250, 1999.
- [81] L. E. Gerweck and K. Seetharaman, "Cellular pH Gradient in Tumor versus Normal Tissue: Potential Exploitation for the Treatment of Cancer," *Cancer Res.*, vol. 56, pp. 194-1198, 1996.
- [82] G. R. Martin and R. K. Jain, "Noninvasive Measurement of Interstitial Ph Profiles in Normal and Neoplastic Tissue Using Fluorescence Ratio Imaging Microscopy," *Cancer Research*, vol. 54, pp. 5670-5674, 1994.
- [83] D. M. Prescott, H. C. Charles, J. M. Poulson, R. L. Page, D. E. Thrall, Z. Vujascovic, and M. W. Dewhirst, "The Relationship between Intracellular and Extracellular pH in Spontaneous Canine Tumors," *Clinical Cancer Research*, pp. 2501-2505, 2000.
- [84] M. Stubbs, P. M. J. McSheehy, and J. R. Griffiths, "Causes and Consequences of Acidic pH in Tumors: A Magnetic Resonance Study," *Advan. Enzyme Regul.*, vol. 39, pp. 13-30, 1999.
- [85] M. L. Wahl, P. M. Pooler, P. Briand., D. B. Leeper, and C. S. Owen, "Intracellular pH Regulation in a Nonmalignant and a Derived Malignant Human Breast Cell Line," *Journal of Cell Physiology*, vol. 183, pp. 373-380, 2000.
- [86] T. Speake and A. C. Elliott, "Modulation of calcium signals by intracellular pH in isolated rat pancreatic acinar cells," *Journal of Physiology-London*, vol. 506, pp. 415-430, 1998.
- [87] J. R. Turner, B. K. Rill, S. L. Carlson, D. Carnes, R. Kerner, R. J. Mrsny, and J. L. Madara, "Physiological regulation of epithelial tight junctions is associated with myosin light-chain phosphorylation," *American Journal of Physiology-Cell Physiology*, vol. 42, pp. C1378-C1385, 1997.
- [88] G. L. Allemain and J. Pouyssegur, "Role of a Na<sup>+</sup> - dependent Cl<sup>-</sup>/HCO<sub>3</sub><sup>-</sup> Exchange in Regulation of Intracellular pH in Fibroblasts," *Journal of Biological Chemistry*, vol. 260, pp. 4877-4883, 1985.
- [89] P. Besson, J. Gore, E. Vincent, C. Hoinard, and P. Bougnoux, "Inhibition of Na<sup>+</sup>/H<sup>+</sup> Exchanger Activity by an Alkyl-Lysophospholipid Analogue in a Human Breast Cancer Cell Line," *Biochemical Pharmacology*, vol. 51, pp. 1153-1158, 1996.
- [90] W. F. Boron and P. DeWeer, "Intracellular pH transients in squid giant-axon caused by CO<sub>2</sub>, NH<sub>3</sub> and metabolic inhibitors," *Journal of General Physiology*, vol. 67, pp. 91-112, 1976.
- [91] A. B. MacLean, "Acetowhite epithelium," *Gynecologic Oncology*, vol. 95, pp. 691-694, 2004.
- [92] T. F. Weiss, "Cellular Biophysics," *MIT eds*, vol. 1, pp. 83-137, 450-620, 1996.
- [93] E. M. Renkin, "Filtration, Diffusion, and Molecular Sieving Through Porous Cellulose Membranes," *Journal of General Physiology*, pp. 225-243, 1954.
- [94] A. L. Hodgkin and K. B., "The effect of sodium ions on the electrical activity of the giant axon of the squid," *Journal of Physiology*, vol. 108, pp. 37-77, 1949.
- [95] L. Langbein, C. Grund, C. Kuhn, S. Praetzel, J. Kartenbeck, J. M. Brandner, I. Moll, and W. W. Franke, "Tight junctions and compositionally related junctional structures in mammalian stratified epithelia and cell cultures derived therefrom," *European Journal of Cell Biology*, vol. 81, pp. 419-435, 2002.
- [96] C. H. Leem, D. Lagadic-Gossman, and R. D. Vaughan-Jones, "Characterization of intracellular pH regulation in the guinea-pig ventricular myocyte," *Journal of Physiology-London*, vol. 517, pp. 159-180, 1999.
- [97] A. Walter and J. Gutknecht, "Permeability of Small Nonelectrolytes through Lipid Bilayer- Membranes," *Journal of Membrane Biology*, vol. 90, pp. 207-217, 1986.
- [98] R. D. Vaughan-Jones, B. E. Peercy, J. P. Keener, and K. W. Spitzer, "Intrinsic H<sup>+</sup> ion mobility in the mammalian ventricular myocyte," *The Journal Of Physiology*, 2002.
- [99] W. H. Moolenaar, L. G. J. Tertoolen, and S. W. d. Laat, "The Regulation of Cytoplasmic pH in Human Fibroblasts," *Journal of Biological Chemistry*, vol. 259, pp. 7563-7569, 1984.
- [100] M. Yamagata and I. F. Tannock, "The chronic administration of drugs that inhibit the regulation of intracellular pH: in vitro and anti-tumor effects," *Br. J. Cancer*, vol. 73, pp. 1328-1334, 1996.

- [101] A. B. MacLean, A. Singer, and H. Critchley, "The use of acetic acid," *Lower genital tract neoplasia, RCOG press, London*, pp. 144-152, 2003.

## Appendix

The Rapid Equilibrium Approximation is a method which exploits the fact that some kinetic steps are faster than other. In many mathematical problems, especially in biology, different time scales arise, corresponding to slow or fast processes. The exact ECS differential system for the  $i$ -th layer from section 4.3 is:

$$\dot{C}_{AA_i}^{ECS} = \rho_{tj} \left( J_{AA_i}^{tj_{in}} - J_{AA_i}^{tj_{out}} \right) + \rho_{ECS} J_{AA_i}^m + J_{ion} \quad (25)$$

$$\dot{C}_{Ac_i^-}^{ECS} = \rho_{tj} \left( J_{Ac_i^-}^{tj_{in}} - J_{Ac_i^-}^{tj_{out}} \right) + \rho_{ECS} J_{Ac_i^-}^m - J_{ion} \quad (26)$$

$$b_{ECS} \dot{C}_{H_i^+}^{ECS} = \rho_{tj} \left( J_{H_i^+}^{tj_{in}} - J_{H_i^+}^{tj_{out}} \right) + J_{H_i^+}^p - J_{ion} \quad (27)$$

The fast process involved in the above system is the AA ionization ( $J_{ion}$ ). Remember from paragraph 4.2.2 that the AA ionization is constantly at chemical equilibrium i.e.

$$K_a = k_1/k_2 = C_{Ac^-}^{ECS} C_{H^+}^{ECS} / C_{AA}^{ECS} \quad (28)$$

By setting:

$$X_i = C_{AA_i}^{ECS} + C_{Ac_i^-}^{ECS} \quad (29)$$

and

$$Y_i = b_{ECS} C_{H_i^+}^{ECS} - C_{Ac_i^-}^{ECS} \quad (30)$$

and rearranging the terms of (29) and (30) we get:

$$C_{Ac_i^-}^{ECS} = X_i - C_{AA_i}^{ECS} \quad (31)$$

and

$$b_{ECS} C_{H_i^+}^{ECS} = Y_i + C_{Ac_i^-}^{ECS} \quad (32)$$

Substituting (31) and (32) to (28) we have:

$$\begin{aligned}
K_a &= \frac{k_1}{k_2} = \frac{C_{Ac^-}^{ECS} C_{H^+}^{ECS}}{C_{AA}^{ECS}} \Leftrightarrow K_a = \frac{C_{Ac^-}^{ECS} (Y_i + C_{Ac^-}^{ECS})}{b_{ECS} C_{AA}^{ECS}} \Leftrightarrow \\
K_a &= \frac{(X_i - C_{AA}^{ECS})(Y_i + X_i - C_{AA}^{ECS})}{b_{ECS} C_{AA}^{ECS}}
\end{aligned} \tag{33}$$

We solve equation (33) for  $C_{AA}^{ECS}$  and after rejecting the negative solution it yields:

$$C_{AA}^{ECS} = \frac{(2X_i - Y_i + K_a b_{ECS}) - \sqrt{(Y_i + K_a b_{ECS})^2 + 4X_i K_a b_{ECS}}}{2} \tag{34}$$

Substitution of (34) to (31) and (32) yields:

$$C_{Ac^-}^{ECS} = X_i - C_{AA}^{ECS} \tag{35}$$

$$C_{H^+}^{ECS} = \frac{X_i + Y_i - C_{AA}^{ECS}}{b_{ECS}} \tag{36}$$

Therefore after adding equations (25) and (26) while subtracting (26) from (27) we can reduce the initial differential system into:

$$\dot{X}_i = \rho_{tj} (J_{AA}^{tj_{in}} - J_{AA}^{tj_{out}}) + \rho_{ECS} J_{AA}^m + \rho_{tj} (J_{Ac^-}^{tj_{in}} - J_{Ac^-}^{tj_{out}}) + \rho_{ECS} J_{Ac^-}^m \tag{37}$$

$$\dot{Y}_i = \rho_{tj} (J_{H^+}^{tj_{in}} - J_{H^+}^{tj_{out}}) + J_{H^+}^p - \rho_{tj} (J_{Ac^-}^{tj_{in}} - J_{Ac^-}^{tj_{out}}) - \rho_{ECS} J_{Ac^-}^m \tag{38}$$

The initial conditions of the simplified differential system are  $X_1 = C_{AA}^{ECS}(0)$ ,  $X_i = 0, i = 2 : n$  and  $Y_i = 0, i = 1 : n$  where n is the number of dysplastic layers. The impact of REA application is obvious: the initial differential system of three equations reduces to the two-equation differential system (37) and(38).